

**THE GEOCHEMISTRY OF THE FOSTERVILLE
GOLDFIELD, VICTORIA.**

A. S. NAND

A thesis submitted in partial fulfilment
of the requirements of the degree of
Bachelor of Science with Honours.



GEOLOGY DEPARTMENT,
UNIVERSITY OF TASMANIA,

November, 1989.

ABSTRACT

The Fosterville goldfield occurs in sandstones, siltstones and shales of Ordovician age, associated with the brecciated shear zones and associated stockworks of the Fosterville Shear Zone. The Fosterville Fault is a planar mineralized structure with significant old mine workings in the oxidized zone over a strike length of 8 km. The present Central Ellesmere and Fosterville prospects are situated along the Fosterville Fault.

The style of mineralization present in the Fosterville goldfield is a sedimentary rock-hosted gold deposit, along the Fosterville Fault Zone. Gold occurs within sediment hosted arsenopyrite and pyrite, in crystal lattice and/or as minute inclusions. The mineralized fault breccia and associated stockworks are vertical to sub-vertical and up to 30 m in width; only very minor quartz veining occurs.

The origin of the Fosterville gold deposit is considered to be genetically related to a granite source, with a temperature for the mineralizing fluid of approximately 370 °C. The depth of the system range from 6.5-10 km.

PIXE (proton-induced x-ray emission) and AAS (atomic absorption spectroscopy) have been very useful in analyzing for trace elements in vein quartz. The Fosterville quartz shows generally high levels of trace elements. The analyses showed positive correlation between the presence of K, Ge, Al and As with Au in the host rock and the intensity of the EPR (electron paramagnetic resonance) of quartz veins. There is a highly significant correlation between the Ge content and EPR of the quartz at the absorption peak at g 2.0027. The present study indicates that the paramagnetic centre is Ge-Al related.

The high correlation between Ge, Au and EPR suggests that EPR and Ge may be used as an indicator of gold mineralization in this type of deposits. Ge is an element typically enriched in late magmatic and hydrothermal minerals.

ACKNOWLEDGEMENTS

I wish to thank Dr. J. Van Moort for his assistance, guidance and supervision throughout the year. Gratitude is also extended to Dr. R. Berry, K. Zaw, Dr. D. Huston, G. Davidson, Dr. M. Banks, Dr. J. Stolz and Dr. A. Crawford for useful discussion, advice and reading parts of this thesis.

Invaluable assistance with preparation and analyses of samples was received from S. Newman, A. Katsaros, W. Jablonski, P. Robinson, M. Power (sen.) and S. Stevens.

Logistic support and access to drill core and technical data for this study was gratefully provided by Bendigo Gold Limited, and accomodation provided by Mrs. E. Wright, to whom I am very grateful. Discussions with Dr. R. Haydon and field assistance from S. Toomey was greatly appreciated.

Thanks are also expressed to Dave, Peter, Darren, John, Tim, Chris and Steve for being very supportive throughout the year.

Finally, I wish to thank my Mum and Dad and my family, without whom I could not have got to this stage of my education.

CONTENTS

	<u>PAGE</u>
ABSTRACT.....	i
ACKNOWLEDGEMENTS.....	ii
CONTENTS.....	iii
LIST OF FIGURES.....	v
LIST OF TABLES.....	viii
LIST OF PLATES.....	x
CHAPTER 1: INTRODUCTION.....	1
CHAPTER 2:	
Part 1 - Regional Geology and Structure.....	9
Part 2 - Local Geology and Structure.....	11
CHAPTER 3: MINERALOGY, PETROLOGY AND VEIN TEXTURES AT FOSTERVILLE.....	16
CHAPTER 4:.....	26
Part 1 - EPR Study of Vein Quartz.....	27
Part 2 - PIXE analysis of Vein Quartz.....	40
Part 3 - AAS analysis of Vein Quartz.....	46

Part 4 - Discussion of EPR Spectra and correlation with PIXE and AAS analyses.....	48
CHAPTER 5: MINERALIZATION AND ALTERATION...	58
CHAPTER 6:	
Part 1 - Sulfur Isotope Study.....	64
Part 2 - Arsenopyrite Geothermometry.....	69
Part 3 - Fluid Inclusion Study.....	74
Part 4 - Gold in arsenopyrite.....	88
CHAPTER 7: GENETIC MODEL AND EXPLORATION STRATEGY:.....	93
CHAPTER 8: SUMMARY AND CONCLUSIONS.....	96
REFERENCES.....	98
APPENDIX 1..... Trace element analysis in quartz by A.A.S.	106
APPENDIX 2..... EPR spectra and their calibration.	109
APPENDIX 3..... EPR spectra after x-ray irradiation.	111
APPENDIX 4..... EPR spectra 15 hrs after x-ray irradiation.	112
APPENDIX 5..... Electron micro-probe analysis of two types of carbonates in sediments at Fosterville.	113
APPENDIX 6..... Rock catalogue.	114

LIST OF FIGURES

<u>FIGURE</u>	<u>PAGE</u>
1.1	Location map of Fosterville goldfield in Victoria.....2
1.2	Location of Fosterville and Central Ellesmere deposits in the Fosterville goldfield.....3
2.1	Bendigo Province, bounded by Avoca Fault and Heathcote Axis..9
2.2	Generalized geology of the Fosterville goldfield.....11
2.3	Location of the Bendigo and Fosterville goldfields.....12
2.4	Typical section through the Central Ellesmere deposit.....14
3.1	Location of drill holes at the Fosterville deposit.....17
3.2	Location of drill holes at the Central Ellesmere deposit.....18
3.3	Infrared spectrum of a quartz vein sample.....25
4.1	Idealized diagram showing the main paramagnetic centres of some typical New Zealand and Tasmanian quartzes (i.e. VM 228 from Ahamuta). See text for discussion of individual centres. Mn ²⁺ standard inserted.....29
4.2	Classification of paramagnetic centres in glass.....32
4.3	Measurement of the intensity of a hypothetical EPR spectrum for a paramagnetic centre.....36
4.4	First derivative EPR powder spectrum of vein quartz, Fosterville, showing main paramagnetic centres under standard instrument conditions and sample weight. Compare with figure 4.1.....36
4.5a	Correlation between Al and Li, H in selected clear rock crystal. Dark circles - Li; Green circles - H.....38
4.5b	Correlation between Al and the sum of Li, H and Na in selected clear rock crystals.....38

4.6	Typical PIXE spectrum for quartz. The dotted line represents the experimental data whereas the solid line is the fit to the data generated by the PIXAN program.....	43
4.7	Scatter plot of the intensity of the paramagnetism of the vein quartz (measured as the height of the first derivative EPR peak at g 2.0025-2.0030) against Au content of the host rocks.....	51
4.8	Scatter plots of the paramagnetism against: (a) Rb, (b) Mg, (c) Al, (d) K, (e) Na and (f) Li for the Fosterville quartz. Also, scatter plots of Al against: (g) K and (h) Rb and K against: (i) Mg and (j) Rb.....	53
4.9	Scatter plot of the paramagnetism against Ge content of Fosterville quartz.....	54
4.10	Phase diagram of the system $\text{SiO}_2\text{-GeO}_2$ on dry studies and hydrothermal studies at 700 bars.....	56
5.1	Idealized section through typical mineralization style at Fosterville.....	58
5.2	Ternary diagram showing two types of carbonate at Fosterville....	63
6.1	Sulfur Isotope Distribution.....	66
6.2	Histogram showing S isotopes (in per mil CDT) in the Ballarat Trough deposits.....	67
6.3	Pseudobinary T-X section along the pyrite-loellingite join showing arsenopyrite composition as a function of temperature and bulk composition. All assemblages include vapour.....	69
6.4	Activity of S_2 -temperature projection of the stability field of arsenopyrite, contoured in atomic % arsenic. All assemblages include vapour.....	70
6.5	Distribution of Fluid Inclusion Homogenization Temperatures, (T_h (L-V)-L) in $^{\circ}\text{C}$	78
6.6	Distribution of Fluid Inclusion Salinity composition	

	(NaCl eq. wt. %)	79
6.7	The quantitative CO ₂ -H ₂ O clathrate equilibria	80
6.8	Solubility of CO ₂ in H ₂ O as a function of pressure at 25 °C	80
6.9	Distribution of Fluid Inclusion first melting temperature, (1st Tm) in °C	81
6.10	Graphs for calculating the mole composition of CO ₂ -CH ₄ mixtures using the final melting of CO ₂ (1st Tm) and the temperature of homogenization (Th (L-V)-L)	82
6.11	P-T diagram of bulk fluid isochores for mixed H ₂ O-CO ₂ fluid inclusions. The values on the curves are volume % CO ₂ for a CO ₂ phase density of 0.6 gm/cc	83
6.12	The four divisions of metamorphic grade representing maximum possible conditions	84
6.13	Temperature-density diagram for the system H ₂ O. The homogenization behaviour of four inclusions, all trapped at 540 °C (but at different pressures) is indicated. Liquid-black; gas-colourless; fluid-grey	85
6.14	P-T-density relationships of water, 5 wt. % and 10 wt. % NaCl solution	86
6.15	Scatter plot of As against Au in DDH 13	90
6.16	Line plot of Au and As with depth in FO 10	91
1	Simultaneous Recording	109

LIST OF TABLES

<u>TABLE</u>	<u>PAGE</u>
1.1 Characteristics of Victorian gold sub-provinces.....	6
3.1 Electron microprobe analysis of sericite from the Fosterville goldfield.....	20
3.2 Chemical and Trace element composition of dyke from Fosterville.....	22
4.1 Intensity of the EPR signal and chemical composition via PIXE analysis of microcrystalline vein quartz, Fosterville. tr - means present (because of better fit between calculated and observed spectra), but peak area is less than minimum detection limit. Au - by fire assay on 1m core length.....	42
4.2 Intensity of the EPR signal and chemical composition via AAS analysis of microcrystalline vein quartz, Fosterville. Au - by fire assay.....	45
4.3 Values of the correlation coefficient for different levels of significance.....	49
4.4 Spearman's rank correlation coefficients between the intensity of the EPR signal, Au and trace elements analyzed by PIXE for the Fosterville quartz (51 samples).....	50
4.5 Spearman's rank correlation coefficients between the intensity of the EPR signal, Au and trace elements analyzed by AAS for the Fosterville quartz (51 samples).....	50
6.1 Sulfur Isotope Data.....	66
6.2 Average composition of 30 arsenopyrite grains obtained from 6 samples (FO 13-42.5; FO 13-48.0; FO 13-48.6; FO 13-71.4;	

FO 12-58.6; FO 12-70.0). Analysis by electron microprobe.....71

6.3 Fluid Inclusion Data.....76

6.4 Electron microprobe analysis of arsenopyrite. C-core; R-rim;
B.D.L-below detection limit.....89

LIST OF PLATESPLATESPAGE

- 1 Sample 12-41.5. Hand specimen. Fine to coarse, grey sandstone with common quartz veins. Abundant clear quartz crystals present.....19 : 1-8
- 2 Sample 12-41.5. Thin section. Quartz grains which are variably angular to sub-rounded. Groundmass is mixed quartz-muscovite-sericite. Minor microcline, albite and hornblende. Plate size = 1.31 x 2.00 mm. (XPL-crossed polarized light)
- 3 Sample 13-33.4. Hand specimen. Massive, coarse, brown sandstone with ferruginous zones which represents oxidized pyrite.
- 4 Sample 11-52.9. Thin section. Ferruginized and oxidized sandstone. Plate size = 0.65 x 0.98 mm. (PPL - plane polarized light).
- 5 Sample 13-74.5. Hand specimen. Weakly bedded, fine, grey siltstone with visible pyrite.
- 6 Sample 13-74.5. Thin section. Fine grained, thinly bedded, quartz siltstone with lenses and blotches of carbonate. Pyrite grain in carbonate.
Plate size = 1.31 x 2.00 mm. (XPL).
- 7 Sample 12-53.0. Hand specimen. Grey-green, well bedded shale. Pits present where pyrite has been removed.

- 8 Sample 12-53.0. Thin section. Thin layers consist of schistose fine muscovite and sericite with very small quartz grains. Irregular patches are oxidized pyrite. Plate size = 1.31 x 2.00 mm. (XPL).
- 9 Sample 13-41.0. Thin section. Laths of plagioclase partially altered by siderite and calcite. Some box-work carbonate veins present. Plate size = 1.31 x 2.00 mm. (XPL).....23 : 9-16
- 10 Sample 13-48.0. Thin section. Bands of carbonate are dissected and sheared forming en-echelon structures through the sediments. Plate size = 1.31 x 2.00 mm. (PPL).
- 11 Sample 13-71.4. Thin section. Quartz vein forming along the path that the carbonate veins formed. Plate size = 1.31 x 2.00 mm. (XPL).
- 12 Sample 13-42.5. Thin section. Sulfides contained in the quartz vein. Plate size = 0.65 x 0.98 mm. (XPL).
- 13 Sample 12-70.0. Thin section. Quartz vein showing a strained texture (fibre veins). Plate size = 1.31 x 2.00 mm. (XPL).
- 14 Sample FO 41-2867. Thin section. Sericite inclusions in vein quartz. Plate size = 0.65 x 0.98 mm. (XPL).
- 15 Sample 13-42.5. Thin section. Pyrite and arsenopyrite randomly distributed through the silty beds. Plate size = 1.31 x 2.00 mm. (PPL).
- 16 Sample 13-52.0. Thin section. Pyrite common through bands of carbonate. Plate size = 1.31 x 2.00 mm. (PPL).
- 17 Sample 12-58.6. Thin section. Growth of pressure shadow around pyrite grain. Plate size = 1.31 x 2.00 mm. (XPL).....61 : 17-21

- 18 Sample 10-45.0. Thin section. Limonite lined voids in sandstone indicating that pyrite has leached out of oxidized zone. Plate size = 1.31 x 2.00 mm. (PPL).
- 19 Sample 13-48.6. Thin section. The alteration comprises predominantly sericite-pyrite-arsenopyrite-carbonate. Plate size = 1.31 x 2.00 mm. (XPL).
- 20 Sample 11-52.9. Thin section. Two types of fluid inclusions studied:
Type 1 - larger, 2-phase, liquid and vapour, and
Type 2 - smaller, 3-phase, CO₂- liquid bearing inclusions.
Plate size = 0.16 x 0.24 mm.
- 21 Sample 12-54.5. Thin section. Star-shaped (rosette) cluster of arsenopyrite in sediments. Plate size = 0.65 x 0.98 mm.
(Reflected light).

CHAPTER 1 - INTRODUCTION

LOCATION, ACCESS AND GEOMORPHOLOGY

The Fosterville Goldfield is located approximately 20 km by road ENE of Bendigo in central Victoria (Figure 1.1) and is situated within the Fosterville Shear Zone. A chain of old open cut mine workings extends over a strike length of some 8 km, most of which occur on subdued low ridges and hills in State forest, Crown land, farming and rural residential zoned areas (McConachy, 1988). The old pits and open cuts can be traced within Lancefieldian (lowermost Ordovician) sediments and are entirely in the oxidized zone with only minor quartz veining, in contrast to the majority of sediment-hosted gold deposits in Central Victoria which are associated with quartz reefs.

THIS STUDY

The research was undertaken to study the mineralogy and geochemistry of the Fosterville Goldfield. The principal areas studied were restricted to the Fosterville and Central Ellesmere fields (Figure 1.2). The first impression obtained during the fieldwork was that disseminated auriferous arsenopyrite-pyrite mineralization exists up to some metres away from the axes of folds in the Fosterville Shear Zone. On visual inspection, in particular of the drill cores and Central Ellesmere open pit, it appears that the rocks are more mineralized if they are more fractured. The mineralization however is, as stated, disseminated throughout the rocks, rather than being confined to fault planes and joints.

Approximately 75 Reverse Circulation percussion hole samples and another 25 diamond drill hole samples from the Fosterville and Central Ellesmere zones, provided by Bendigo Gold Limited, were studied during the course of this project.

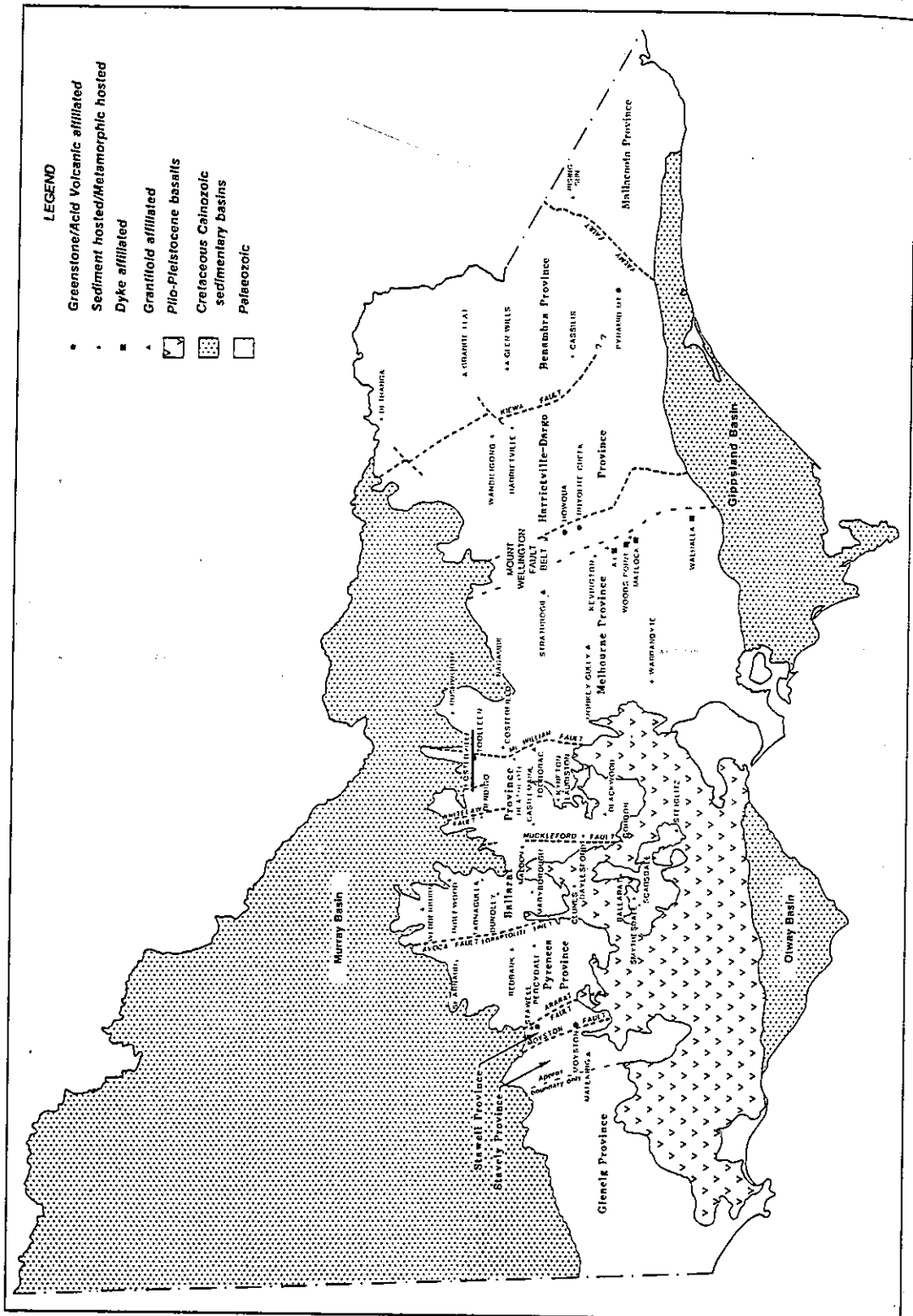


FIGURE 1.1 Location map of Fosterville goldfield in Victoria (After Douglas & Ferguson, 1988).

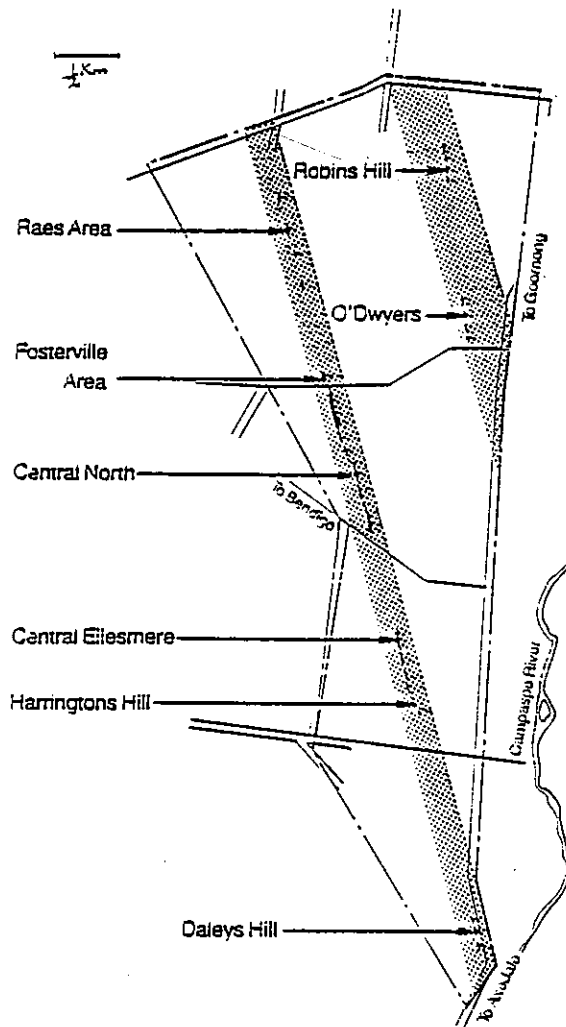


FIGURE 1.2 Location of Fosterville and Central Ellesmere deposits in the Fosterville goldfield (From Bendigo Gold Limited).

AIMS:

The aims of this project were to study:

- (1) the local geology of the prospect,
- (2) the mineralogy and petrology of the oxidized and primary host rock zones to the Fosterville Gold Deposit, and vein textures associated with gold mineralization,

- (3) the relationship between the paramagnetism of the small quartz veins present to gold grade and concentrations of other elements in the quartz,
- (4) the mineralogy of primary sulfide ores and alteration,
- (5) the geochemistry of the mineralization, and to
- (6) develop a genetic model for the Fosterville Gold Deposit.

To carry out this study, the following analytical systems and equipment were used: polished thin sections, electron microprobe analysis, electron spin resonance spectrometry, atomic absorption spectrometry, proton induced x-ray emission analysis, x-ray fluorescence spectrometry, infrared spectroscopy, carbon/ oxygen/ sulfur isotope extraction lines and VG micromass 602D stable isotope mass spectrometer and a fluid inclusion thermometric stage.

PREVIOUS WORK

1884 - 1910: The Fosterville Goldfield yielded a recorded 1480 kg of Au, at an average grade of 3.2 g/t from the oxidized zone.

1910 - 1952: Small scale operators worked on the goldfield and later abandoned it, due to a gradual decline in production.

1973 -1983: Recent exploration for gold in the Fosterville area was carried out by Lone Star Exploration N.L., Noranda Australia Ltd., J.B.Griffith and P.M.Rush in joint venture with Pennzoil of Australia Limited, Newmont Pty. Ltd., and Apollo International Minerals N.L. These companies abandoned the goldfield, as the tonnage potential determined did not meet with their high tonnage extraction criteria.

1982 - 1984: McNiece Wright Mining, now Bendigo Gold Limited (BGL), recovered approximately 108 kg of gold, at a recovered grade of 1.0 g/t, by cyanide treatment of the battery tailings.

1989: Brunswick N.L., part of the Normandy-Poseidon Group, took over BGL in July.

CURRENT EXPLORATION

BGL holds title to approximately 130 km² of tenements covering a major proportion of the Fosterville Goldfield. The company has continued a successful exploration and development programme:

(1) An intensive drilling programme has now defined seven significant deposits, combining a measured and indicated *in situ* geological resource of 3.6 million tonnes at an average grade of 2.3 g/t Au. Six deposits, namely Raes Area, Fosterville, Central North, Central Ellesmere, Harringtons Hill and Daleys Hill are located along the Fosterville Fault Zone which is a major steeply dipping mineralized structure that widens into a series of splay faults as it crosses fold-hinges or runs along the anticlinal axes. The seventh deposit is located at Robins Hill, which occurs within a similar structure to the Fosterville Fault Zone, known as O'Dwyers Fault Zone, located 1.5 km to the east (Figure 1.2). Limited testing of sulfides suggests 70-80% of gold is associated with arsenopyrite while the remaining 20-30% is associated with pyrite.

(2) Old pits have been geologically mapped.

(3) An exploration shaft was sunk to 28m at Central Ellesmere to collect bulk sample for metallurgical tests.

(4) Channel sampling of pit floors at Central Ellesmere has been completed.

(5) A bedrock geochemical program was undertaken at Robins Hill with excavation, mapping and sampling of two costeans.

BGL is currently evaluating near-surface oxidized gold mineralization and work on the Development Lease (DL 57) has advanced to the stage whereby a Mining Lease Application (MLA 1868) has been made. A final feasibility study on an open cut/ore processing plant has been commissioned.

HISTORY AND PRODUCTION OF THE BENDIGO GOLDFIELD

Victoria is one of the major gold provinces of the world, with the production of 2450 tonne of gold up to 1988 (Ramsay & Willman, 1988). Gold was discovered in Victoria during the great gold rushes in 1851 at Clunes, 120 km north-west of Melbourne and at Warrandyte, 24 km east of Melbourne. Productive shallow placer deposits were discovered at Bendigo during late 1851; followed rapidly by the discovery of gold-bearing quartz veins (reefs) beneath the alluvial deposits. Working of the reefs commenced in 1854 at Bendigo (Bowen & Whiting, 1976).

REGIONAL MINERALIZATION STYLES

Bowen & Whiting (1976) grouped the Victorian goldfields into a number of sub-provinces (Table 1.1) which suggest several different periods of mineralization.

Sub-province	Mineralization is quartz with	Host rocks	Probable age of mineralization	K-Ar age of granites
Stawell	gold, gold-sulphides	Camb.(?)-L. Ordo. sediments	Ordo.	L. Dev.
Bendigo-Ballarat	gold	L. Ordo. sediments	late Ordo.	U. Dev.
Warrandyte	gold-stibnite	sil.-L. Dev. sediments	late M.-early U. Dev.	U. Dev.
Walhalla-Wood's Point	gold	late M. Dev. dykes	late M.-early U. Dev.	nil
Harrierville	gold	U. Ordo. sediments	U. Ordo. or younger	U. Dev.
Glen Wills	gold-sulphides	U. Ordo. meta.	U. Ordo.	L. Dev.
Bendoc	gold-quartz	U. Ordo. sediments	U. Ordo. or younger	Sil.-Dev.

TABLE 1.1 Characteristics of Victorian gold sub-provinces (After Bowen & Whiting, 1976).

The Bendigo and Fosterville Goldfields are situated in the Bendigo-Ballarat sub-province. The Bendigo goldfield is the second largest goldfield in Australia and has a recorded production of approximately 700 tonne of reef gold. The gold occurs in saddle reefs at the crests of anticlines in tightly folded Lower Ordovician sequences of slate, sandstone and greywackes in the Bendigo goldfield. The repetitive nature, and degree of predictability of saddle reefs, contributed vastly to the success of the Bendigo field; as the economic mineralization occurs in "shoots" and "legs" of these reefs. "Legs" are reefs occurring in the bedding plane below the saddle. A great deal of gold was also derived from fault-related reefs and spur (irregular veins of quartz that do not conform regularly to the bedding planes or the fault planes) systems (Ramsay & Willman, 1988). Gold is unevenly distributed in these reefs but is often concentrated where they truncate certain broad favourable beds called "indicators" and also where reefs are more massive.

The majority of the gold ores are free milling and contain minor amounts of sulfides, of which pyrite, arsenopyrite and pyrrhotite are the most common. Galena, sphalerite and chalcopyrite are also present on most of the fields in minor amounts. Quartz is the main gangue mineral and may be associated with ankerite, chlorite, calcite and albite (Chace, 1949).

The major quartz-Au deposits in the Bendigo-Ballarat sub-province formed when the host Ordovician turbidites were folded, but the age of this event is not known for certain. It is certainly no younger than the mid-Devonian Tabberabberan Orogeny and cannot be older than the late Ordovician Benambran Orogeny (Ramsay & Vandenberg, 1986).

There have been several theories proposed for the origin of the gold in the Bendigo-Ballarat sub-province. These are:

- (1) remobilization of gold from the slates during cleavage formation (Cox et al., 1983),

- (2) derivation of gold from interflow sediments in the underlying Cambrian "greenstones" (Sandiford & Keays, 1986), and
- (3) gold related to granites (Clappison, 1965).

Another style of mineralization less frequently encountered, occurs at Fosterville which is sediment hosted and fault controlled. The gold is not free milling in the primary zone at Fosterville. The age of the mineralization is somewhere between late Ordovician and mid-Devonian (ie. 440-370 Ma), as mentioned above.

CHAPTER 2 - REGIONAL AND LOCAL GEOLOGY

PART 1: REGIONAL GEOLOGY AND STRUCTURE

The Palaeozoic Lachlan Fold Belt system, which encompasses much of southeastern Australia dominates the geology of Victoria. The system comprises the Cambrian to Lower Carboniferous sequences which were deformed during the mid-Palaeozoic (Cas, 1983). Sedimentation in Victoria during the early to middle Palaeozoic occurred in three major basins; the Omeo Trough, Melbourne Trough and Ballarat Trough.

The Ballarat Trough contains thick sequences of Cambro-Ordovician marine sediments. The Bendigo Province is situated in the Ballarat Trough which is bounded by the Avoca Fault and the Heathcote Greenstone Belt (Figure 2.1), and contains flyschoid sediments such as quartz-rich greywacke-shale sequence of Ordovician age.

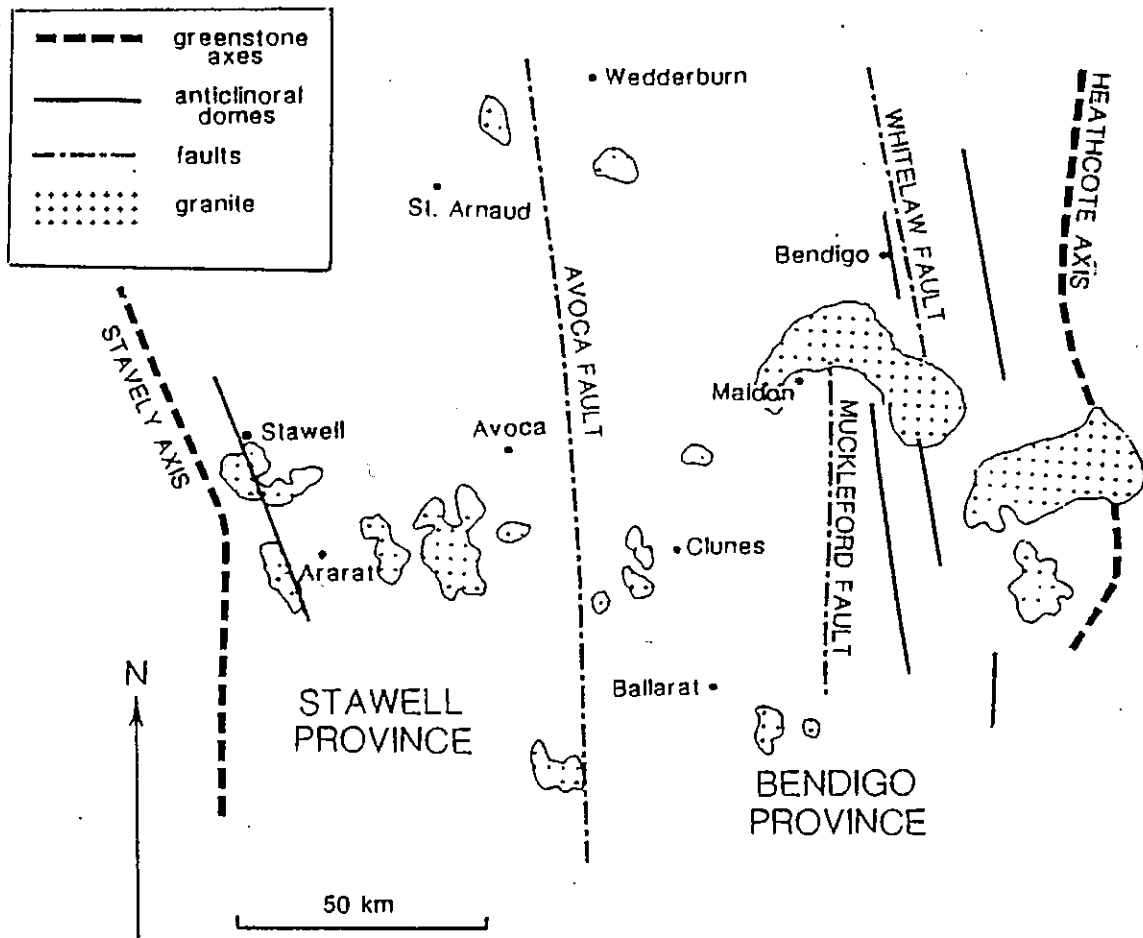


FIGURE 2.1 Bendigo Province, bounded by Avoca Fault and Heathcote Axis (After Sandiford & Keays, 1986).

These rocks are grouped in the Castlemaine Supergroup, which comprises the entire Lower to Middle Ordovician sequence of the Bendigo Province from the Lancefieldian to upper Darriwillian. The Castlemaine Supergroup is largely undifferentiated. The Lancefieldian appears to contain a greater proportion of sandstone compared with the other stages, and has a higher lithic component. In the other stages, interbedded sandstone-rich, and mudstone-rich intervals are dispersed uniformly throughout the succession (Cas & Vandenberg, 1988). Volcanism was completely absent during this period (Spencer-Jones & Vandenberg, 1976). The Ordovician flysch sequence was metamorphosed during the Devonian. The mineralogy of the metasediments indicates a low temperature-low pressure metamorphic regime typical of lower greenschist facies (Sandiford & Keays, 1986).

The principal structures in the Castlemaine Supergroup rocks are double plunging, upright folds which define a dome and basin pattern with axes that have a shallow westerly dip on a strike of approximately 345° . Several orders of folds define regional anticlines and synclines, with wavelengths in the order of 10 to 15 km, whereas higher order folds have wavelengths from 100 to 300 m (Gray, 1988).

The Muckleford, Whitelaw and Avoca faults are near vertical, north-trending faults and define the largest scale fault structures in the Ballarat Trough which expose successively older sequences to the west (Figure 2.1). These faults have throws in the order of 1000-1500 m and do not contain auriferous reefs. This distinguishes them and from the smaller strike faults which are parallel to bedding and approximately parallel to the axial planes of the folds. The smaller strike faults have localized the gold-bearing quartz bodies and are abundant in well-defined fracture systems, particularly on the anticlines (Chace, 1949).

PART 2 : LOCAL GEOLOGY AND STRUCTURE

The Whitelaw Fault divides the Bendigo Province in two; to the west is the Bendigo Goldfield, to the east, the poorly auriferous Strathfieldsaye Synclinorium. The Strathfieldsaye Synclinorium contains the youngest Ordovician sediments of the Bendigo Province, outcropping along the eastern side of the Whitelaw Fault and the oldest sequence outcrops to the west of the Campaspe river. The youngest sequence is subdivided into two stages (Yapeenian and Darriwillan) on the basis of the abundant diplograptid fauna. The Strathfieldsaye Synclinorium shows a normal succession of zones eastwards from the Whitelaw Fault, from Darriwillan at the fault to Lancefieldian towards the Campaspe river. Sugarloaf Range arenites which form a prominent strike ridge at Axedale are characteristic of the Lancefieldian (Figure 2.2).

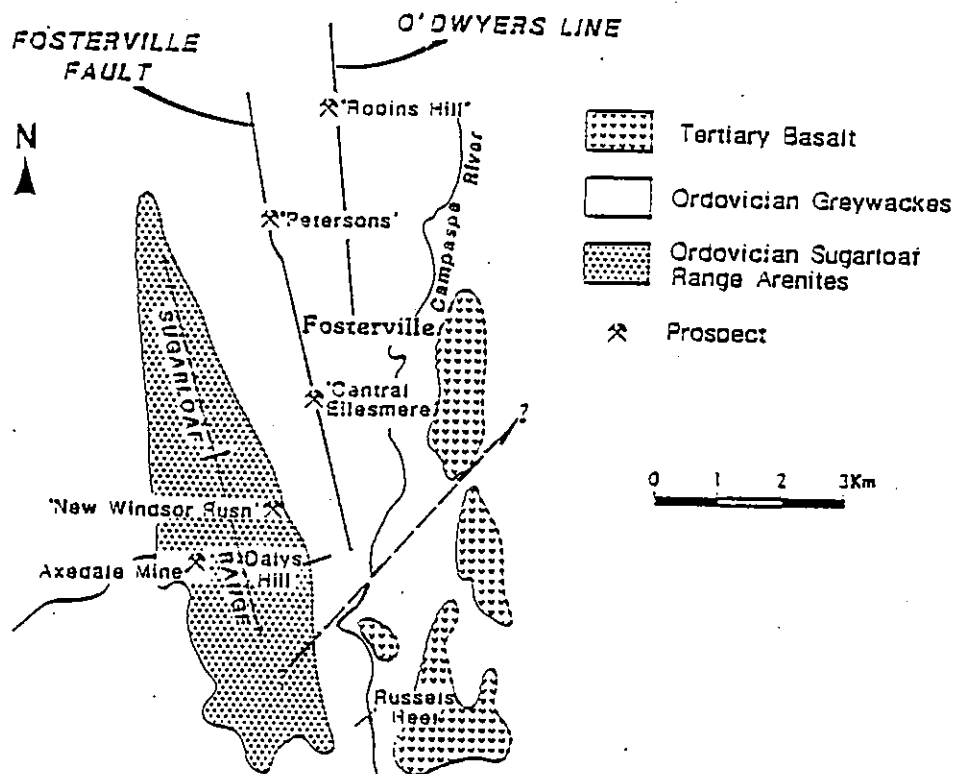


FIGURE 2.2 Generalized geology of the Fosterville goldfield (After McConachy, 1988).

The Campaspe Lancefieldian beds are succeeded westwards into the Strathfieldsaye Synclinorium by middle Bendigonian beds. Chewtonian beds occur in normal succession west of the Bendigonian and Castlemainian succeeds Chewtonian westwards (McAndrew & Marsden, 1973). Patchy outcrops of Tertiary basalt occur along the Campaspe river.

The Fosterville Goldfield occurs in sedimentary rocks of Lower Ordovician age (Lancefieldian) and is situated on the eastern limb of the Strathfieldsaye Synclinorium, some 22 km north-east of Bendigo (Figure 2.3).

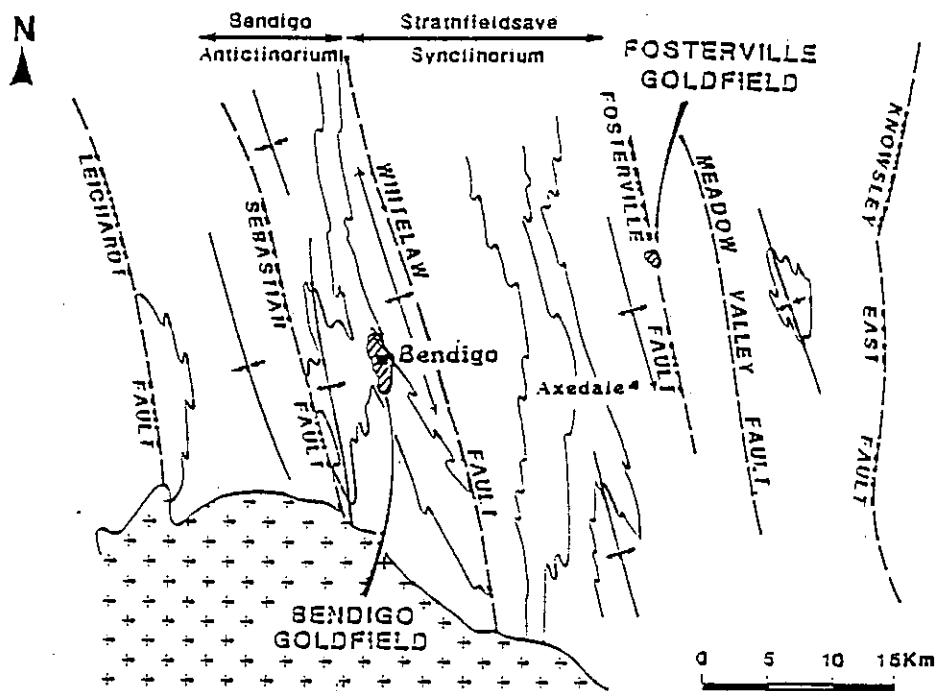


FIGURE 2.3 Location of the Bendigo and Fosterville goldfields (After McConachy, 1988).

The sedimentary sequence consists of marine greywackes, sandstones, mudstones, shales and slates which are characterized by tight to isoclinal folding with shallow plunge reversals. The Fosterville Fault, a major strike fault, is a planar mineralized structure which extends over a strike length of approximately 8km (McConachy, 1988). An adjacent strike fault, sub-parallel to and approximately 1.5km east of the Fosterville

Fault, hosts the O'Dwyers Line of mineralization (Figure 2.2). In some places fault zones are characterized by limonitic fault breccia several metres thick.

The Lower Ordovician host rocks are poorly exposed in the area other than in mine workings, mapped in detail by White (1988). The mine workings are situated entirely in the oxidized zone.

The prospect area is characterized by steep westerly dipping reverse faults uplifting west over the east. There is also evidence in the slickensides along the faults that a horizontal motion was involved late in the movement, which carried the west block to the south and the east block moved north as uplift progressed, producing an overall sinistral wrench movement accompanying the thrust. Gold mineralization along the Fosterville Fault Zone occurs in oxidized shear zones associated with oxidized sulfide (mainly pyrite) and in the primary zone with disseminated pyrite and arsenopyrite.

Central Ellesmere Deposit:

The Central Ellesmere deposit extends 650m along the Fosterville Fault zone, and contains a west dipping, thinly bedded and micaceous siltstone and pink, ferruginized and micaceous sandstone sequence to the west (hanging wall) and an east dipping, thinly bedded siltstone, silicified sandstone and shale sequence to the east (footwall). The footwall contains intense, fine, ferruginized quartz veining which is more common in the sandstone horizons. A typical cross-section from west to east of the Central Ellesmere deposit is shown in Figure 2.4. The structure represented is an antiform, but this has not been confirmed, as it was not possible to match beds across the fault, which appears to dip steeply west. There is a 15-30 cm, highly altered, kaolinised monchiquite dyke along the axis of the structure, a common feature of anticlines in the Bendigo area (White, 1988). The fault is marked by a thin black gouge and ferruginised breccia which is usually approximately 4 m wide and intensely silicified on the footwall side and contains SW striking quartz veins.

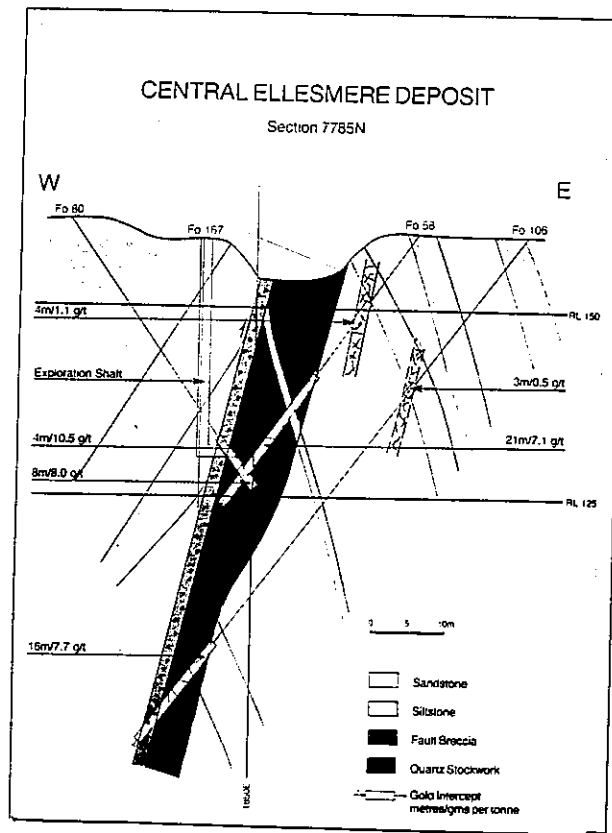


FIGURE 2.4 Typical section through the Central Ellesmere deposit (From Bendigo Gold Limited).

Three splay-faults, in a 310° - 320° direction branch off the eastern side of the main fault and dip at 60° - 70° W. The junction of each of these splays is marked by fine, ferruginized quartz stockwork and silicified sandstone showing a great deal of fracturing. The splay faults are usually accompanied by smaller parallel faults.

Fosterville Deposit:

The Fosterville field occurs 2km north of Central Ellesmere (Figure 1.2) and extends 600m along the Fosterville Fault zone. The Fosterville Deposit is one of the three splayed zones that occur in the Fosterville field. The other two splay zones are known as Hunt-Worcester and Thomas United (White, 1988).

The Fosterville splay cuts across a major east dipping sandstone unit in an anticline and becomes a normal thrust in the west dipping limb. The massive grey-cream sandstone is interbedded with siltstone and dip at 30° - 60° E on the eastern side of the fault. The western side is a highly oxidized and ferruginized, brecciated sandstone and heavily stockworked, with bedding dipping at approximately 45° to 55° E.

CHAPTER 3 - MINERALOGY, PETROLOGY AND VEIN TEXTURES AT FOSTERVILLE

In this section the sedimentology, both on hand specimen and microscopic scale (thin sections) as well as mineralogy except sulfide mineralogy are described and discussed. The quartz and carbonate vein textures associated with the faults are also described.

The samples used in this study were collected from four inclined ^{diamond} drill holes which penetrated both limbs of the anticline in the mine area. The location of the drill holes are indicated in Figures 3.1 & 3.2). Drill holes have outlined the oxidized zone from surface to 30 - 45 m depth.

The drill cores consist of an alternation of three main lithologies:

SANDSTONE

The sample taken from DDH 12 (at a depth of 41.5 m) is a typical sandstone unit from the primary zone. In hand specimen, the fine to coarse, grey sandstone contains abundant clear quartz grains (Plate 1).

In thin section, the sandstone consists essentially of quartz and a close aggregation of sericite-muscovite (Plate 2). At least 40% of the rock consists of a microscopically heterogeneous matrix of fine muscovite and sericite (including minor detrital muscovite), with abundant braided extremely fine foliae defined by oriented sericite, commonly clouded by leucoxenitic dust and probably sparse carbonaceous material. There are accessory detrital grains of albite, tourmaline, zircon and flakes of graphite and no visible chlorite. The quartz grains are angular to subrounded and have a weakly bedded distribution through the matrix. They are unsorted with a size range of very fine sand (0.1 mm) to coarse sand (0.5 mm). There are also minor small lithic fragments of carbonaceous shale. Sideritic and Fe-Mg rich carbonate is also present in

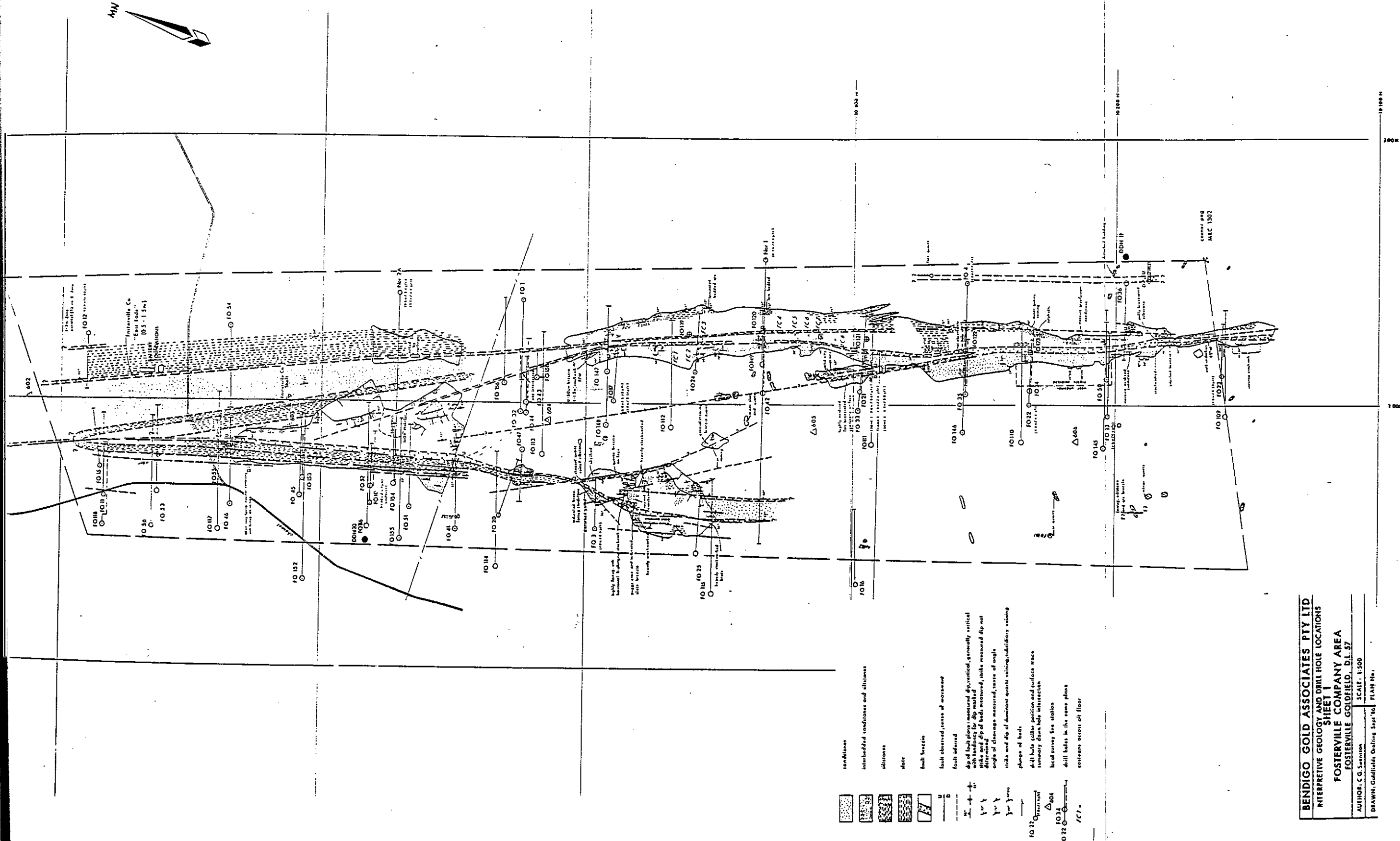


FIGURE 3.1 Location of drill holes at the Fosterville deposit. Splays marked as (From Bendigo Gold Limited).

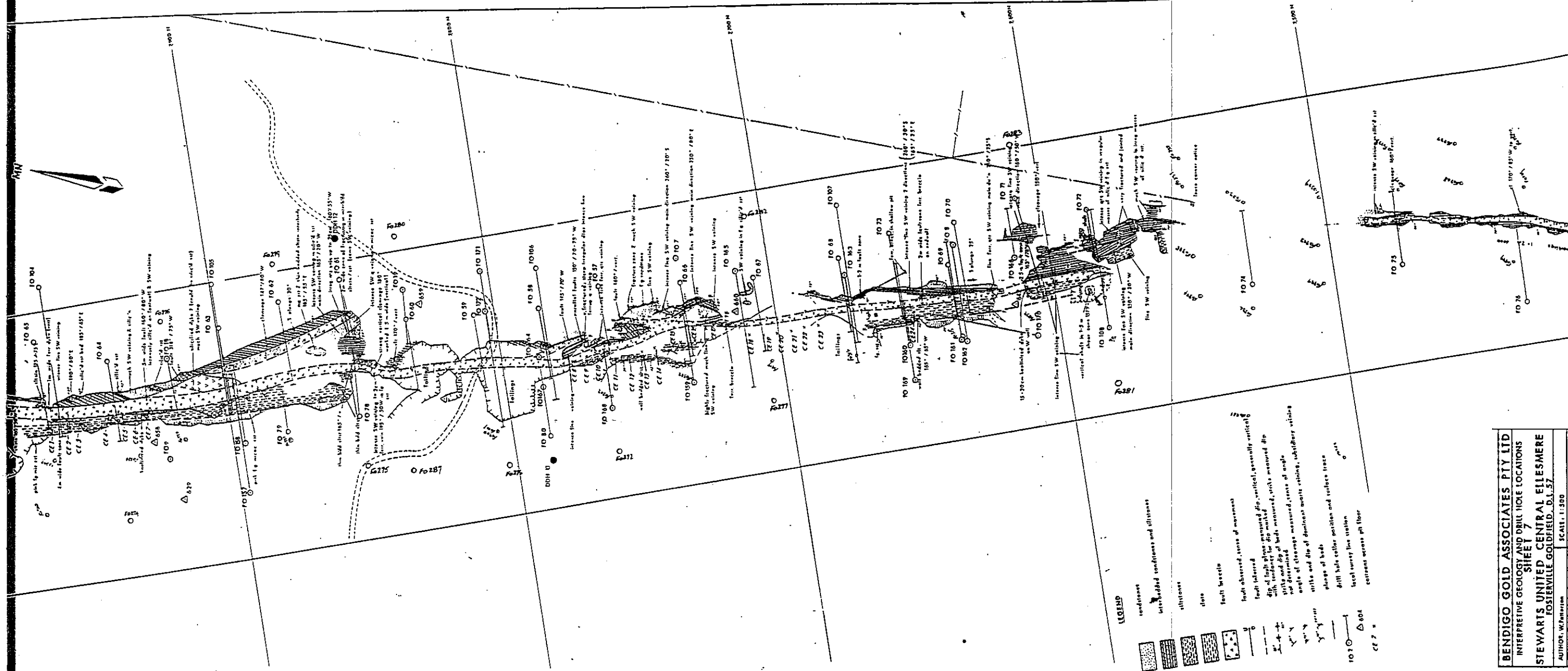


FIGURE 3.2 Location of drill holes at the Central Ellesmere deposit. Splays marked

as

(From Bendigo Gold Limited).

BENDIGO GOLD ASSOCIATES PTY LTD
 INTERPRETIVE GEOLOGY AND DRILL HOLE LOCATIONS
 SHEET 7
 STEWARTS UNITED CENTRAL ELLESMERE
 FOSTERVILLE GOLDFIELD, D.I. 57
 AUTHOR: W. PARKINSON
 SCALE: 1:500

- PLATE 1 Sample 12-41.5. Hand specimen. Fine to coarse, grey sandstone with common quartz veins. Abundant clear quartz crystals present.
- PLATE 2 Sample 12-41.5. Thin section. Quartz grains which are variably angular to sub-rounded. Groundmass is mixed quartz-muscovite-sericite. Minor microcline, albite and hornblende. Plate size = 1.31 x 2.00 mm. (XPL-crossed polarized light).
- PLATE 3 Sample 13-33.4. Hand specimen. Massive, coarse, brown sandstone with ferruginous zones which represents oxidized pyrite.
- PLATE 4 Sample 11-52.9. Thin section. Ferruginized and oxidized sandstone. Plate size = 0.65 x 0.98 mm. (PPL - plane polarized light).
- PLATE 5 Sample 13-74.5. Hand specimen. Weakly bedded, fine, grey siltstone with visible pyrite.
- PLATE 6 Sample 13-74.5. Thin section. Fine grained, thinly bedded, quartz siltstone with lenses and blotches of carbonate. Pyrite grain in carbonate. Plate size = 1.31 x 2.00 mm. (XPL).
- PLATE 7 Sample 12-53.0. Hand specimen. Grey-green, well bedded shale. Pits present where pyrite has been removed.
- PLATE 8 Sample 12-53.0. Thin section. Thin layers consist of schistose fine muscovite and sericite with very small quartz grains. Irregular patches are oxidized pyrite. Plate size = 1.31 x 2.00 mm. (XPL).

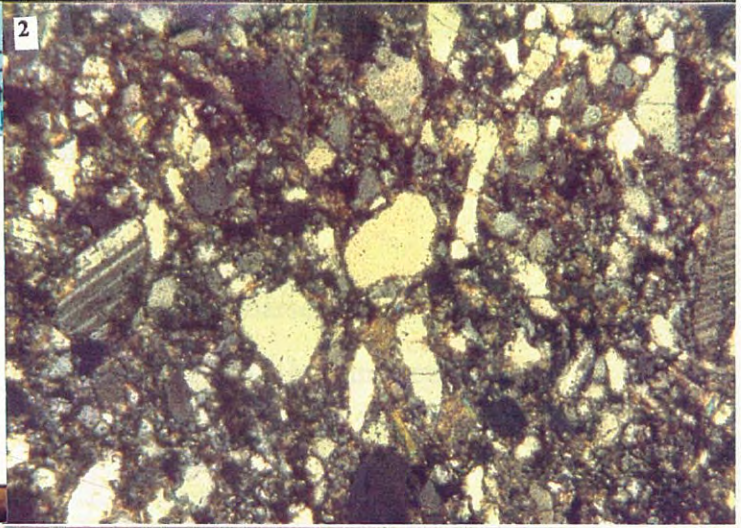
1

TYPE B 45T NEW ZEALAND



SAMPLE 12/41.5

2



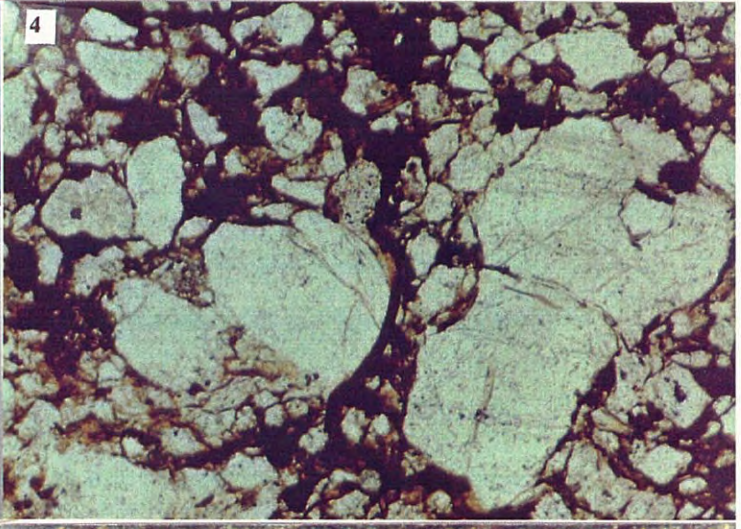
3

TYPE B 45T NEW ZEALAND



SAMPLE 13/33.4

4



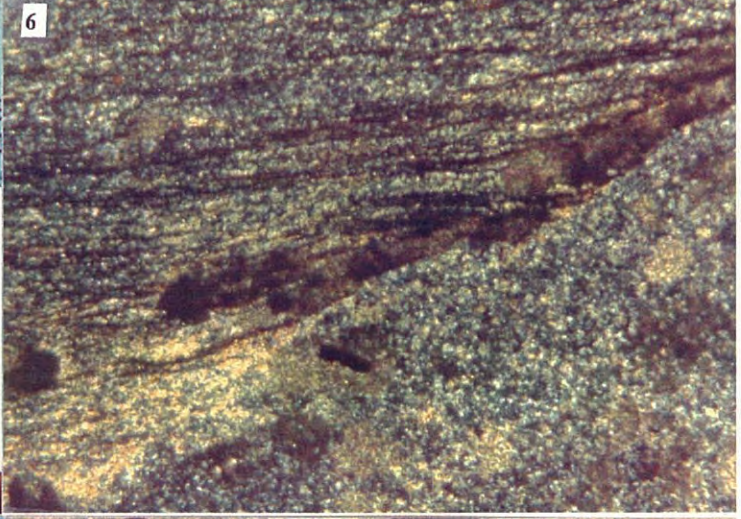
5

TYPE B 45T NEW ZEALAND



SAMPLE 13/74.5

6



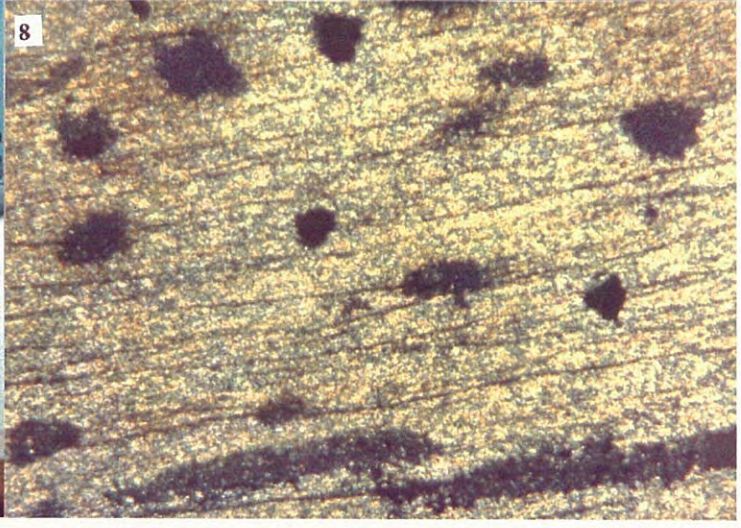
7

TYPE B 45T NEW ZEALAND

SAMPLE 12/53.0



8



some altered sandstones. The sandstone also contains scattered crystals of pyrite and arsenopyrite (discussed later).

Sandstone from the oxidized zone is massive, fine to coarse and brown with ferruginous zones which represent oxidized pyrite (Plates 3 & 4). In thin section, the sandstone is very similar to primary zone sandstone except for the presence of limonite.

Quartz veins, from 1 mm and up to 4mm wide, cut the sandstone (Plate 1).

SILTSTONE

The siltstone outcrops as a characteristically light to dark green massive unit in the primary zone (Plate 5), in which is sometimes interbedded with sandstone and very thin shale beds.

In thin section, the rock consists of schistose fine muscovite, and sericite (Table 3.1), as fine foliae (partly defined by ultrafine leucoxene), variably spaced and variably continuous through fine to coarse quartz silt (Plate 6).

		WT. %	CATIONS
SiO ₂	50.3767	Si 23.5484	6.6642
TiO ₂	0.3309	Ti 0.1994	0.0329
Al ₂ O ₃	29.9226	Al 15.8369	4.6652
MgO	2.3990	Mg 1.4469	0.4730
CaO	0.0000	Ca 0.0000	0.0000
MnO	0.0721	Mn 0.0558	0.0081
FeO	2.1950	Fe 1.7070	0.2429
Na ₂ O	0.4909	Na 0.3542	0.1259
K ₂ O	9.7293	K 8.0769	1.6418
H ₂ O	4.4083		
F	0.2631		
Cl	0.0000		
TOTAL	100.4520		13.8541
O = F	-0.1108		
O = Cl	0.0000		
TOTAL	100.3412		

TABLE 3.1 Electron microprobe analysis of sericite
from the Fosterville goldfield.
Cations based on 22 oxygen.
H₂O by stoichiometry

There are rare detrital heavy minerals, authigenic tourmaline, and rare graphite. Several quartz veinlets up to 2.5 mm wide are present in the siltstone beds. The siltstone contains oxidized sulfides in the oxidized zone.

SHALE

The shale unit in the primary zone outcrops as a characteristically fine-grained, thinly-bedded dark green to black shale which is fissile parallel to bedding and interbedded with siltstone and sandstone as mentioned above. Beds are usually only a few millimetres thick.

In hand specimen, the shale is finely laminated, with the lamination relatively undisturbed (Plate 7). The rock also displays a weak cleavage oblique to the lamination.

In thin section, the lenticular shale layers consist essentially of compact sericite \pm fine discrete flakes of muscovite (some detrital), and with very closely-spaced ultrafine leucoxene, along a cleavage which is oblique to the bedding. The sericite and muscovite define the cleavage in the rock (Plate 8). Quartz veins up to a few mm wide intersect the shale horizons. The shale usually contains sulfides which are oxidized in the oxidized zone.

IGNEOUS PETROLOGY

The only outcropping igneous rock in the prospect area is a dyke, intruded parallel to the strike of the folded Ordovician sediments in the axial region of the anticline at Central Ellesmere and a quartz-feldspar porphyry dyke at Robbins Hill (R. Haydon, pers. comm.). The quartz-feldspar porphyry dyke at Robbins Hill was not studied during the field work.

In hand specimen, the Central Ellesmere dyke is green-grey to black in colour and strongly weathered. In thin section, approximately 30% of the rock contains fine laths (approximately 1 mm long) of plagioclase which have been partially altered or

replaced by siderite, calcite and chlorite (Plate 9). Another 20% of the rock is siderite and calcite replacing olivine and pyroxene phenocrysts. Fine carbonate is also dispersed through the plagioclase-rich groundmass. Abundant leucocene replicas after magnetite are dispersed throughout the rock.

Whole rock and trace element geochemical analysis using XRF indicated that the dyke rock is a monchiquite-basalt (Table 3.2).

Chemical composition			Trace element composition	
OXIDE	WT%	MOLE%	ELEMENT	CONCENTRATION(ppm)
SiO ₂	34.45	41.21	Nb	149
TiO ₂	5.66	5.09	Zr	459
Al ₂ O ₃	13.47	9.50	Sr	329.8
Fe ₂ O ₃	3.28	1.48	Y	37
FeO	26.55	26.56	Rb	41.6
MnO	1.16	1.18	Ni	245.8
MgO	3.28	6.74	Cr	155.1
CaO	4.04	5.18	V	308.3
Na ₂ O	0.41	0.48		
K ₂ O	1.75	1.34		
P ₂ O ₅	2.49	1.26		

TABLE 3.2 Chemical and Trace element composition of dyke from Fosterville.

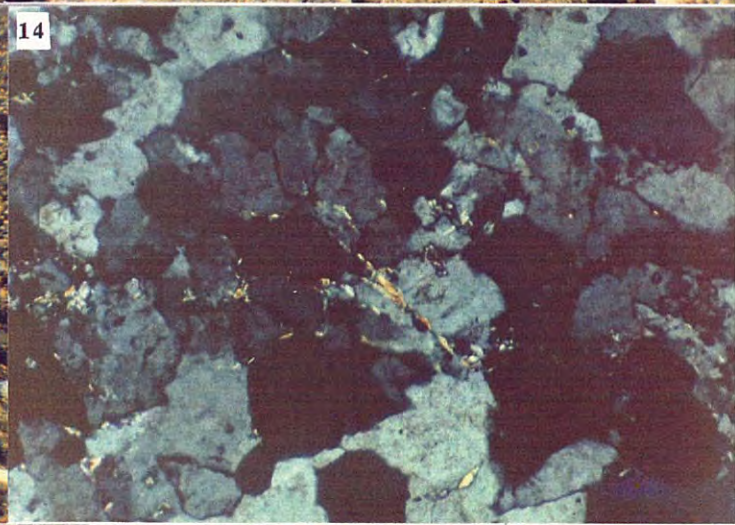
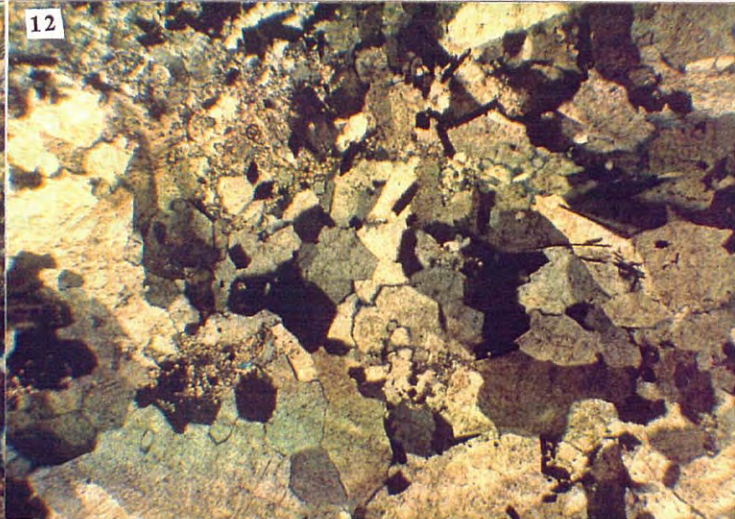
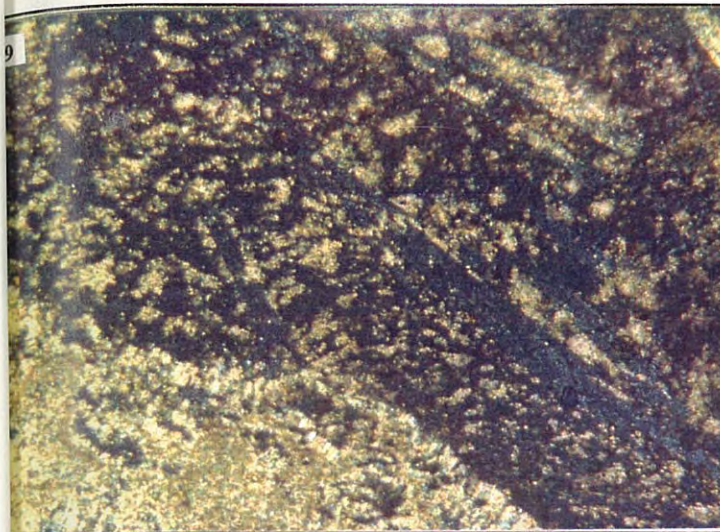
Monchiquite basalts are transitional between monchiquite and olivine basalt and contain variable amounts of plagioclase.

VEIN TEXTURES

Mineralization at Fosterville occurs in the quartz stockworks within the fault zones. The very thin siderite and Fe-Mg carbonate veins (see Appendix 5 for electron microprobe analysis) at Fosterville occurred prior to cleavage development in the rocks and are very discontinuous throughout the sediments, forming en-echelon structures (first deformational phase) (Plate 10). The majority of the sulfides are disseminated through the carbonate veins or related to it and are referred to as Phase 1.

Quartz veins which are a few millimetres wide form alongside the carbonate veins, taking the same path as that of the carbonate veins (Plate 11). These quartz veins

- PLATE 9 Sample 13-41.0. Thin section. Laths of plagioclase partially altered by siderite and calcite. Some box-work carbonate veins present.
Plate size = 1.31 x 2.00 mm. (XPL).
- PLATE 10 Sample 13-48.0. Thin section. Bands of carbonate are dissected and sheared forming en-echelon structures through the sediments.
Plate size = 1.31 x 2.00 mm. (PPL).
- PLATE 11 Sample 13-71.4. Thin section. Quartz vein forming along the path that the carbonate veins formed. Plate size = 1.31 x 2.00 mm. (XPL).
- PLATE 12 Sample 13-42.5. Thin section. Sulfides contained in the quartz vein.
Plate size = 0.65 x 0.98 mm. (XPL).
- PLATE 13 Sample 12-70.0. Thin section. Quartz vein showing a strained texture (fibre veins). Plate size = 1.31 x 2.00 mm. (XPL).
- PLATE 14 Sample FO 41-2867. Thin section. Sericite inclusions in vein quartz.
Plate size = 0.65 x 0.98 mm. (XPL).
- PLATE 15 Sample 13-42.5. Thin section. Pyrite and arsenopyrite randomly distributed through the silty beds. Plate size = 1.31 x 2.00 mm. (PPL).
- PLATE 16 Sample 13-52.0. Thin section. Pyrite common through bands of carbonate. Plate size = 1.31 x 2.00 mm. (PPL).



are very fine grained (approx. 100 μ m), interlocking sparry crystals of quartz dusted with fluid inclusions and cut the cleavage in the rocks and therefore are post-deformation (referred to as Phase 2). Sulfides are also associated with these quartz veins (Plate 12) and some veins in the oxidized zone show no evidence of existing sulfides except for a few limonite-lined voids which appear to represent original sulfides, that have been oxidized and selectively leached out. Hence, Phase 2 veins are also mineralizing veins at Fosterville. Alternatively, the sulfides could have been remobilized into the quartz veins, but there is no evidence for this.

Phase 2 (quartz) veins show a strained texture (fibre veins) (Plate 13) and undulose extinction suggesting syn-deformation (second deformation phase) that was weak, due to the fact that the quartz veins were not folded. An alternative explanation is that there was only one continuous phase of deformation, strongest during and just after carbonate veins developed and weak when the quartz veins were formed.

Phase 3 quartz veins are the latest phase and are associated with fractures (fracture-fill) in the sediments. These veins also show fibre vein texture and undulose extinction suggesting formation during the second deformational phase.

TYPE OF QUARTZ

An infra-red(IR) spectrum of a quartz vein sample (F0 3-30) was run in order to define the type of quartz present at Fosterville. By comparing the characteristic peak wavenumber from the IR spectrum (Figure 3.3) and the literature data from Gadsden, 1975 it was concluded that the sample represented α -quartz. It may be assumed that all quartz at Fosterville is α -quartz.

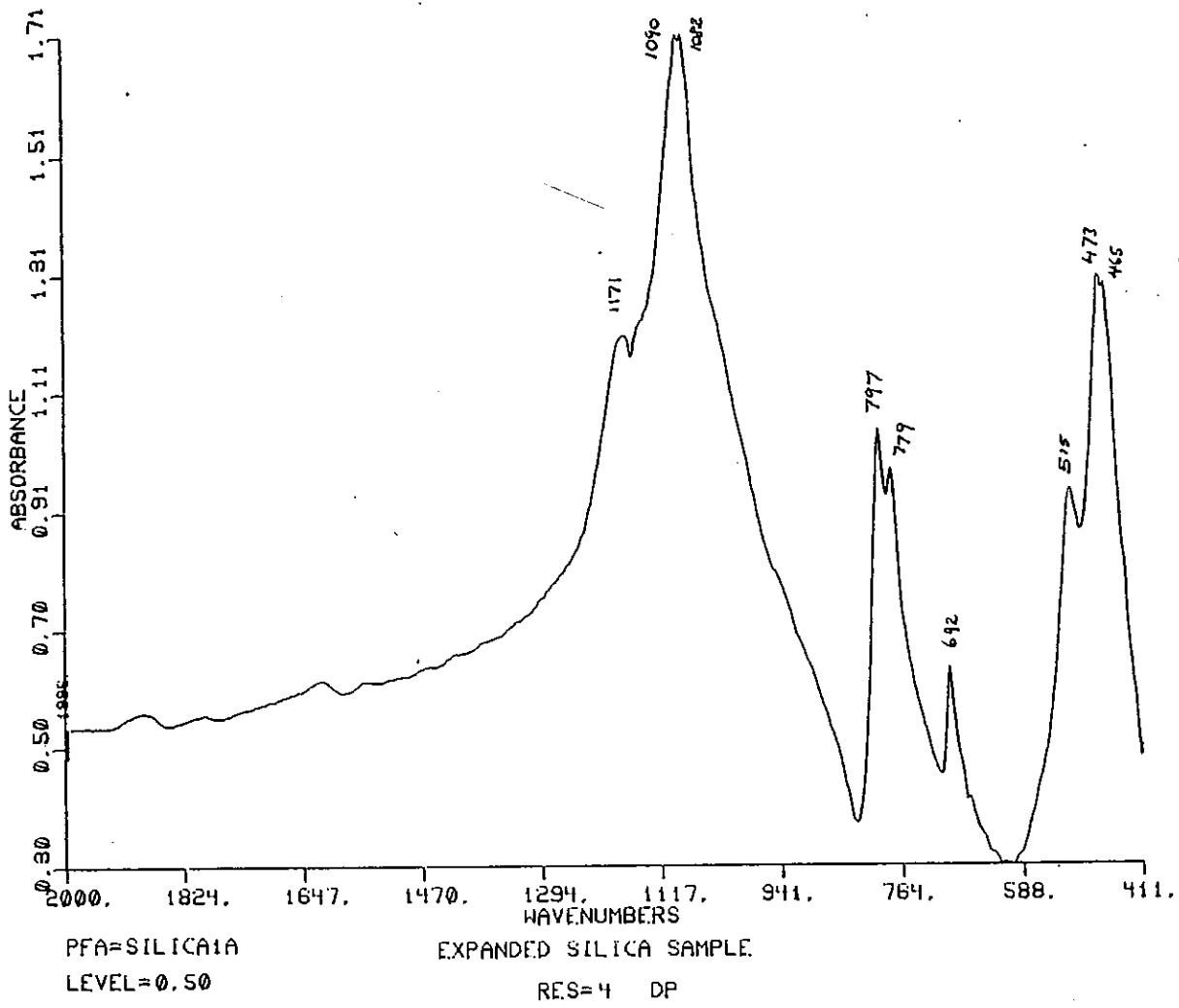


FIGURE 3.3 Infrared spectrum of a quartz vein sample..

CHAPTER 4 - GEOCHEMICAL STUDY OF VEIN QUARTZ FROM FOSTERVILLE

INTRODUCTION

This chapter investigates the relations between trace elemental composition of vein quartz and its paramagnetism. The theory of electron paramagnetic resonance (EPR) is described and discussed in Part 1.

Elemental analysis by proton induced x-ray emission (PIXE) discussed in Part 2, and atomic absorption spectroscopy (AAS) discussed in Part 3, have been used to provide a rapid and accurate and precise elemental analysis of microcrystalline vein quartz. Particular trace element concentrations were shown to correlate strongly with the intensity of EPR spectra of the same material (Part 4).

SAMPLE SELECTION AND PREPARATION FOR THIS PROJECT

51 samples were obtained from percussion drill and diamond drill cores from locations at Fosterville near Bendigo given in Figures 3.1 & 3.2. The quartz samples were selected carefully in order to avoid contamination from minerals such as carbonates (as they show marked electron paramagnetism) or sulfide and other impurities. The microcrystalline quartz samples were hand ground in an agate mortar and pestle, leached overnight in hot nitric acid, rinsed three times in distilled water and dried at 90 ° C. Several quartz chips were taken from each sample and the derived powder represents a mixture of the various types of quartz present as discussed in chapter 3. The same powders were used for all analyses.

PART 1: EPR STUDY OF VEIN QUARTZ

INTRODUCTION

Paramagnetism is caused by the alignment of elementary atomic dipoles in a magnetic field and occurs when unpaired electrons are present in the atomic orbitals. It is much weaker than the well known ferromagnetism, in which the interaction between adjacent atoms couples their magnetic moments in rigid parallelism.

For most atoms and ions the magnetic effect of the electrons, including both their spins and orbital motions, exactly cancel, so that the atom or ion is not magnetic. For atoms or ions with unpaired electrons, the magnetic effects of the electrons do not cancel. Examples are found amongst the transition elements such as Mn^{2+} and Fe^{3+} and compounds thereof.

Theoretically, quartz, neglecting surfaces, does not contain unpaired electrons and shows no paramagnetism. Real quartz, natural or cultured, contain numerous atoms out of place, broken bonds and interstitial impurities. In other cases, spin unpairing by external stimulus, for example irradiation, creates detectable paramagnetism (Weil, 1984).

Electron Paramagnetic Resonance Spectroscopy (EPR), also known as Electron Spin Resonance Spectroscopy (ESR), was first established by Zavoiskii in 1945. The method is able to detect down to 1×10^{15} electron spins and is as such one of the more sensitive analytical techniques¹. EPR is widely used to understand details of the atomic structure of material, mainly through single crystal studies, and further as an empirical tool to characterize material.

EPR of quartz as a guide to mineralization was used by Scherbakova et al. (1976) and Matyash et al. (1982). Both groups of authors determined at 77K the intensity of what

¹ Avogadro's number is 6.02×10^{23}

they called the O-(Al) centre in quartz and did correlate it, not very successfully, with the Au content of ore. Van Moort (1987) established a significant correlation between the gold content of quartz and its paramagnetism at room temperature.

A completely different aspect of the paramagnetism of quartz is its use as an age dating tool, as stressed since 1985 by Ikeya in several papers on ESR. As the response to radiation varies between samples, the individual response to the types of (natural) radiation to which the samples probably have been subjected has to be determined for each case in ESR dating studies.

Both applications of EPR can be compatible as, on one hand, lattice impurities and broken bonds will increase the inherent paramagnetism of a substance and, on the other hand, external radiation of either cosmic or terrigenous origin, will stimulate spin-unpairing or electron dislocation. This chapter will only dwell on the aspect of lattice impurities in quartz and its relation to EPR.

A general discussion on what empirically can be seen in powder spectra of quartz will be given below, prior to the discussion of the theory of paramagnetic resonance.

GENERAL CHARACTERISTICS OF QUARTZ POWDER SPECTRA

The EPR powder spectrum at room temperature of clear quartz or quartz with visible crystal faces is, with some exceptions, featureless, but for a faintly developed E'. Microcrystalline vein quartz however may show pronounced spectra. Van Moort and Barth (1987, 1989) (see Figure 4.1) found the following paramagnetic centres as most commonly occurring:

and Van Moort (1989)

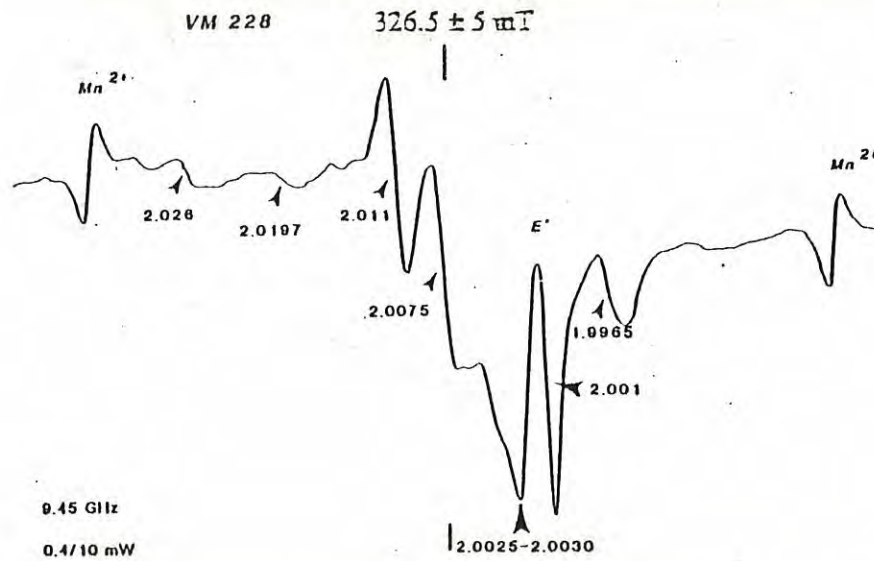


FIGURE 4.1 Idealized diagram showing the main paramagnetic centres of some typical New Zealand and Tasmanian quartzes (i.e. VM 228 from Ahamura). See text for discussion of individual centres. Mn^{2+} standard inserted (After van Moort & Barth, 1987).

E' centre

It is easily identified at $g\ 2.001^2$. It is interpreted as an electron trapped in a vacancy left by an oxygen missing from a normal bridging location (Yip & Fowler, 1975). The E' centre is strongly enhanced by irradiation, but the response varies very much from sample to sample. This diminishes its value for age dating (Ikeya, 1985; Fukuchi et al., 1986).

Hole centres

Whereas non bridging oxygen seems to be ubiquitous in silica glasses, its presence in the quartz structure is a debated issue. A detailed discussion on this subject was given by Maschmeyer and Lehmann (1983).

² The definition of the effective spectroscopic splitting factor g will be discussed below. It is used here as a parameter to characterize EPR absorption peaks.

The centre at g 2.011, which is usually not well developed in vein quartz, is considered to be an oxygen hole centre, caused by the presence of a non-bridging oxygen. The centre is prominent in quartz next to radioactive minerals (van Moort, 1989). The centre is used for age dating (Fukuchi et al., 1986).

The germanium centres

EPR studies on Ge ions substituted at Si sites in quartz were carried out on synthetic quartz by Anderson and Weil (1959). Resonance lines of Ge centres are usually not seen in non activated pure quartz samples. After short x-ray irradiation $[\text{GeO}_4]^-$ at g 1.9985 becomes visible, decaying at room temperature rapidly to the $[\text{GeO}_4/\text{M}^+]^0$ centre at g 1.9976 (van Moort & Barth, 1989). The centre is frequently used for age dating (e.g. Fukuchi et al., 1986).

Anderson & Weil, 1959; Leyderman et al., 1985; and van Moort & Barth, 1989 showed for single quartz crystals and quartz powders respectively that Ge centres, which are not visible at room temperature, become observable after irradiation.

Four Fosterville quartz powder samples were irradiated for 10 minutes using a Au x-ray tube at 50 kV and 50 mA. After irradiation and immediate EPR analysis at room temperature, the samples showed a pronounced EPR centre at g 1.9988 (see Appendix 3). This g value corresponds to the $[\text{GeO}_4]^-$ centre studied by van Moort & Barth, 1989 for quartz powders. The samples with higher Ge content showed the stronger signals. At room temperature the centre decays within 15-20 hrs (see Appendix 4).

Fe³⁺ centre

The Fe³⁺ in α - quartz has received considerable attention because of the presence of both substitutional $[\text{FeO}_4]^-$ and interstitial ion (Weil, 1984). In practice, substitutional iron shows up in very iron rich quartz powder spectra at $g \sim 3.8$.

Mn²⁺ centre

The characteristic sextet for Mn²⁺ ions can be observed in many impure quartzes (Ikeya et al., 1986; van Moort, 1987), chert (Robins et al., 1981), and it is also present in perfectly clear euhedral quartz from Rosebery. No detailed study of this centre is available in the EPR literature. The centre is absent in the Fosterville spectra as its quartz contains little manganese.

Other centres

Other centres of unknown origin at g 2.4, 2.26, 2.026, 2.075, 2.020, 2.007, 2.005 and 1.995 may be observed in many vein quartz samples.

The centre at g 2.0025 - 2.0030

McMorris (1970) was the first to observe a pronounced EPR centre at g~ 2 for " a dozen extracts of igneous, sedimentary and metamorphic quartz, most of several pegmatitic quartzes and one alpha active obsidian". He attributed the signal to a radiation damage, without substantiation. The same centre can also be observed in some silica glasses (Schnadt & Rauber, 1971) and flint (Garrison et al., 1981). After irradiation and immediate EPR analysis at < 100K, the signal frequently shows hyperfine splitting due to the presence of aluminium. This observation indicates that there is a relation between the signal and the presence of aluminium in the sample.

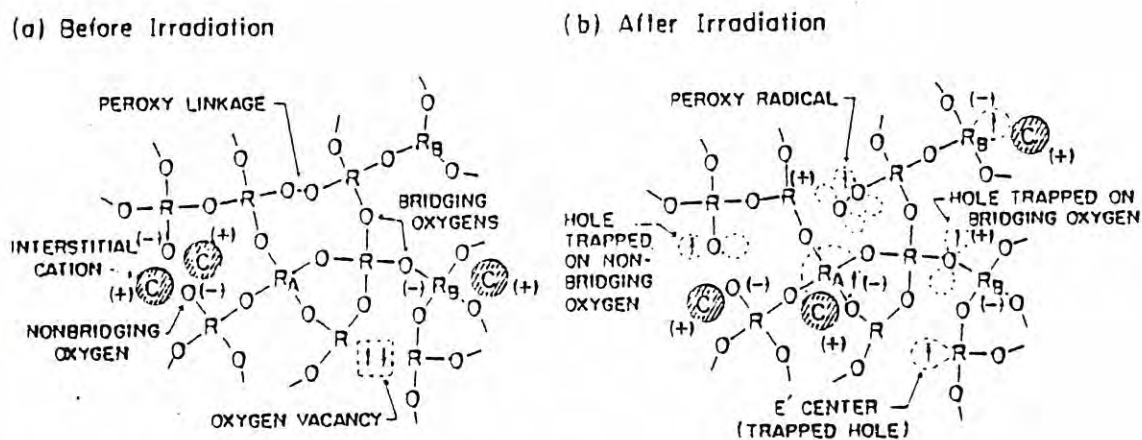
Presumably the centre represents what Scherbakova et al., (1976) and Matyash et al., (1982) observed in vein quartz and what they called the Al-O centre which, they claim, can only be observed at cryogenic temperatures. Confusion reigns as to the characteristics of this centre as for one and the same quartz from a welded tuff, Shimakowa et al., (1984) report that it is visible at room temperature and cannot be enhanced by x-rays, Imai et al., (1985) report that it is visible at 77K only and can be enhanced by x-rays and Shimakowa and Imai (1985) report that there are two centres,

one superimposed on the other. They use the (combined) centre for age dating as did Garrisson et al., (1981) and Odom and Rink (1989).

Study of glasses led Friebele and Griscom (1979) and Griscom (1980) to the belief that there is a double oxygen link in the silica lattice, which they called peroxy centre or peroxy radical centre. This supposed centre occurs at the same g value of 2.0025 - 2.0030. Their explanation is not universally accepted and it is preferable to call the centre for the time being by its g value.

The centre is well developed in the Fosterville quartz and it does not change its intensity on x-ray irradiation, as was determined on the four irradiated samples mentioned above. Its peak height is used in this study as a measure of the intensity of the EPR signal.

Figure 4.2 gives Griscom's classification of paramagnetic centres in glass, which can also be used as an illustration of what can be expected in quartz.



R, R_A, R_B = Network Formers = Si, B, P, Ge, Al, ...

C = Monovalent Network Modifying Cation = H, Li, Na, K, ...

FIGURE 4.2 Classification of paramagnetic centres in glass (After Griscom, 1980).

THEORY

EPR is a technique for detecting paramagnetism, a physical property produced by the alignment of elementary atomic dipoles in a magnetic field and occurs when unpaired (or odd) electrons are present in atomic orbitals. It is therefore applicable, as stated shortly in the introduction, to most transition-metal ions and rare-earth ions and complexes, free radicals, biradicals, triplet states and conduction electrons in metals, all of which are characterized by one or more unpaired electrons (Cubitt & Burek, 1980).

The theory of EPR is very complex, and consequently, the reader is referred to standard texts like Poole (1983) or Wertz & Bolton (1986), for better understanding of the theoretical concepts. The theory of EPR of α - quartz was reviewed by Weil (1984).

EPR spectroscopy is carried out at microwave frequencies whereby the sample is irradiated with microwave radiation of fixed energy. EPR phenomena are best explained by considering the behaviour of a free electron. According to quantum theory, the free electron spins about its axis at a fixed rate. Consequently, the negative charge carried by the electron is also spinning and constitutes a circulating electric current. The circulating current sets up a magnetic moment (β) which, if the electron is subjected to an externally applied steady magnetic field, causes the electron to experience a torque and hence tends to align the magnetic moment with the field. The ground state arises when the magnetic moment of the electron is parallel to the applied magnetic field. The excited state occurs only when the magnetic moment of the electron is antiparallel with the applied magnetic field. At a particular intensity of the magnetic field, this Zeeman splitting of energy levels occurs and leads to resonance; that is, rapid alternation between the parallel and antiparallel state of the electrons. The degree of Zeeman splitting of the energy levels at which the energy required to cause a transition of electron to the excited state is dependant on the intensity of the suitable excitation (magnetic) field. No absorption of microwave energy occurs if the magnetic field is above or below this intensity. Hence, in order to

obtain electron resonance, the energy difference, ΔE between the two spin levels is given by;

$$\Delta E = g \beta B_{res} \quad (1)$$

where B_{res} is the flux density of the magnetic field at resonance,

g is a spectroscopic splitting factor that describes the position of an absorption line, and allows the characteristics of free electrons to be determined. The electron free-spin factor in g is 2.0023.

Thus, the frequency (ν) at which EPR occurs is given by;

$$\nu = \Delta E/h = g \beta B_{res}/h \quad (2)$$

where h = Plancks constant.

Single crystal EPR spectra of artificially doped or impure quartz as measured parallel and perpendicular to the crystallographic c -axis are very detailed. As all vein quartz studied was of microcrystalline nature, only powder spectra could be made for this study. The calculated effective spectroscopic splitting factor g_{eff} , as derived from equation (2) can be used to characterize the spectrum as was done above in the discussion of the general characteristics of the quartz powder spectra.

Although it is theoretically feasible to calculate a powder spectrum from a known single crystal spectrum (Taylor et al., 1975), this has not been achieved satisfactorily in practice.

INSTRUMENTATION

A simple EPR spectrometer consists of a cavity in which a standing microwave is created by an external constant frequency generator of the klystron type or a Gunn diode. The klystron is the source of monochromatic microwave radiation and is operated within a superhigh frequency range. The monochromatic radiation passes through the

waveguide and into a resonance cavity where the sample is located. The cavity system is the heart of an EPR spectrometer and is located in the centre of a strong homogeneous magnetic field between two large electromagnets. The cavity system includes the components which hold the sample (resonant cavity) and which direct and control the microwave beam to and from the sample. Usually instruments are run in the X-band³ (~ 9 GHz frequency and medium B~ 320mT). For technical details see Wilmshurst (1967).

The intensity of the microwave coming back from the resonance cavity is by means of a circulator and a crystal detector compared with the incoming microwave intensity. When the narrow band amplifier and phase-sensitive detector are tuned to the modulation frequency, and the modulation amplitude is much less than the linewidth, then the recorded lineshape becomes the first derivative of the absorption line. The signal is measured as the first derivative of the absorption of microwave energy coming back from the sample against the intensity of the magnetic field. The peak height (Figure 4.3) is used as a measure of the paramagnetism of the sample as it is proportional to the area under the peak and the concentration of the paramagnetic species; the observed peak widths were constant for all quartz studied. The peak height of the centre at g 2.0025-2.0030 was measured on the analogue spectrum charts recorded under standard instrument conditions and standard sample weight as given in Figure 4.4.

APPLICATION OF EPR ON QUARTZ

Crystalline silicon dioxide is an ideal material to demonstrate the use of EPR at optimal potency. EPR absorption lines in α - quartz are usually narrow (~0.01 mT) because silicon and oxygen nuclei are predominantly spin-less, enabling highly accurate line position measurement.

³ Old U.S. Military Microwave Band designation.

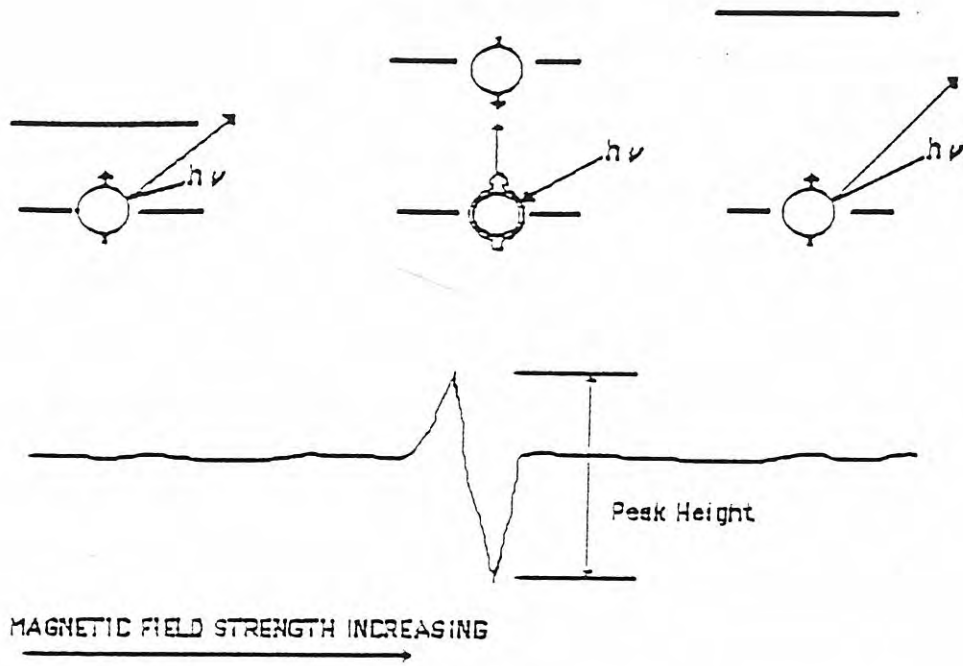


FIGURE 4.3 Measurement of the intensity of a hypothetical EPR spectrum for a paramagnetic centre (After Hamdorf, 1987).

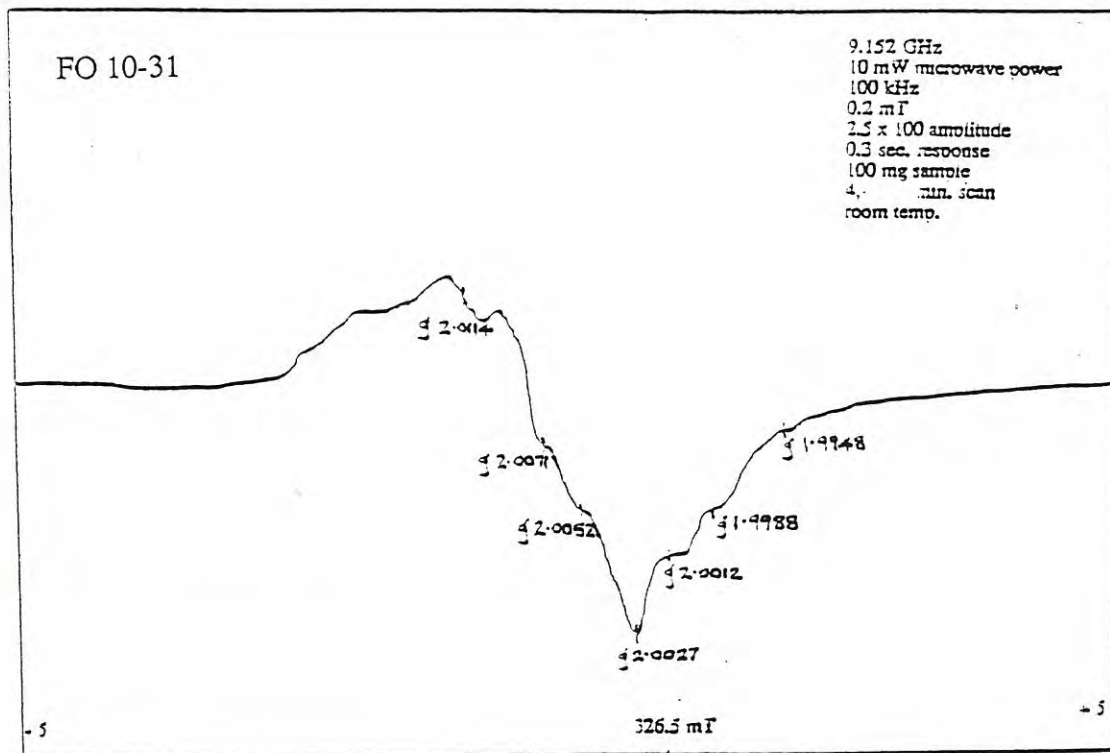


FIGURE 4.4 First derivative EPR powder spectrum of vein quartz, Fosterville, showing main paramagnetic centres under standard instrument conditions and sample weight. Compare with figure 4.1.

As stated above, perfect quartz does not contain unpaired electrons and hence shows no EPR signals. The solid state chemistry of paramagnetic defect centres in α -quartz in general was reviewed by Weil (1984). He discussed in particular the impurity-related centres; of these, $[\text{AlO}_4]^0$, $[\text{AO}_4/\text{M}^+]^0$ and $[\text{DO}_4]^0$ are the most important:

where A is the electron acceptor replacing Si (eg. Ge, Ti,),

M^+ is the compensating ion (eg. H^+ , Li^+ , Na^+ ,), and

D is the electron donor replacing Si (eg. Al, Ga,)

and the centres of atomic copper and silver, phosphorous, manganese, iron and in addition, the oxygen vacancy centre called E'. The correlation between the compensating ions Li^+ , Na^+ , H^+ and the electron donor Al is perfect for the selected clear and euhedral quartz studied by Bambauer (1961) as shown in Figure 4.5 a & b. This relation exists in a study by Poty (1969) as a trend only. The relation in the Fosterville samples, as discussed later, is obscured by the inferred presence of K, Li, Na, Mg, and Rb bearing sericite and alkaline chloride bearing fluid inclusions.

All these centres have been determined on carefully oriented single crystals at cryogenic and room temperature, with and without irradiation. All the above mentioned paramagnetic centres in α - quartz have been linked to established point defects in the quartz crystal lattice, with the exception of manganese.

The EPR spectra of powdered quartz show far less resolution than those of single crystals. Consequently, quartz powder studies have only been made when good single crystals were not available.

INSTRUMENT SETTINGS

A JEOL JES FE3X ESR Spectrometer at the Central Science Laboratory department of the University of Tasmania was used to record the analogue EPR spectra of the samples. Appendix 2 contains only EPR spectra of a selected number of samples

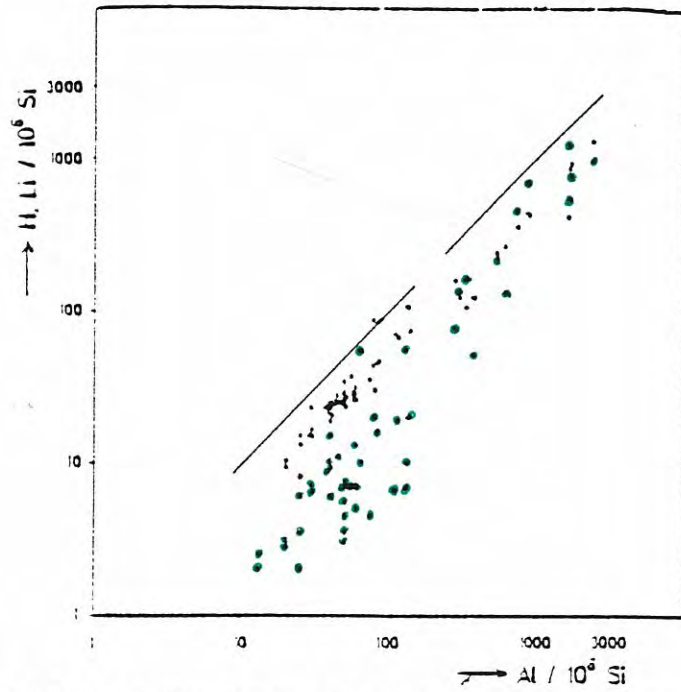


FIGURE 4.5a Correlation between Al and Li, H in selected clear rock crystal.

Dark circles - Li: GREEN circles - H (After Bambauer, 1961).

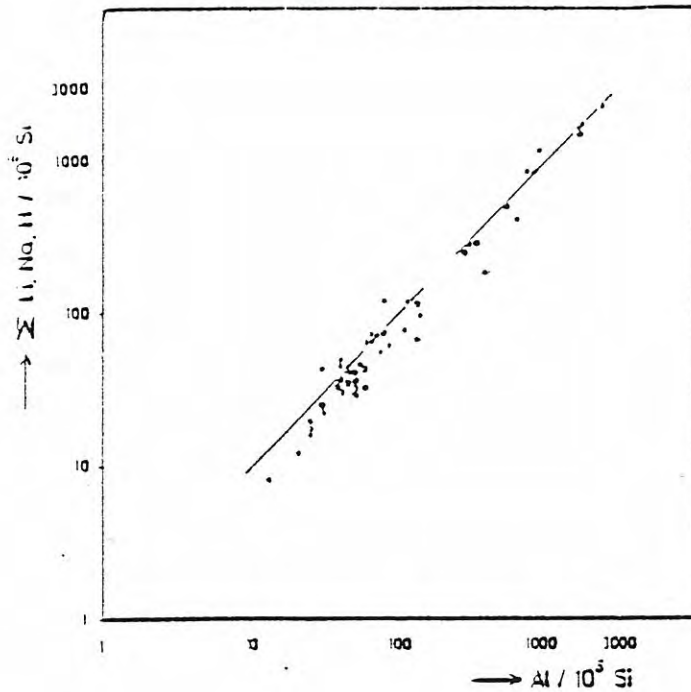


FIGURE 4.5b Correlation between Al and the sum of Li, H and Na in selected clear rock crystals (After Bambauer, 1961).

as they were all very similar. Finely ground quartz samples of 100 mg placed in an annealed silica tube were inserted in a multipurpose cavity and subjected to a microwave frequency of 9.15 GHz, 10 mW microwave power, modulation at 100 KHz \pm 0.2 mT, amplitude at 2.5×100 and with a nominal magnetic field of 326.5 mT. Spectra were run over sweeps of 326.5 ± 5 mT, 326.5 ± 100 mT and 326.5 ± 250 mT respectively; the first spectrum providing details of the peaks in the middle of the range and the second and third spectrum providing the general shape. All the samples were run under standard instrumental conditions at room temperature, and sweep times were usually of 4, 8 and 16 minutes for the respective spectra.

The JEOL ESR spectrometer used has provided reproducible spectra over a period of several years and the peak height of the standards B4 1708' 6" and B4 1706' has not changed.

PART 2: PIXE ANALYSIS OF VEIN QUARTZ

INTRODUCTION

Most PIXE (proton induced x-ray emission) probes use linear accelerators (eg. van de Graaff accelerator or pelletron) in which static electricity is deposited on non conductive belts or ladders and scraped off at the top where some hydrogen is released. The resulting protons accelerated in a high vacuum in a field of usually 2 to 4 MV are screened by an analyzing magnet, switched to a subsequent magnet and brought down the vacuum in the beam line of at least several tens of metres long. This enormous length is required to achieve full acceleration and focussing by diaphragms and focussing magnets. PIXE analysis was used for all elements with an atomic number higher than 14 because it enables rapid scan at sub-ppm levels and permits analysis of elements like Ga, Ge and As which cannot be determined by conventional methods.

INSTRUMENTATION

The target is usually some millimetres across. It is possible to manipulate the proton beam to a scanning 2 μm target, but this is extraordinarily expensive, and less than 10 scanning PIXE probes exist in the world.

The produced spectrum shows less bremsstrahlung than the spectrum of electron probe because the protons shoot rather through the target than being decelerated. The bremsstrahlung (continuum) is reduced by filters.

The counters are energy dispersive Si (Li) or Ge (Li) types and allow simultaneous analysis.

Because of the minute beam current (~ 50 nA or less) it is possible to have, as stated above, rather large beam radius, allowing a bulk analysis of the sample. PIXE probes are extraordinarily sensitive and can analyse at < 1 ppm level.

SAMPLE PREPARATION

The samples were cleaned the same way as done for EPR analysis. 400 mg of the clean, ground quartz sample was mixed mechanically with 100 mg of spectroscopically pure graphite for 10 minutes in a SPEX mixer and pressed into 13 mm diameter pills for the PIXE analysis. The data are presented in Table 4.1.

PIXE ANALYSIS

The PIXE analyses were carried out on the 3 MV van de Graaff at the Lucas Heights Research Laboratories. The proton energy used was 2.5 MeV, with a beam current of 50 nA, the beam spot size was 3 mm in diameter and run times were adjusted so that the total charge received per sample was 80 μC .

The main interest was in x-rays with energies above 3 KeV so a 100 μm thick mylar filter was placed in front of the target and the Si (Li) detector to reduce the count rate from the Si $K\alpha$ x-rays from quartz to a manageable level. A typical Pixe spectra is shown in Figure 4.6. Unless otherwise stated, the $K\alpha$ lines are used.

The PIXAN analysis package of Clayton (1986) was used to find the peak areas associated with each element. This area is then converted to a concentration normalized to an SiO_2 concentration of 47.0 weight percent, quartz being the internal standard. The program uses as input variable:

- (1) the mylar filter thickness and a possible ice layer on the detector surface (affects the detector efficiency),
- (2) the solid angle subtended by the detector at the target and
- (3) the accumulated current through the target.

Sample No.	Peak (cm)	P (ppm)	S (ppm)	Cl (ppm)	K (ppm)	Ca (ppm)	Ti (ppm)	V (ppm)	Cr (ppm)	Mn (ppm)	Fe (ppm)	Co (ppm)	Ni (ppm)
FO3-23	58.25	0.0	0.0	80.1	2805.2	65.0	227.2	12.0	3.4	3.3	739.1	0.0	22.4
FO3-30	103.50	0.0	0.0	83.6	1545.3	11.4	60.4	0.0	17	0.8	95.6	0.0	14.2
FO3-36	58.75	0.0	0.0	57.5	590.5	152.5	54.0	0.0	0.5	5.9	97.6	0.0	8.6
FO10-30	20.00	0.0	0.0	395.1	1547.8	28.4	101.9	0.0	14.5	1.6	327.4	0.0	15.6
FO10-31	18.00	0.0	0.0	82.2	1304.9	11.0	84.4	0.0	11	0.0	113.7	0.0	10.5
FO10-32	13.00	0.0	0.0	58.2	721.8	31.1	68.7	0.0	9.0	1.7	870.8	0.0	11.6
FO23-747	67.50	0.0	0.0	44.1	1270.9	16.3	72.1	0.0	0.0	1.1	261.9	0.0	12.5
FO23-748	65.00	0.0	0.0	178.2	1598.5	66.6	155.0	0.0	70.7	0.0	703.0	0.0	13.1
FO41-2853	35.00	0.0	0.0	37.1	417.1	15.0	31.5	0.0	0.0	0.6	65.5	0.0	10.5
FO41-2854	37.50	0.0	0.0	40.6	663.6	18.1	95.5	0.0	0.3	2.2	221.2	0.0	13.4
FO41-2857	4.50	0.0	0.0	190.2	170.9	43.9	10.3	0.0	14.1	42.0	295.9	0.0	15.9
FO41-2887	4.50	0.0	0.0	237.0	159.5	17.6	0.0	0.0	0.0	17	320.8	17	8.8
FO52-3937	10.50	0.0	0.0	60.4	735.4	18.1	63.5	0.0	0.0	1.3	43.1	0.0	16.9
FO59-4159	58.75	0.0	0.0	110.6	1966.9	17.9	236.2	0.0	1.5	0.8	234.3	0.0	7.6
FO59-4160	40.00	0.0	0.0	76.1	2483.5	8.1	202.9	0.0	17	0.0	156.9	0.0	14.2
FO59-4164	53.75	0.0	0.0	57.6	373.1	16.5	25.9	0.0	0.0	3.8	132.7	0.0	7.7
FO108-6468	17.50	0.0	0.0	134.8	2888.5	24.5	238.3	0.0	2.8	2.2	206.2	0.2	14.8
FO108-6518	52.50	0.0	0.0	92.2	1377.8	17.9	105.1	0.0	1.7	2.4	120.7	0.0	6.5
FO108-6523	75.00	0.0	0.0	88.9	1283.7	13.8	65.2	0.0	4.4	1.1	244.8	0.0	9.5
FO108-6640	41.00	0.0	0.0	32.9	526.5	21.2	24.6	0.0	0.0	0.7	109.2	0.0	13.0
FO108-6641	71.21	0.0	0.0	80.5	2945.1	9.7	213.1	0.0	4.3	1.7	317.7	0.0	8.8
FO108-6645	19.50	0.0	0.0	45.3	202.1	14.9	16.9	0.0	0.0	0.5	37.2	0.0	12.6
FO109-6735	65.00	0.0	0.0	24.1	194.6	17.2	0.0	0.0	0.0	0.7	38.4	0.0	9.2
FO109-6736	20.50	0.0	0.0	116.3	650.5	21.1	43.2	0.0	3.4	0.9	158.9	0.0	9.2
FO147-15736	58.25	0.0	0.0	136.6	3602.1	5.0	314.8	0.0	3.6	1.3	197.3	0.0	18.2
FO148-15789	48.80	0.0	0.0	65.9	783.6	19.2	61.0	0.0	16.1	0.7	220.5	0.0	15.5
FO148-15793	68.25	0.0	0.0	25.8	227.0	17.8	0.0	0.0	5.7	1.5	61.5	0.0	14.3
FO172-17031	88.87	0.0	0.0	45.3	1844.6	6.1	223.2	0.0	0.9	1.1	317.8	0.0	11.6
FO172-17032	86.00	0.0	0.0	170.6	281.2	27.3	9.6	0.0	6.4	2.6	2804.9	5.2	7.2
FO172-17035	21.00	0.0	0.0	90.3	1299.3	12.6	105.5	0.0	0.5	1.2	87.7	0.0	17.8
FO224-20626	9.80	0.0	0.0	32.0	1025.0	10.9	80.5	0.0	1.5	0.0	81.8	0.0	8.4
FO224-20640	11.70	0.0	0.0	61.1	576.5	23.8	26.1	0.0	18.4	1.2	1495.8	17	12.8
FO236-21309	62.50	0.0	0.0	184.2	717.5	48.3	41.4	0.0	1.7	1.5	69.1	0.0	10.1
FO237-21381	13.30	0.0	0.0	95.8	322.8	18.3	14.4	0.0	0.0	0.5	50.5	0.0	15.8
FO276-23574	57.50	0.0	0.0	210.7	677.6	19.3	26.9	0.0	8.6	1.2	77.4	0.0	13.5
FO276-23601	50.00	0.0	0.0	70.9	200.7	15.9	14.6	0.0	0.0	3.2	82.4	0.0	20.6
FO327-28787	60.00	0.0	0.0	38.6	308.4	16.1	94.3	0.0	0.0	0.0	87.4	0.0	9.7
FO327-28804	5.80	0.0	0.0	52.6	1230.1	10.6	103.1	0.0	0.0	1.5	125.2	0.0	9.6
DD1112-43.0	7.00	0.0	0.0	52.6	2203.1	9.9	253.9	0.0	1.4	1.3	129.1	0.0	8.5
DD1112-54.5	50.50	0.0	0.0	52.5	314.2	73.8	70.1	0.0	2.7	2.2	678.4	0.0	14.7
DD1112-58.8	63.00	0.0	0.0	73.0	1981.7	17.8	216.3	0.0	2.0	1.6	109.0	0.5	11.5
DD1113-6.8	10.00	0.0	0.0	51.9	3320.2	11.7	512.4	0.0	5.2	3.7	288.4	17	15.7
DD1113-42.5	47.00	0.0	0.0	60.8	656.9	15.8	163.9	0.0	0.4	1.5	63.9	0.0	8.2
DD1113-48.0	49.00	0.0	0.0	160.4	1714.8	17.8	262.7	0.0	1.6	2.7	197.8	0.0	13.1
DD1113-48.6	34.50	0.0	0.0										
DD1113-71.4	35.50	0.0	0.0										

Sample No.	Cu (ppm)	Zn (ppm)	Ga (ppm)	Ge (ppm)	As (ppm)	Rb (ppm)	Sr (ppm)	Y (ppm)	Zr (ppm)	Pb (ppm)	Aut (ppm)	Bi (ppm)	Au (ppm)
FO3-23	0.0	8.3	17	2.2	2.3	10.9	6.2	5.6	4.8	2.2	17	0.0	0.05
FO3-30	0.2	0.3	1.0	2.6	1.2	5.3	2.3	1.8	1.3	0.0	0.0	0.0	4.00
FO3-36	0.0	0.0	0.0	2.5	0.9	2.2	1.6	0.0	2.2	2.0	17	0.0	1.40
FO10-30	1.0	1.1	1.1	1.9	6.6	7.2	2.1	0.0	5.8	0.0	17	17	7.20
FO10-31	17	17	0.1	1.4	1.0	7.1	1.7	0.0	2.3	0.0	17	0.0	10.6
FO10-32	0.7	0.9	0.0	0.4	16.9	1.9	1.8	1.2	7.5	3.8	0.0	0.0	3.40
FO23-747	17	0.0	0.0	3.4	2.4	5.6	2.6	0.0	31.2	0.0	17	0.0	11.17
FO23-748	1.2	1.2	1.0	5.4	21.1	7.6	3.8	0.0	8.8	0.0	3.1	4.0	8.17
FO41-2853	0.0	0.0	0.5	0.6	0.0	0.7	1.1	0.0	0.0	0.0	0.0	0.0	0.02
FO41-2854	1.0	0.7	0.7	1.0	1.7	2.2	1.2	0.0	0.0	0.0	0.0	0.0	0.02
FO41-2857	0.9	1.4	0.0	0.0	1.4	1.0	0.0	9.4	0.0	0.0	1.8	0.0	0.02
FO41-2887	1.3	1.0	17	1.0	0.8	0.0	0.0	0.0	0.0	0.0	0.0	0.0	0.02
FO52-3637	0.6	0.0	0.0	2.6	3.1	2.0	2.6	0.0	3.4	0.0	0.0	0.0	1.53
FO59-4159	0.6	0.8	1.0	2.2	9.2	7.5	0.3	1.9	3.7	4.8	0.0	0.0	6.77
FO59-4160	0.0	0.0	0.9	2.5	1.9	10.6	2.7	2.3	2.7	0.0	0.5	1.4	4.30
FO59-4164	0.6	0.0	0.0	0.5	1.7	1.9	0.6	0.0	0.0	0.0	0.0	0.0	0.13
FO108-6468	0.9	0.0	0.0	1.7	5.8	11.4	1.9	0.0	4.7	0.0	0.0	17	6.60
FO108-6518	0.9	0.0	1.5	1.7	5.8	11.4	1.9	0.0	1.1	0.0	0.0	0.0	11.00
FO108-6523	0.1	0.6	0.7	1.9	2.0	5.7	0.8	0.0	1.1	0.0	0.0	0.0	0.78
FO108-6640	0.5	1.1	0.0	1.5	5.5	5.3	1.4	0.0	2.8	0.0	0.0	0.0	4.10
FO108-6641	0.0	17	0.0	1.6	1.3	2.8	1.5	0.0	0.0	0.0	0.0	0.0	0.40
FO108-6645	0.7	0.8	0.9	2.3	3.7	11.8	2.6	17	7.7	0.0	18.6	1.6	11.60
FO109-6735	1.2	0.5	0.5	0.8	0.0	0.0	0.7	0.0	1.0	0.0	1.1	0.0	0.03
FO109-6736	0.6	17	0.0	17	0.6	0.0	0.0	0.0	17	0.0	0.0	0.0	0.04
FO116-7278	0.8	0.6	17	2.0	0.0	2.9	0.8	0.0	0.0	0.0	0.0	1.3	0.78
FO147-15736	17	0.5	0.9	3.4	7.3	17.2	1.5	0.0	14.2	0.0	17	0.7	1.47
FO148-15789	1.4	0.8	0.2	3.8	4.1	3.3	1.3	0.0	1.7	2.5	0.0	17	12.10
FO172-17031	17	17	0.5	2.3	2.1	0.0	0.0	0.0	0.0	0.0	0.0	0.0	3.54
FO172-17032	0.6	0.5	0.5	0.5	1.6	8.9	0.6	0.0	0.0	0.0	0.0	17	1.86
FO172-17035	0.6	1.8	0.0	0.9	33.3	0.0	1.4	1.6	1.3	0.0	17	0.0	1.85
FO224-20626	0.0	0.0	0.0	2.0	1.6	5.1	1.9	0.0	2.4	0.0	0.0	0.0	0.49
FO236-21309	0.8	0.0	0.5	2.1	1.1	5.2	0.9	0.0	1.6	0.0	0.0	0.0	0.01
FO236-21317	5.9	2.0	17	0.6	18.3	0.0	0.0	0.0	3.6	17	1.4	0.0	3.83
FO237-21381	2.5	1.4	3.5	5.0	3.8	2.1	2.2	0.0	2.4	0.0	4.6	1.8	0.02
FO276-23574	0.8	0.4	0.6	2.3	1.0	1.7	0.8	0.0	1.3	0.0	0.0	0.0	4.32
FO276-23601	17	0.0	0.0	1.9	0.0	3.1	1.8	17	1.1	0.0	17	0.0	0.64
FO327-28787	17	0.7	0.0	1.1	4.6	0.0	0.0	1.9	1.7	0.0	0.0	0.0	0.01
FO327-28804	0.6	0.7	0.4	1.4	1.0	0.5	0.7	3.0	1.0	0.0	0.0	0.0	0.01
DD1112-43.0	0.6	17	17	1.1	1.3	4.7	2.0	0.0	4.3	0.0	17	17	18.30
DD1112-54.5	0.1	0.0	0.0	1.7	1.3	7.3	1.4	0.0	23.3	0.0	17	17	3.03
DD1112-58.8	0.7	17	0.0	0.0	0.0	1.4	1.6	0.0	9.7	0.0	0.0	0.0	0.01
DD1113-6.8	0.6	17	0.6	2.0	7.7	8.8	1.3	1.2	3.6	2.1	0.0	0.0	6.90
DD1113-42.5	0.6	17	0.6	5.3	8.3	15.0	1.0	1.3	31.6	0.0	17	17	13.70
DD1113-48.0	0.0	0.0	0.0	1.8	0.8	2.3	0.0	0.0	13.1	0.0	17	0.0	9.44
DD1113-48.6	0.0	1.7	0.4	2.2	1.8	5.6	6.2	1.7	14.1	1.9	0.0	0.0	6.30
DD1113-71.4	5.5	0.0	0.0	0.8	0.8	2.3	0.0	0.0	0.0	0.0	0.0	0.0	2.30

TABLE 4.1 Intensity of the EPR signal and chemical composition via PIXE

analysis of microcrystalline vein quartz, Fosterville, Ir - means present (because of better fit between calculated and observed spectra), but peak area is less than minimum detection limit.

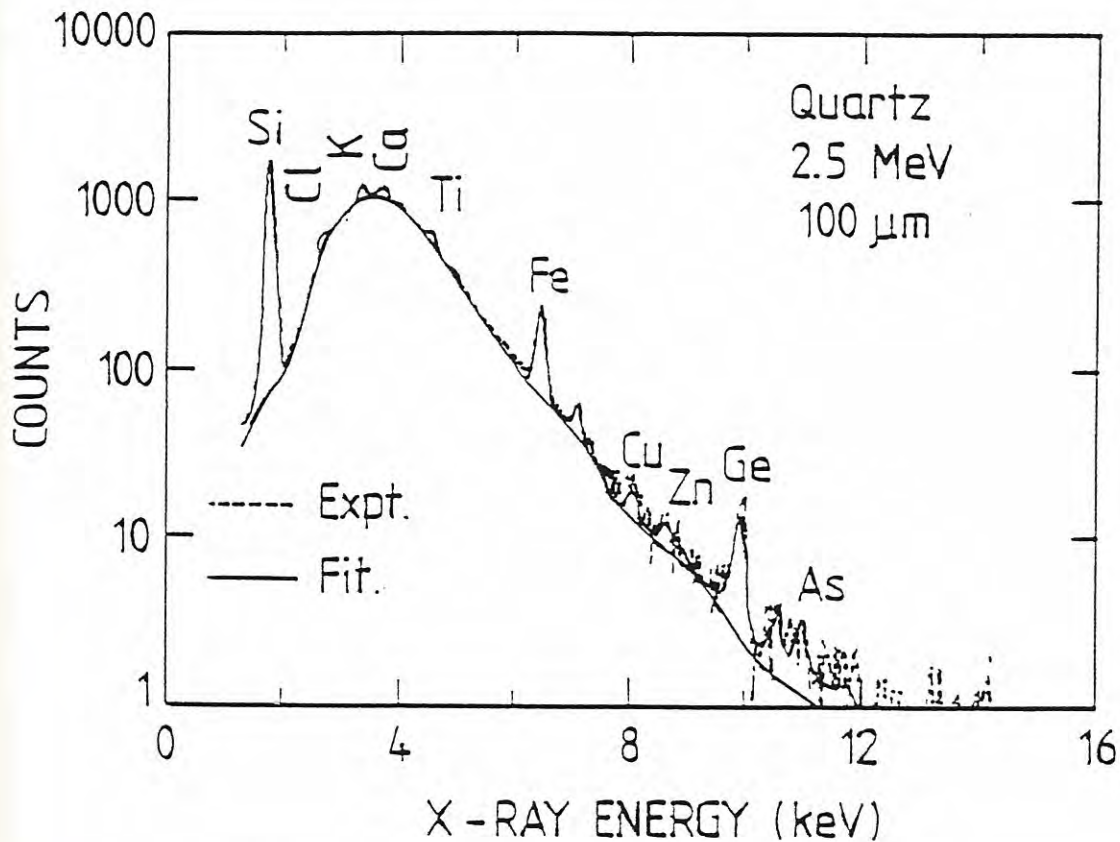


FIGURE 4.6 Typical PIXE spectrum for quartz. The dotted line represents the experimental data whereas the solid line is the fit to the data generated by the PIXAN program.

These parameters are 'juggled' to give as good a fit as possible to the Si peak, which is effectively the internal standard, and then all of the other concentrations are estimated from this.

The x-ray yield is calculated from

$$Y = \frac{C \cdot N_0 \cdot \Omega \cdot Q \cdot \epsilon}{W \cdot 4 \cdot \pi \cdot e} \cdot \int \sigma_p(E) \frac{T(E)}{S(E)} dE$$

where Y - yield

N_0 - Avogadro's number

Ω - solid angle

Q - charge

- ϵ - detector efficiency
- W - element atomic weight
- σ_p - x-ray production cross-section
- T (E) - matrix attenuation
- S (E) - matrix stopping power
- e - electron charge

where the integral basically allows for the loss of energy of the incident proton beam and emerging x-ray beam due to elastic and inelastic scattering in the sample. For most of the samples, the solid angle and filter dimensions are fixed with the charge $Q = 80 \mu\text{C}$.

The most probable cause for errors on the experimental side are fast random beam current fluctuations which affect the detected x-ray yield through dead-time corrections. Clayton's (1986) PIXAN analysis package compares the calculated spectrum with the observed spectrum and accepts analytical values on the basis of a best chi-squared fit.

The calculated spectrum usually involves some low concentrations of elements, where the standard error of the count exceeds the actual count. These elements (e.g. Zn, Ga, Bi, etc. in my samples) are recorded as trace (tr) in Table 4.1. The analytical value of the cut off is in the order of 0.5 ppm, varying from element to element and from sample to sample.

Assuming an analytically efficient proton penetration depth of $60 \mu\text{m}$ into the sample, the analyzed mass of the quartz will be about 1 mg for the 3 mm diameter beam target. This amount is so small that the slightest amount of impurity, like a mineral fragment other than quartz, will cause deviations from the analytical composition, which would be shown, if the sample had been larger. This may be the main causes of the differences between the analytical values of K, Fe, Zn, and Sr which were analyzed by PIXE (see Table 4.1) and AAS (see Table 4.2).

SAMPLE No.	EPR (cm)	Au (ppm)	Al (ppm)	Mg (ppm)	Fe (ppm)	Li (ppm)	Zn (ppm)	Na (ppm)	K (ppm)	Ca (ppm)	II (ppm)	Sr (ppm)
F03-23	58.25	0.05	9173	151.8	19.0	10.5	2.6	151.2	2826.4	877.3	893	8.9
F03-30	103.50	4.00	5130	74.1	9.9	14.3	0.3	98.8	1785.9	123.1	325	8.0
F03-36	58.75	1.40	2180	36.5	3.2	20.9	0.0	85.9	681.8	84.2	62	2.8
F010-30	20.00	7.20	4883	92.4	9.3	14.6	0.6	77.0	1732.8	265.8	257	2.8
F010-31	18.00	10.60	5029	87.4	10.5	8.2	0.1	136.8	1889.0	136.8	393	3.0
F010-32	13.00	3.40	2582	46.5	3.9	5.2	1.5	70.6	952.8	875.2	325	6.0
F023-747	67.50	11.17	5343	77.1	10.1	12.6	0.8	111.5	1700.2	167.1	325	1.4
F023-748	65.00	6.17	5890	69.7	12.0	13.5	1.0	109.3	1814.6	634.3	463	5.7
F041-2853	35.00	0.02	1678	34.9	2.1	13.2	0.3	53.8	561.9	73.7	257	2.2
F041-2854	37.50	0.02	2346	50.5	3.2	14.0	0.4	57.4	689.1	263.2	191	1.7
F041-2857	4.50	0.02	272	5.5	1.5	0.7	0.4	35.4	55.7	224.8	191	0.0
F041-2867	4.50	0.02	192	1.7	0.0	0.7	0.8	33.0	32.0	425.6	126	2.8
F052-3637	10.50	1.53										
F058-4159	58.75	6.77	3342	34.1	5.0	20.7	0.4	99.1	989.1	51.9	128	5.7
F059-4160	40.00	4.30	6925	74.2	11.7	11.8	0.7	120.7	2264.1	277.4	325	8.9
F059-4164	53.75	0.13										
F0108-6468	17.50	0.02	1362	22.6	1.3	3.4	3.2	80.7	409.5	184.1	760	2.2
F0108-6518	62.50	6.60	10348	115.9	18.5	7.5	0.7	118.3	2787.5	240.4	693	2.8
F0108-6523	75.00	11.00	5262	68.8	8.4	10.9	0.9	101.9	1922.5	121.0	463	3.3
F0108-6840	41.00	0.76										
F0108-6841	71.21	4.10	3893	49.2	7.4	17.3	1.1	92.3	1471.8	293.9	191	2.8
F0108-6845	19.50	0.40	2071	27.7	2.5	10.7	1.0	77.1	641.0	184.0	126	2.2
F0108-6735	65.00	11.60	11277	138.5	21.6	14.5	0.7	144.9	2631.7	489.2	760	4.4
F0108-6738	20.50	3.54	2846	44.0	4.4	11.5	3.0	89.7	1101.7	1181.9	191	5.7
F0116-7278	26.25	0.03	494	12.6	0.6	0.9	0.3	35.3	169.8	33.1	128	1.7
F0116-7279	26.25	0.04	478	8.5	0.0	1.2	0.4	26.5	124.9	19.9	191	1.7
F0147-15736	58.25	2.81										
F0148-15769	48.80	0.78	1275	22.6	1.3	6.3	0.3	49.5	441.1	34.6	257	2.8
F0148-15793	58.25	1.47	11622	110.6	18.9	17.8	0.4	136.6	2681.2	180.9	393	0.5
F0172-17031	66.67	12.10	3484	36.6	4.4	47.3	0.4	101.6	1128.7	117.7	325	2.8
F0172-17032	88.00	3.54	14475	135.8	21.3	32.1	1.1	172.8	2926.4	410.7	803	4.4
F0172-17035	21.00	1.88	802	6.8	0.5	9.3	0.2	53.7	190.4	30.5	62	3.0
F0172-17038	65.76	1.65	7164	40.7	10.3	32.1	0.7	158.6	1931.2	410.5	393	4.4
F0224-20826	9.80	0.48	666	10.1	0.7	5.2	4.1	58.9	127.9	1381.9	128	2.8
F0224-20840	11.70	0.01										
F0236-21309	50.00	3.83	5075	59.5	9.4	15.6	0.9	90.0	1771.3	100.2	191	4.3
F0236-21317	62.50	31.50	3945	59.5	7.5	18.7	1.0	81.4	1383.6	89.7	325	2.2
F0237-21361	13.30	0.02	1641	31.7	2.2	6.0	3.2	54.4	638.3	1211.7	191	3.0
F0276-23574	57.50	6.62	1911	32.9	2.7	6.5	2.2	93.5	771.8	47.0	191	2.2
F0276-23601	50.00	4.32	890	18.4	0.0	8.2	0.5	60.2	301.5	31.2	0	1.7
F0327-28797	60.00	0.64	2027	37.1	2.6	4.2	0.5	80.8	801.6	94.5	62	1.7
F0327-28804	5.80	0.01	514	13.8	0.8	3.7	2.1	44.0	160.8	1067.6	325	5.6
DD112-430	7.00	0.01	1292	14.5	0.0	1.3	4.7	80.8	283.2	69.6	62	0.0
DD112-545	50.50	19.30	4212	73.3	4.0	1.7	0.0	101.1	1636.2	156.2	393	0.0
DD112-586	53.00	3.03	8853	67.9	16.2	16.1	0.6	217.6	2495.5	141.0	760	7.4
DD113-66	10.00	0.01										
DD113-425	47.00	8.90	7207	70.8	6.5	8.6	1.2	106.8	2407.3	104.2	608	0.0
DD113-485	76.00	13.70										
DD113-480	49.00	9.44	2598	41.8	1.4	13.1	0.0	80.8	829.8	66.1	257	0.0
DD113-486	34.50	8.30										
DD113-714	35.50	2.30										

TABLE 4.2 Intensity of the EPR signal and chemical composition via AAS

analysis of microcrystalline vein quartz, Fosterville, Au - by fire assay.

PART 3: ATOMIC ABSORPTION ANALYSIS OF VEIN QUARTZ

INTRODUCTION

Atomic absorption spectroscopy (AAS) is an analytical method based on the absorption of ultraviolet or visible light by gaseous atoms. The material to be analyzed is converted to an atomic vapour by spraying into a flame. A hollow-cathode lamp containing the element to be determined is used as the light source. The atoms of this element in the flame absorb at precisely the wavelength emitted by the light source (Fritz & Schenk, 1979).

INSTRUMENTATION

The instrument used was an upgraded Varian Techtron Atomic Absorption A4 Spectrophotometer in the Geology Department. The absorbance versus concentration curves flatten out at higher concentrations and AAS cannot accommodate high concentrations in the liquid analyzed. This requires stringent dilution. Absorbance is defined as,

$$D = \log \frac{I_{\text{incident}}}{I_{\text{transmitted}}}$$

In addition to acetylene-air, the higher temperature flame mixture of acetylene-nitrous oxide, was used for the determination of the elements Al, Mg, Ti and Sr .

SAMPLE AND STANDARD PREPARATION

The same vein quartz powder samples that were used for EPR and PIXE study were used for AAS analysis. The procedure for the preparation of the standard solutions are described in Appendix 1.

1 g of powdered quartz sample was dissolved in HF and diluted 25 times. This was then analyzed against the prepared standards.

A computer program, designed by the departmental analyst, was used to calculate the actual concentration of the samples. The results are shown in Table 4.2.

PART 4: DISCUSSION OF EPR SPECTRA AND CORRELATION WITH PIXE AND
AAS ANALYSES

INTRODUCTION

Inspection of the analytical results presented in Tables 4.1 and 4.2 suggest numerical relations between the respective trace elemental concentrations of the quartz and its paramagnetism. These relations were investigated by Spearman's ranking.

This technique is characterized by a simplicity in the calculations, and its use is not restricted by the distribution law of the observed data. Spearman's Rank Correlation is defined as the sum of the squared differences in the paired ranks of two variable overall cases, divided by a quantity best described as: it is what the sum of the squared differences in ranks would have been, had the two sets of rankings been totally independent. This quotient is then subtracted from 1 to produce the standardized coefficient. The rank correlation is determined using

$$r_n = 1 - \frac{6 \sum (\Delta^2)}{n(n^2 - 1)} \quad (1)$$

where $\sum (\Delta^2)$ is the sum of the squares of differences between ranks and n is the number of samples.

If some of the ranks are tied, the equation for calculating rank correlation is given by

$$r_n = 1 - \frac{6 (\sum (\Delta)^2 \pm T_x + T_y)}{n(n^2 - 1)} \quad (2)$$

where T_x and T_y represent corrections for each of the tied ranks. These corrections are determined by

$$T_x = \frac{\sum t^3 - t}{n} \quad (3)$$

Similarly T_y is determined.

The significance of the correlation is evaluated using Table 4.3 from Fisher & Yates (1963). For example, if the number of samples analysed were 50 and r_n was calculated to be 0.4433, then the probability or significance is still 99.999%, in spite of the correlation coefficient being below 0.5.

n	.1	.05	.02	.01	.001	n	.1	.05	.02	.01	.001
1	.98769	.99692	.999507	.999877	.9999988	16	.4000	.4683	.5425	.5897	.7084
2	.90000	.95000	.98000	.990000	.99900	17	.3887	.4555	.5285	.5751	.6932
3	.8054	.8783	.93433	.95873	.99116	18	.3783	.4438	.5155	.5614	.6787
4	.7293	.8114	.8822	.91720	.97406	19	.3687	.4329	.5034	.5487	.6652
5	.6694	.7545	.8329	.8745	.95074	20	.3598	.4227	.4921	.5368	.6524
6	.6215	.7067	.7887	.8343	.92493	25	.3233	.3809	.4451	.4869	.5974
7	.5822	.6664	.7498	.7977	.8982	30	.2960	.3494	.4093	.4487	.5541
8	.5494	.6319	.7155	.7646	.8721	35	.2746	.3246	.3810	.4182	.5189
9	.5214	.6021	.6851	.7348	.8471	40	.2573	.3044	.3578	.3932	.4896
10	.4973	.5760	.6581	.7079	.8233	45	.2428	.2875	.3384	.3721	.4648
11	.4762	.5529	.6339	.6835	.8010	50	.2306	.2732	.3218	.3541	.4433
12	.4575	.5324	.6120	.6614	.7800	60	.2108	.2500	.2948	.3248	.4078
13	.4409	.5139	.5923	.6411	.7603	70	.1954	.2319	.2737	.3017	.3799
14	.4259	.4973	.5742	.6226	.7420	80	.1829	.2172	.2565	.2830	.3568
15	.4124	.4821	.5577	.6055	.7246	90	.1726	.2050	.2422	.2673	.3375
						100	.1638	.1946	.2301	.2540	.3211

TABLE 4.3 Values of the correlation coefficient for different levels of significance (After Fisher & Yates, 1963).

Doing the calculation by hand is very time consuming, therefore a statistics package called STATWORKS was used to calculate all the Spearman's rank coefficients. Correlation coefficients for all the elements analyzed by PIXE and AAS have been calculated and presented in Tables 4.4 & 4.5 respectively. Only the major positive correlations will be discussed.

EPR	Au	Cl	K	Ca	Ti	Mn	Fe	Al	Co	Zn	As	Pb	Sr	Zr
Au	0.617													
Cl	0.021	0.141												
K	0.575	0.284	0.220											
Ca	-0.287	-0.212	0.284											
Ti	0.489	0.443	0.120											
Mn	-0.133	-0.122	0.087	-0.336										
Fe	0.047	0.083	0.213	0.284	0.220									
Al	-0.248	-0.083	0.112	0.146	0.082	0.283								
Co	-0.242	-0.076	0.312	0.421	-0.253	0.016	0.100							
Pb	0.360	0.223	0.453	0.383	-0.111	0.020	0.284	0.041						
Sr	0.711	0.597	0.220	-0.232	0.499	0.115	0.559	0.028	0.583					
Zr	0.201	0.296	0.131	-0.127	-0.118	-0.130	-0.102	0.115	0.052	0.102				
As	0.657	0.578	0.215	0.609	0.482	0.229	0.592	0.229	-0.128	-0.107	0.489			
Pb	0.498	0.392	0.230	-0.308	0.350	0.039	0.182	0.158	0.241	0.103	0.275	0.309		
Sr	0.353	0.584	0.282	0.035	0.881	-0.031	0.225	0.168	-0.288	0.058	0.339	0.619	0.301	
Zr		0.482	0.151	-0.118	0.733	0.181	0.375	0.181	-0.005	-0.008	0.147	0.530	0.361	0.533
									0.054			0.638	0.479	
												0.620		

TABLE 4.4 Spearman's rank correlation coefficients between the intensity of the EPR signal, Au and trace elements analyzed by PIXE for the Fosterville quartz (51 samples).

EPR	Au	Al	Sr	Mg	Pb	Li	Zn	Na	Ti	K	Fe	
Au	0.617											
Al	0.652	0.479										
Sr	0.220	0.941	0.401									
Mg	0.572	0.956	0.577	0.924								
Pb	0.622	0.653	0.418	0.544	0.652							
Li	0.685	0.037	0.157	-0.022	0.038							
Zn	-0.184	0.037	0.157	-0.022	0.038	0.154						
Na	0.713	0.925	0.442	0.800	0.871	-0.154	0.120					
Ti	0.346	0.727	0.382	0.701	0.710	0.616	0.105	0.648				
K	0.639	0.990	0.503	0.945	0.955	0.266	0.032	0.910	0.728			
Fe	-0.127	0.282	0.466	0.304	0.376	0.611	0.532	0.229	0.357	0.267		

TABLE 4.5 Spearman's rank correlation coefficients between the intensity of the EPR signal, Au and trace elements analyzed by AAS for the Fosterville quartz (51 samples).

EPR and GOLD CORRELATION

The intensity of the major EPR signal of the vein quartz correlates positively with gold content (i.e. 0.617), as was calculated for the 51 samples (Figure 4.7).

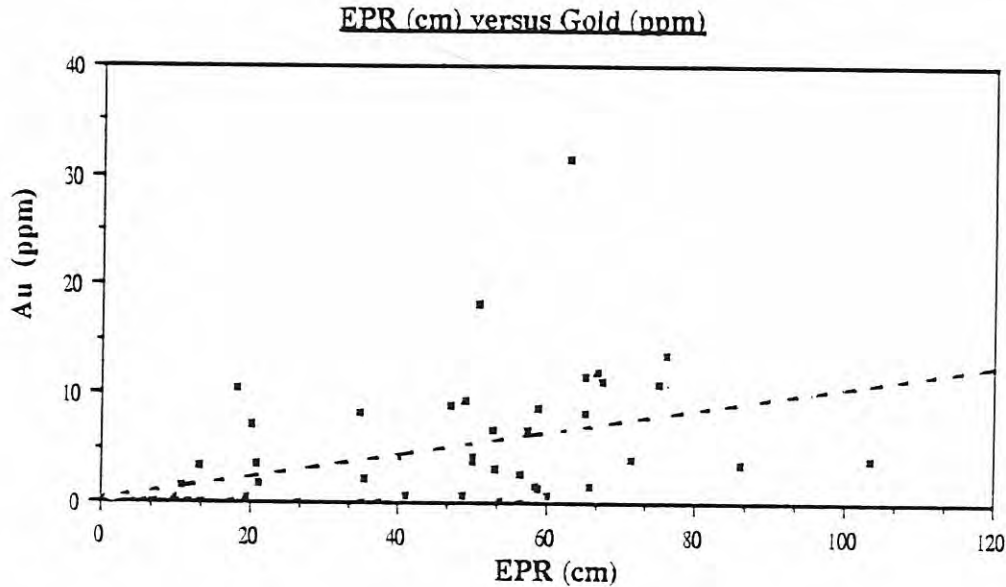


FIGURE 4.7 Scatter plot of the intensity of the paramagnetism of the vein quartz (measured as the height of the first derivative EPR peak at g 2.0025-2.0030) against Au content of the host rocks.

For this number of samples, the coefficient > 0.44 indicate with 99.999% probability that the ranking order correlates positively. This is surprisingly good, as most of the gold occurs in arsenopyrite, distributed in the host rock outside the quartz vein. The gold content was determined by industrial fire assay, derived from splits of 1 m long drill core and the EPR signal on 100 mg samples only. The positive correlation between the paramagnetism of quartz and gold content is not restricted to Fosterville, but also occurs at Beaconsfield (van Moort & Russell, 1987; van Moort et al., in press).

Gold has a large ionic radius and is unlikely to fit in the quartz lattice. Hence, the relation between the paramagnetism and the gold mineralization must consequently be of a secondary nature.

EPR and Al, K, Rb, Mg, Na, and Li CORRELATION

There are also very strong positive correlations between Al, K, Rb, Mg, Na, and Li respectively and the EPR signal of the quartz as demonstrated in Figure 4.8 and Tables 4.4 & 4.5. The observed positive correlations between the concentrations of the elements with the paramagnetism may be traced to specific mineral inclusions of submicroscopic sericite in the quartz (Plate 14) (van Moort, in press.) and sericite was observed in one case microscopically. Assuming 10 % K_2O in sericite, the Fosterville quartz would contain up to 0.4% sericite. However, sericite does not produce intense paramagnetism and therefore, the paramagnetism in the samples must originate from some source other than sericite. Subtraction of a standardized muscovite from the chemical composition of the quartz does not yield more relevant trace element relations for the remaining calculated quartz and its EPR.

The correlation coefficient between Al and Li is much lower than the correlation coefficient between Al and K, Rb, Mg and Na. This is due to the fact that part of the Li will be in the form of compensating ions in the quartz lattice, as discussed in the section on the application of EPR on quartz.

Alkaline chloride waters in hydrothermal areas are characterized by their relatively high Li, Na, K, and Rb concentrations (Mann et al., 1986) which could lead to enrichment of these elements in quartz, either in the form of mineral inclusions, or as lattice substitutions.

GOLD and Na, K, Al, Mg, Rb and Li CORRELATION

Na, K, Al, Mg, Rb, and Li show a highly significant correlation with Au as is observed in Tables 4.4 & 4.5, particularly in the case of Na. This observed correlation would be of a secondary nature, due to the fact that these elements can be largely traced to the specific mineral inclusions of sericite in the quartz and gold in the adjacent host rock.

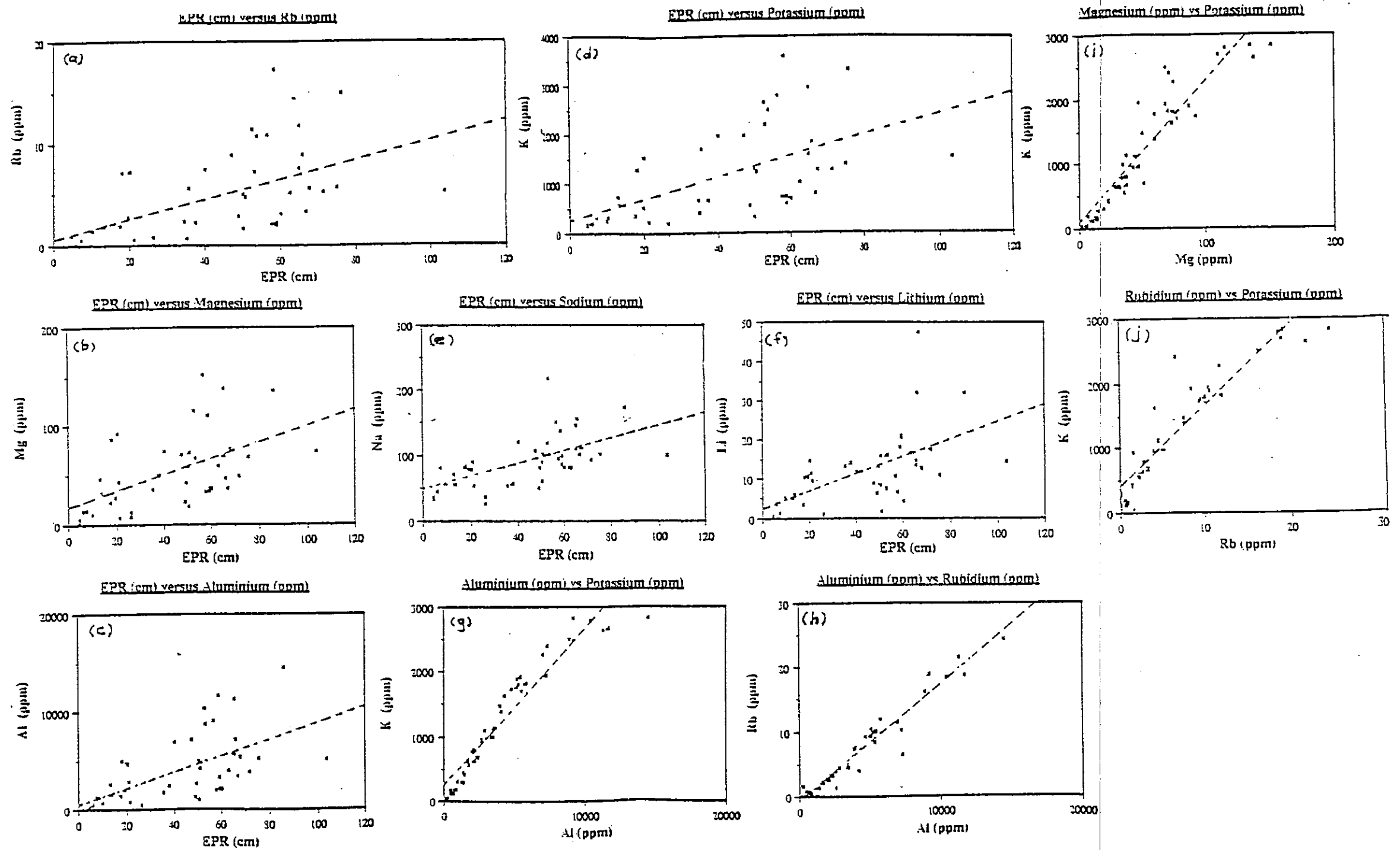


FIGURE 4.8 Scatter plots of the paramagnetism against: (a) Rb, (b) Mg, (c) Al, (d) K, (e) Na and (f) Li for the Fosterville quartz. Also, scatter plots of Al against: (g) K and (h) Rb and K against: (i) Mg and (j) Rb.

EPR and Ge CORRELATION

The Ge content of the quartz correlates particularly well with the paramagnetism at g 2.0025-2.0030 for the samples from Fosterville (see Table 4.4 & Figure 4.9) suggesting a proportional relationship.

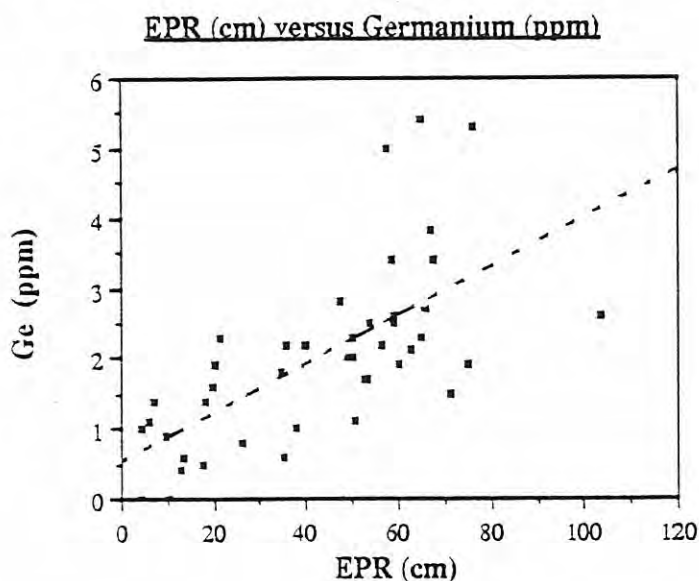


FIGURE 4.9 Scatter plot of the paramagnetism against Ge content of Fosterville quartz.

The established Ge centres however, cannot be seen in the EPR spectra, unless irradiated as stated in the introduction of this chapter. The highly significant correlation between the paramagnetic centre and the Ge content mentioned above may consequently be accidental. The relation is however strong and the spectrum is reminiscent to (but stronger than) that of Ge-doped Al bearing quartz, corroborating a direct relation between the Ge content of the quartz and its paramagnetism.

The alternative possibility of broken bonds contributing to the paramagnetism of the quartz, can neither be ruled out nor be proven, as their abundance cannot be determined.

EPR and As CORRELATION

There is a poorer but still significant correlation between the paramagnetism and arsenic content of the quartz samples (i.e. 0.201) for the 51 samples studied. There are no sulfide minerals present in the samples, as the sulfides have been removed by the hot nitric acid treatment, leaving no proton probe detectable sulfur. Therefore, the As must be present in the quartz lattice. Arsenic concentrations in some geothermal waters from New Zealand are in excess of 4.8 ppm (Mann et al., 1986) and sinter precipitates from Waiotapu have been shown to contain up to 13 wt. % As (Hedenquist & Henley, 1985). There is only one reference in the older literature to As in quartz, which gives a range of 0.4 - 1.3 ppm (Onishi & Sandell, 1955). Hamdorf (1987) found As in quartz at Elliott Bay in the range 0.1 to 5.0 ppm.

DISCUSSION

Table 4.4 & 4.5 indicate trace element levels in the Fosterville quartz as above what is recorded for vein quartz (Fron del, 1962; Bambauer, 1961; Poty, 1969; Wedepohl, 1978). The relation between Al, K, Rb, Mg and also Li with essentially submicroscopic sericite was discussed above.

The Fosterville quartz also contains several ppm As and usually some ppm Ge. The presence of Ge is of particular importance as it enhances the paramagnetism of quartz and is the common dopant in artificially grown piezo-electric quartz.

Although the geochemical similarities between silicon and germanium are generally known (i.e. tetrahedral coordination, similar ionic and covalent radii), there is very little information in literature on the trace element studies of Ge in quartz (Wedepohl, 1978). This may be due to the fact that the Ge content of quartz is generally less than 1 ppm (Schroen, 1968), and its occurrence in quartz is well explained by simple substitution: $\text{Ge}^{4+} \rightarrow \text{Si}^{4+}$.

GeO_2 is very much more soluble in water than SiO_2 at higher temperatures (Morey, 1957; Kennedy, 1950). Consequently, it is enriched in late magmatic and hydrothermal fluids. This leads to enrichment of Ge in quartz, sinters, sulfides, and as was recently established, in agate (Blankenberg & Schroen, 1982). At relatively low pressure and temperature (700 bars & 300 °C), germania solid solution in α - quartz occurs to about 24 mole % (Miller et al., 1963). Increasing the temperature to about 750 °C with constant pressure, results in a slight increase in solubility up to about 31 % (Figure 4.10). The system SiO_2 - GeO_2 has not been investigated at lower temperatures. Extrapolation of the data from Figure 4.10 would indicate that the SiO_2 still can incorporate considerable amounts of GeO_2 at lower temperatures. Consequently, the amount of Ge in quartz would be governed by availability during crystallization.

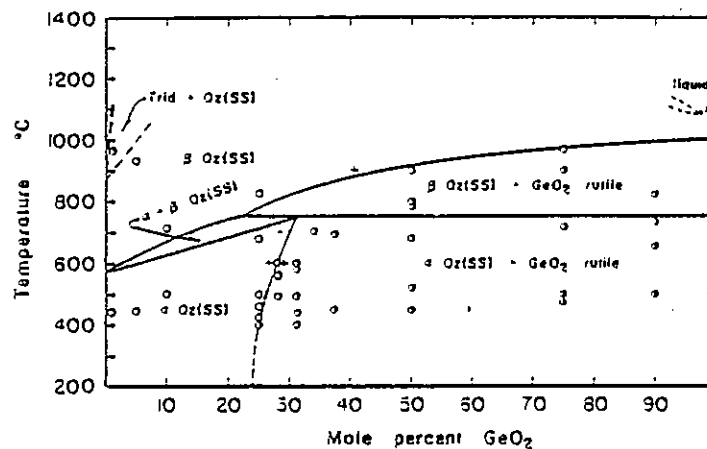


FIGURE 4.10 Phase diagram of the system SiO_2 - GeO_2 on dry studies and hydrothermal studies at 700 bars (After Miller et al., 1963).

Natural quartz usually does not contain more than about 2 ppm Ge (Wedepohl, 1978). Quartz associated with pegmatites contain values up to 8 ppm Ge (Schroen, 1969). Higher values such as 8 ppm are also observed in quartz from hydrothermal veins (Balitskiy et al., 1969) or even 25 ppm in case of hydrothermal vein quartz associated with polymetallic sulfide deposits (Tikhomirova, 1966). Siliceous hot spring sinters from Rotorua and Rotokawa in New Zealand contain up to 17 and 20 ppm Ge respectively

(O'Shea, 1987; Krupp & Seward, 1987) and those from Hokkaido in Japan contain approximately 25 ppm Ge (Uzumasa et al., 1959). The main carriers of Ge in hydrothermal mineralization are sulfide minerals such as sphalerite, bornite and chalcopyrite, which contain up to 1000 ppm Ge (Wedepohl, 1978). Consequently, it can be assumed that quartz, related to such mineralization, may be germanium enriched.

The high correlation between Ge, Au and EPR suggests that EPR and Ge may be used as an indicator of gold mineralization in Quartz-Au type deposits. In metamorphic quartz vein systems which have lost their paramagnetism through annealing (van Moort & Barth, 1987), Ge can probably still be used as an indicator of the presence of gold, as quartz would be unlikely to lose low level trace element concentrations during metamorphism.

ORIGIN OF THE PARAMAGNETISM

The observed paramagnetism of the quartz is not unlike what can be expected for a Li, Na or H compensated Ge bearing quartz (which will always contain Al) at cryogenic temperature (Weil, 1984). It is however visible at room temperature and consequently much of the recent literature on use of the centre at g 2.0025-2.0030 for dating, is referring to it as the peroxy centre, which is visible in glass, at room temperature.

The present study indicates that the centre is Ge-Al related. The question why the centre is visible at room temperature however cannot be answered. It may be of importance that all samples (except 3) contain > 0.6 ppm As. As^{5+} would provide the free electron to compensate Al^{3+} in the $Si^{4+}O_2$ lattice.

McMorris (1970) and Odom & Rink (1989) believe that the centre is the result of the damage due to alpha-emitting nuclides present as impurities. King et al., (1987) indeed determined the concentration of ^{40}K , ^{232}Th , ^{235}U and ^{238}U in quartz from granites. The presence of these elements in concentrations above 0.1 ppm in the Fosterville quartz is excluded because of the nature of PIXE scans.

CHAPTER 5 - MINERALIZATION AND ALTERATION

STYLE OF MINERALIZATION AND GOLD GRADE

Gold mineralization along the Fosterville fault zone occurs in quartz stockworks within oxidized brecciated shear zones and fractured sandstones. The mineralized fault breccia and associated stockworks are nearly vertical and up to 30 m wide. Stockwork zones occur more commonly on the eastern side of the main fault breccia (Figure 5.1).

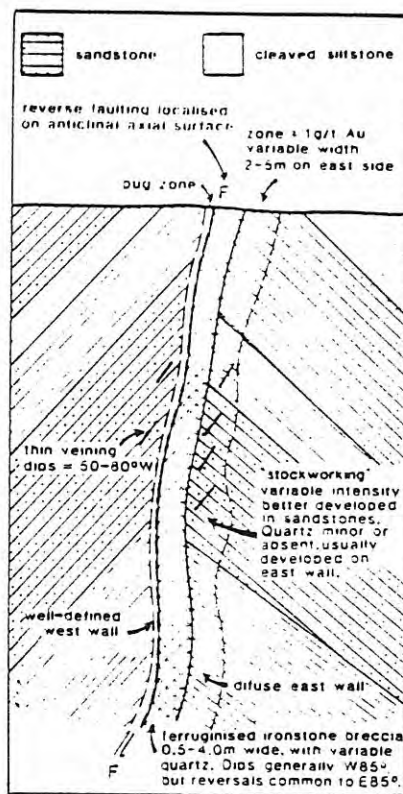


FIGURE 5.1 Idealized section through typical mineralization style at Fosterville (After McConachy, 1988).

The mineralized zones occur as two distinct types. These are :

- (1) wide and planar mineralized zones, and

(2) shallow plunging ore shoots, which are controlled by

- (i) brecciation along the Fosterville Fault Zone,
- (ii) lithology,
- (iii) presence of cross faulting, and
- (iv) presence of drag folds.

Mineralization in the Fosterville goldfield comprises of disseminations of pyrite and arsenopyrite, and there is a strong geochemical association between arsenic and gold (discussed later).

Most of the Fosterville field had original head grades of 3.5 to 4.5 g/t. No gold grains have been observed in core or thin section, but PIXE and electron-probe analysis have identified gold in quartz and sulfides respectively.

ORE MINERALOGY

Ore minerals (pyrite and arsenopyrite) were studied by polished thin sections prepared at the Geology Department of Tasmania.

PYRITE

Pyrite is the most common sulfide mineral observed at Fosterville. Individual euhedral crystals of pyrite are commonly fractured or cracked. Being relatively hard, pyrite tends to fracture during deformation rather than flow. Pyrite usually comprises between 5 and 7 % of the whole rock in the mineralized zones. The grains are randomly distributed, but are most abundant in the silty beds, (Plate 15) and generally absent from the sericitic-shale. Euhedral pyrite grains are also common through bands of siderite and Fe-Mg rich carbonate (Plate 16).

A common feature of the individual pyrite grains are growths of quartz and sericite pressure shadows (Plate 17). Quartz and sericite grows as fibres perpendicular to the free surface and attains lengths up to half the diameter of the pyrite grains. Pressure shadows develop during deformation which indicates the presence of pyrite prior to or during deformation. The pyrite crystals are almost invariably $< 0.5\text{mm}$ in size and average about 0.1mm .

ARSENOPYRITE

Arsenopyrite is the other sulfide mineral present and is sometimes associated with pyrite. The great majority of arsenopyrite crystals occur independent to pyrite but some of the coarser crystals are composites of both sulfide species.

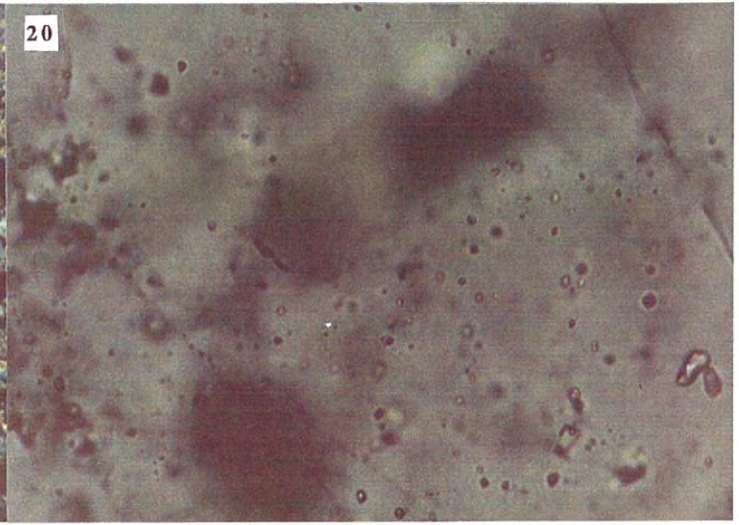
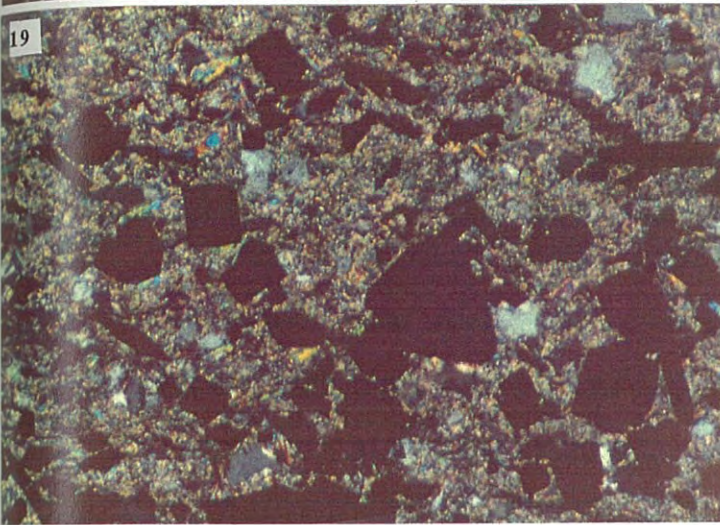
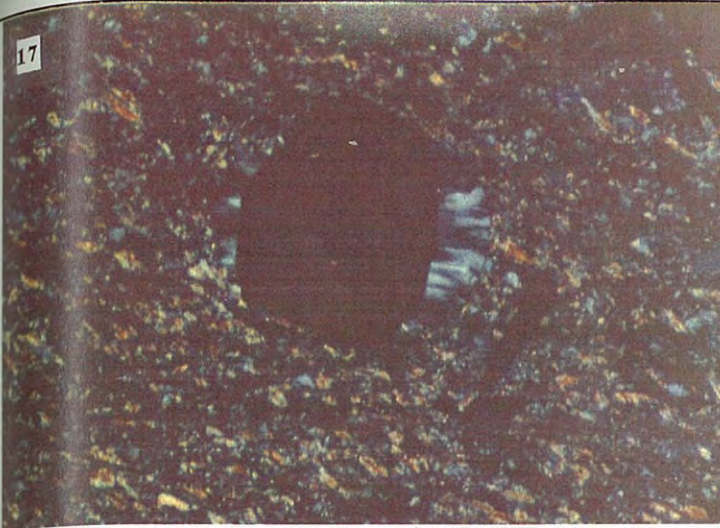
Individual rhombic or prismatic crystals of arsenopyrite (Plate 15) make up 4 to 6 % of the whole rock, have a random, but sometimes vague layered to somewhat patchy distribution, throughout the sediment.

The fact that there are composites of both sulfide species suggests that pyrite and arsenopyrite deposition occurred contemporaneously.

OXIDIZED ZONE

Hematite is a very common phase at Fosterville in the oxidized zone, from surface to 30-45m depth, as a weathering product. Anhedral primary hematite was not observed in the oxidized zone but rare quartz veins containing limonite (Plate 18) (replacement of pyrite and arsenopyrite) were found which suggests the hematite is probably all secondary and associated with oxidation. Hematite associated with the oxidized zones along the strike of the Fosterville Fault indicates that oxidizing conditions were present at some period of time, at least within and immediately adjacent to the fault zone.

- PLATE 17 Sample 12-58.6. Thin section. Growth of pressure shadow around pyrite grain. Plate size = 1.31 x 2.00 mm. (XPL).
- PLATE 18 Sample 10-45.0. Thin section. Limonite lined voids in sandstone indicating that pyrite has leached out of oxidized zone.
Plate size = 1.31 x 2.00 mm. (PPL).
- PLATE 19 Sample 13-48.6. Thin section. The alteration comprises predominantly sericite-pyrite-arsenopyrite-carbonate.
Plate size = 1.31 x 2.00 mm. (XPL).
- PLATE 20 Sample 11-52.9. Thin section. Two types of fluid inclusions studied:
Type 1 - larger, 2-phase, liquid and vapour, and
Type 2 - smaller, 3-phase, CO₂- liquid bearing inclusions.
Plate size = 0.16 x 0.24 mm.
- PLATE 21 Sample 12-54.5. Thin section. Star-shaped (rosette) cluster of arsenopyrite in sediments. Plate size = 0.65 x 0.98 mm.
(Reflected light).



ALTERATION AT FOSTERVILLE

INTRODUCTION

Wall rock alteration effects are commonly minimal in auriferous deposits hosted by turbidites and associated sedimentary rocks. Hydrothermal alteration at Fosterville is confined to the brecciated shear zones and quartz stockworks. The alteration comprises predominantly sericite-pyrite-arsenopyrite-carbonate alteration (Plate 19).

SERICITE ALTERATION

Sericitic alteration is the most intense type of alteration and occurs in the quartz stockworks and shear zones. Sericite, a white mica, occurs within the groundmass and associated with quartz veins as masses. Sericite in unaltered rocks from Fosterville commonly occur as laths that are aligned, giving the rock its schistosity.

In this section, sericite is very fine grained and fibrous and shows moderate to high birefringent colours.

CARBONATE ALTERATION

Hydrothermal carbonate alteration has produced carbonate minerals (see Appendix 5) within the quartz stockworks and shear zones and sediments immediately adjacent to the shear zones. The carbonates are either siderite or Fe/Mg carbonate (Figure 5.2). These commonly occur as irregular veins, which cut through the rocks, and as vugs and masses disseminated through the groundmass. Vein carbonate occurs with quartz and sometimes with pyrite. The carbonate veins form en-echelon patterns (as mentioned earlier) and are discontinuous through the sediments as a result of later stress.

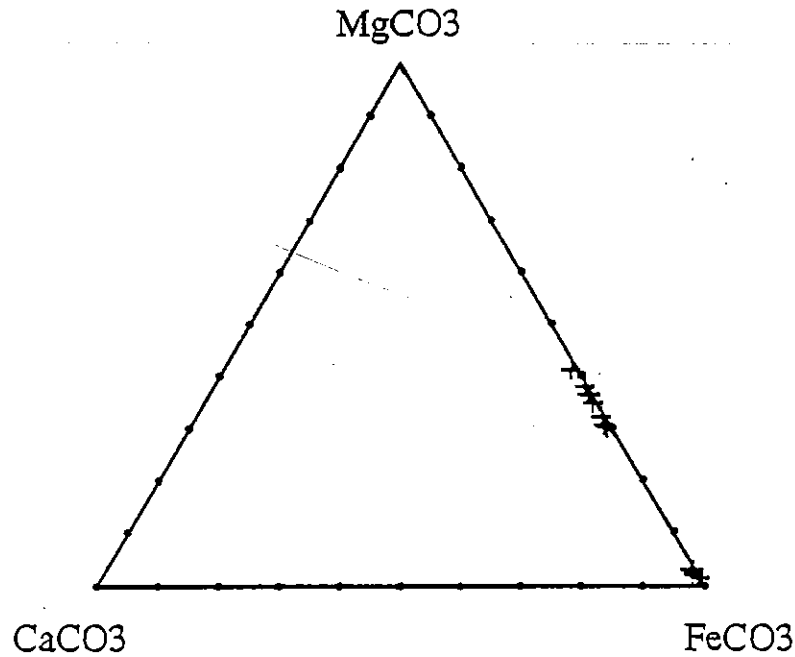


FIGURE 5.2 Ternary diagram showing two types of carbonate at Fosterville.

SUMMARY

Hydrothermal alteration has produced a variety of mineral assemblages within the shear zones at Fosterville, with sericite alteration being the most widespread. Pyrite alteration is also widespread but only present with sericite and arsenopyrite alterations. Carbonate alteration, which is sometimes associated with sulfides is common and indicates that a later stress event occurred after mineralization as the carbonate veins are discontinuous through the sediments.

The only silica alteration at Fosterville occurs as silicification of the sandstone at the junctions of splays (see chapter 2). There are no evidence for chlorite alteration at Fosterville.

CHAPTER 6 - GEOCHEMISTRY OF THE MINERALIZATION AT FOSTERVILLE

INTRODUCTION

The geochemistry of the disseminated gold mineralization at Fosterville was studied by various methods. These were:

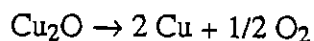
- (1) sulfur isotope study,
- (2) arsenopyrite geothermometric study,
- (3) fluid inclusion study, and
- (4) study of gold-rich arsenopyrite.

The aim of this study is to determine and infer the source of sulfur, conditions of deposition, such as aS_2 , temperature, pressure and depth of formation, and to investigate the occurrence and distribution of gold.

PART 1 : SULFUR ISOTOPE STUDY

INTRODUCTION

A limited sulfur isotope study was conducted in order to deduce the potential source of sulfur in the hydrothermal system at Fosterville. Samples were obtained by drilling pyrite from diamond drill cores using a dentist's drill. The sulfide was converted to sulfur dioxide (SO_2) using Cu_2O as an oxidizing agent at $\sim 800^\circ C$, according to the following reactions:



The samples were subsequently analysed on a VG Micromass 602D Stable isotope mass spectrometer in the Central Science Laboratory at the University of Tasmania and the results are reported as δ values in per mil (‰). The accuracy of the results are generally ± 0.2 per mil. The procedure used for the isotopic analysis is described in Ohmoto & Rye (1979). Results are expressed as $\delta^{34}\text{S}^1$. The $\delta^{34}\text{S}$ notation is defined as :

$$\delta^{34}\text{S}_{\text{sample}} = \left(\frac{(\text{}^{34}\text{S} / \text{}^{32}\text{S})_{\text{sample}}}{(\text{}^{34}\text{S} / \text{}^{32}\text{S})_{\text{standard}}} - 1 \right) \times 1000$$

and is expressed in parts per thousand (‰).

Sulfur in hydrothermal ore deposits can originate from a large number of different sulfur sources. These are:

- (1) magmatic,
- (2) rock sulfur,
- (3) seawater sulfur,
- (4) evolved seawater , and
- (5) evaporites.

RESULTS OF ISOTOPIC ANALYSIS

The results of the sulfur isotopic analysis for seven disseminated pyrite samples are presented in Table 6.1 and their distribution plotted in Figure 6.1.

¹ $\delta^{34}\text{S}$ is defined as the ratio $^{34}\text{S} / ^{32}\text{S}$ of the sample relative to the standard sulphide, namely troilite (FeS) phase of the Canon Diablo Meteorite in California.

SAMPLE No.	SULPHIDE	$\delta^{34}\text{S}$ VALUE	STYLE
DDH 13/42.5	pyrite	-0.931	disseminated
DDH 13/46.5	pyrite	-1.214	disseminated
DDH 13/48.0	pyrite	-1.141	disseminated
DDH 13/48.6	pyrite	-1.230	disseminated
DDH 13/52.0	pyrite	-2.622	disseminated
DDH 13/71.4	pyrite	-0.819	disseminated
DDH 13/74.5	pyrite	-0.384	disseminated

TABLE 6.1 Sulfur Isotope Data.

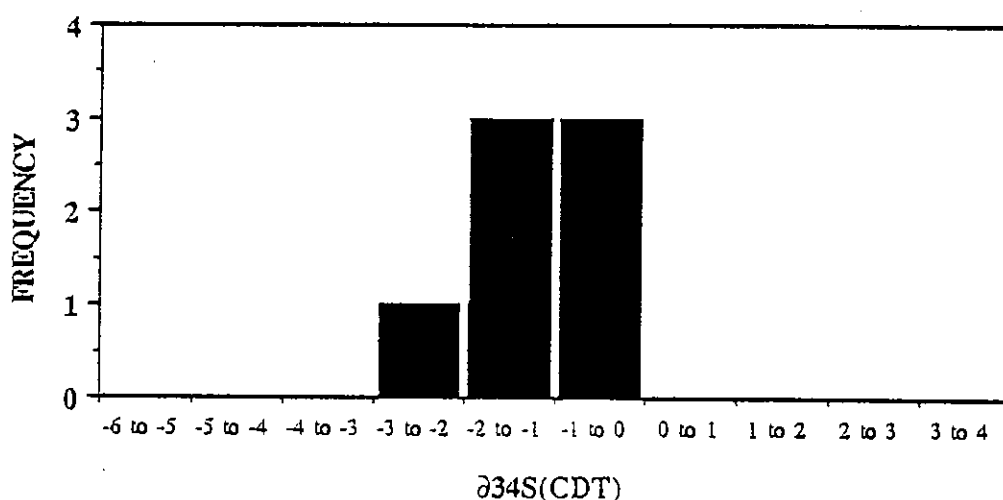


FIGURE 6.1 Sulfur Isotope Distribution.

DISCUSSION OF RESULTS

Sulfides in igneous rocks are isotopically similar to those in meteorites with average $\delta^{34}\text{S}$ close to 0 ‰. Ore deposits in which sulfides have $\delta^{34}\text{S}$ values near $0 \pm 3\%$ have been interpreted to have formed from magmatic fluids. Fluids derived from one magmatic source cannot have $\delta^{34}\text{S}$ values greater than approximately 8 ‰, but can be as low as approximately -30 ‰ (Ohmoto & Rye, 1979). Seawater sulfate has $\delta^{34}\text{S}$ of about +10 to +30 ‰ depending on geological age. Sulfides in sedimentary environments have highly variable but usually negative $\delta^{34}\text{S}$ values.

The $\delta^{34}\text{S}$ values obtained from pyrite disseminated in the sediments from Fosterville range from -2.6 to -0.4 ‰ and are comparable with the sulfur isotopic composition of magmatic source fluids. Figure 6.2 shows the sulfur isotopic variations of other deposits in the Ballarat Trough.

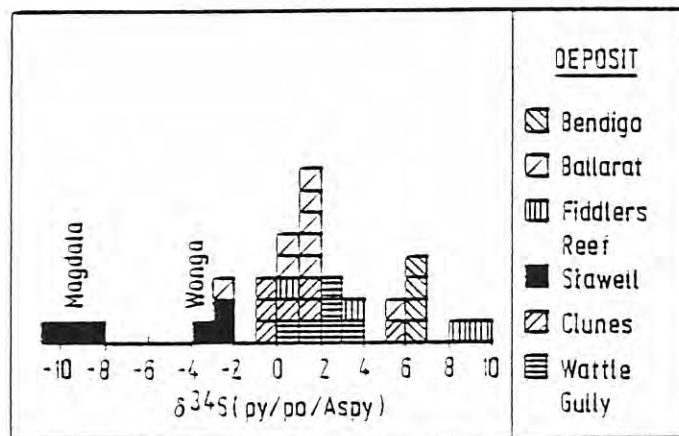


FIGURE 6.2 Histogram showing S isotopes (in per mil CDT) in the Ballarat Trough deposits (After Gulson et al., 1988).

The sulfur isotopic results of Fosterville are similar to that of the Clunes deposit. The S isotope values from the alteration halo at the Clunes deposit ($\delta^{34}\text{S} = -2.7$ to 2.7) are depleted in ^{34}S compared with values measured on coarse metamorphic pyrite ($\delta^{34}\text{S} = 5.7$ to 7.8) outside the alteration halo (Gulson, et al., 1988).

R. Haydon (pers. comm.) noted the presence of a quartz-feldspar porphyry dyke at Robbins Hill, approximately 4 km NNE of Fosterville and along the O'Dwyers fault (Figure 1.2), which is located in sediments and contain sericite alteration and associated with mineralization. The Robbin's Hill area comprises a significant shallow deposit with mineralization in shears and stockworks in the sandstone over a wide area. This indicates a similar relation between mineralization at Fosterville and Central Ellesmere and the felsic porphyry dyke. Therefore, Fosterville and Central Ellesmere fields may be situated close to the edge of a batholith and the mineralization is related

with this batholith. The sulfur isotope results, which indicate a magmatic signature for the mineralizing fluids supports the above proposition.

PART 2: ARSENOPYRITE GEOTHERMOMETRY

INTRODUCTION

Arsenopyrite is the most refractory of the common sulfides. It can range in composition from $\text{FeAs}_{0.9}\text{S}_{1.1}$ to $\text{FeAs}_{1.1}\text{S}_{0.9}$ (Clark, 1960a). Within the Fe-As-S system, the composition of arsenopyrite is a function of temperature and pressure (Kretschmar & Scott, 1976). This makes arsenopyrite a potentially useful geochemical tool for determining the conditions of its deposition in certain restricted assemblages (Barton & Skinner, 1979). Clark (1960 a,b) determined detailed phase relationships in the Fe-As-S system between 702 °C to less than 281 °C. The essence of the arsenopyrite geothermometer is to determine the atomic percentage of arsenic in arsenopyrite as a function of temperature (Figure 6.3).

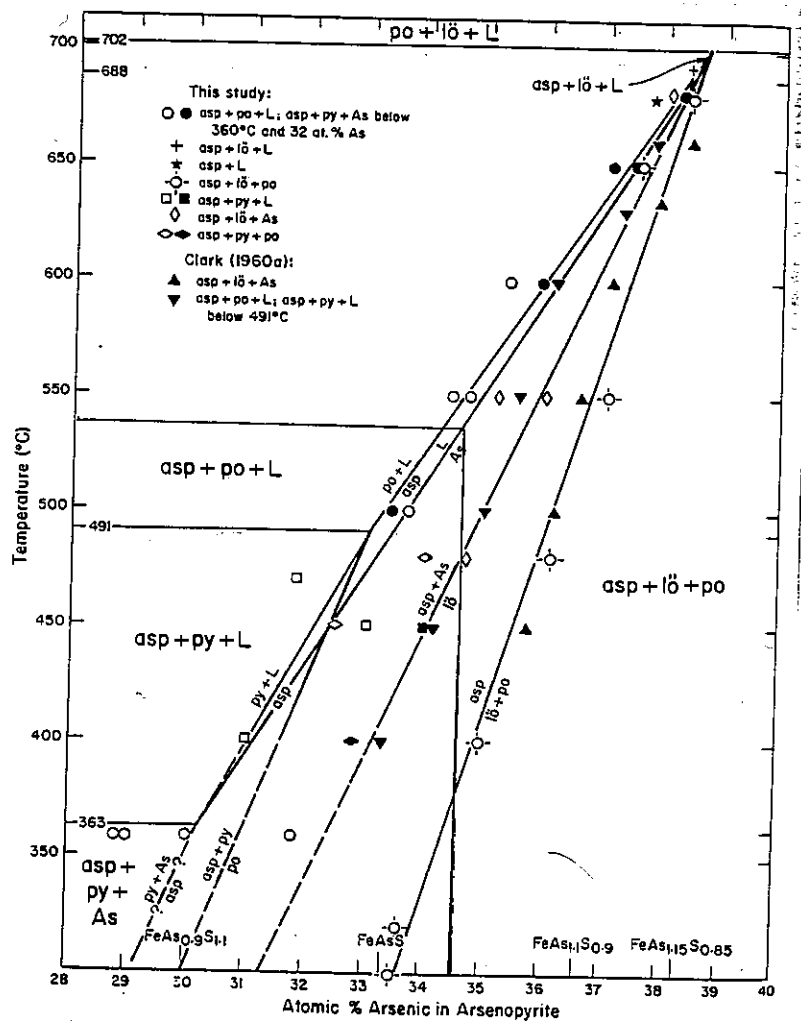


FIGURE 6.3 Pseudobinary T-X section along the pyrite-loellingite join showing arsenopyrite composition as a function of temperature and bulk composition. All assemblages include vapour (After Kretschmar & Scott, 1976).

ELEMENT	Ave. At. %	Range At. %	1 Std. dev.
S	29.5	27.6 - 30.2	0.5
Fe	34.7	34.5 - 35.6	0.4
As	34.3	33.1 - 36.4	0.3

TABLE 6.2 Average composition of 30 arsenopyrite grains obtained from 6 samples (FO 13-42.5; FO 13-48.0; FO 13-48.6; FO 13-71.4; FO 12-58.6; FO 12-70.0). Analysis by electron microprobe.

grains taken from 6 different samples and analysed using the JEOL electron microprobe in the CSL at the University of Tasmania.

Figures 6.3 & 6.4 were used to estimate the temperatures and a_{S_2} at the time of mineralization at Fosterville. The temperatures obtained from this method (approximately 540 °C) was compared with those obtained from Fluid Inclusion Study (Part 3).

RESULTS OF GEOTHERMOMETRY AND a_{S_2}

The compositional variation of atomic As (%) in arsenopyrite from Fosterville was from 33.1 to 36.4 atomic As (%) with an average value of 34.7 atomic As (%) for the 30 grains analysed. Also the atomic percentage of S ranged from 27.6 to 30.2 with the atomic percentage of Fe being very close to the stoichiometric value, which supports the accuracy of the analysis. From Figure 6.3, the temperature for the deposition of arsenopyrite in equilibrium with pyrite at Fosterville is 540 °C for the 30 arsenopyrite grains from 6 samples. This is obtained by taking the average atomic As (%) of arsenopyrite at Fosterville and extrapolating the temperature data onto Figure 6.3. This temperature of 540 °C for the arsenopyrite indicates a_{S_2} of $10^{-4.5}$ at the time of deposition (see Figure 6.4).

DISCUSSION

Temperature obtained from arsenopyrite geothermometry are approximately 170 °C higher than those obtained from fluid inclusion study (Part 3) for quartz. Pyrite and arsenopyrite in equilibrium is a low-temperature assemblage with a temperature of 491 ± 12 °C (Clark, 1960a). Also, the temperature range represented by greenschist facies metamorphic grade ranges from approximately 330 °C to 500 °C (Winkler, 1976). Possible reasons for the discrepancy for temperature values obtained from arsenopyrite geothermometry are:

- (1) disequilibrium existed between pyrite and arsenopyrite, although textural evidence suggests this is not so,
- (2) early arsenopyrite could have been epitaxially overgrown by younger arsenopyrite of different composition,
- (3) mineralization is pre-metamorphism (ie. pre-Tabberabberan Orogeny) and that the sulfides reequilibrated post-depositionally, and/or
- (4) fluid inclusion temperatures indicate minimum values for the temperature of the mineralizing fluids.

CONCLUSION

The average atomic As (%) obtained from Table 6.2 for arsenopyrite was 34.3. Extrapolation of this value on Figure 6.3 suggests lower a_{S_2} conditions for the Fosterville mineralization is required since no pyrrhotite was recorded at Fosterville. In other words, arsenopyrite was reequilibrated at lower a_{S_2} and/or higher temperature at Fosterville.

In this case, the arsenopyrite geothermometer has not been successful, therefore the temperature indicated by fluid inclusion study represents the minimum temperature of ore deposition at Fosterville.

PART 3 : FLUID INCLUSION STUDYINTRODUCTION

Study of fluid inclusions from gold mineralization systems provide valuable information on the nature and source of ore fluid and ore components and gold depositional conditions. Measurements of the homogenization temperature (T_h)¹ upon heating provides an indication of the temperature at which the fluids became trapped. T_h can be corrected for pressure effects during formation of the quartz veins to obtain the actual trapping temperature. Information on the composition of the fluids and salinity can be acquired by measuring the freezing point depression and first ice melt (1st T_m) or clathrate decomposition temperature ($T_{e-clathrate}$). 'Clathrates' are gas hydrates which are a result of interaction between the aqueous and non-aqueous phases.

Fluid inclusions were characterised using criteria defined by Roedder (1984) in order to distinguish between inclusions of primary origin and those of secondary origin. These criteria are:

Primary inclusions - usually have a large size,

- often occur as isolated inclusions, away from groups of inclusions,
- are randomly distributed within or along grain boundaries.

Secondary inclusions - usually small size ($< 10 \mu m$),

- occur in planar groups and grow across grain boundaries, and
- often occur as thin and flat inclusions.

¹ T_h - temperature at which the fluid inclusion becomes a homogenous phase, ie. temperature of disappearance of bubble in inclusion.

METHOD OF STUDY

Two samples (DDH 11/52.9 & DDH 12/43.0) from Fosterville were taken from quartz veins for fluid inclusion study. The quartz veins were chosen as they appeared to be related to the mineralization, known as phase 2 quartz veins (see chapter 3). Sample DDH 12/43.0 is from the oxidized and unmineralized zone and sample DDH 11/52.9 is from the primary zone and mineralized. Only 37 primary and secondary inclusions were measured (Table 6.3), because most of the inclusions in the samples, were very small and difficult to measure.

Sections used for this study were cut to less than 1 mm thickness and polished on both sides. The doubly polished plates were examined in detail under the petrographic microscope prior to microthermometric experiment. The reasons for this inspection was to :

- (1) identify inclusions of primary and secondary origins, and
- (2) classify inclusions into various types, depending on the nature of the phases within each inclusion.

The fluid inclusions were analyzed with the Fluid Inc. modified U.S.G.S. gas flow heating/freezing stage at the Geology Department of the University of Tasmania. The temperature uncertainty were ± 1 °C for heating and ± 0.3 °C for freezing measurements as the experiments were performed at least twice on one inclusion.

Sample No.	min. facies	Inclusion size	type	Au grade	flomarks	1st Tm	To-Clnthrate	Th (L-V)-L	Th CO ₂	NaCl eq. wt. %
DDH 11/52.9	quartz vein	20-25 μ	1	2.75 ppm	primary zone	-57.0	8.0	254.3	15.0	9.9
		20 μ	1			-58.0	8.6	254.1	16.7	2.8
		15-20 μ	1			-58.0	8.1	254.3	19.7	3.7
		<5 μ	2			-57.0	7.2	156.2	18.2	5.4
		10-15 μ	1			-58.0	6.5	254.2	16.2	6.6
		10 μ	1			-57.0	6.7	251.8	16.1	6.3
		20 μ	1			-58.0	7.6	255.8	14.6	4.7
		10 μ	1			-57.0	6.4	254.3	19.7	6.8
		10 μ	1			-57.0	5.9	253.7	13.6	7.6
		<5 μ	2			-50.0	3.9	169.8	18.8	10.7
		<5 μ	2			-49.0	2.4	169.2	18.5	12.8
		<5 μ	2			-56.0	4.9	152.5	15.4	9.2
		<5 μ	2			-56.0	4.8	152.7	15.2	9.4
		<5 μ	2			-57.0	7.1	141.5	15.0	5.6
		<5 μ	2			-56.0	5.0	172.8	18.8	9.1
DDH 12/43	quartz vein	<5 μ	2	0.01 ppm	oxidized zone	-57.0	7.2	178.8	19.1	5.4
		5-10 μ	1			-57.0	7.1	156.1	18.2	5.6
		<3 μ	2			-58.0	8.1	249.6	18.2	3.7
		<5 μ	2			-56.0	6.7	170.8	18.8	6.3
		<5 μ	2			-56.0	7.2	162.1	18.3	5.4
		<5 μ	2			-56.0	7.6	138.8	14.6	4.7
		<2 μ	2			-56.0	7.2	138.7	14.7	5.4
		~10 μ	1			-57.0	8.0	248.8	16.1	3.9
		<5 μ	2			-56.0	6.5	236.8	15.5	6.6
		5-10 μ	1			-58.0	8.6	252.3	14.8	2.8
		<5 μ	2			-56.0	4.6	172.9	18.9	9.7
		<2 μ	2			-57.0	7.1	156.1	18.2	5.6
		<2 μ	2			-56.0	5.1	235.7	15.6	8.9
		<2 μ	2			-57.0	7.0	210.8	15.0	5.7
		<5 μ	2			-57.0	7.8	210.2	14.8	4.7
	5-10 μ	1			-58.0	8.1	250.9	17.6	3.7	
	10 μ	1			-58.0	8.6	288.5	18.2	2.8	
	<5 μ	2			-57.0	5.3	224.6	15.5	8.8	
	<5 μ	2			-56.0	5.0	175.2	18.0	8.1	
	<3 μ	2			-56.0	4.8	180.1	17.9	9.4	

TABLE 6.3 Fluid Inclusion Data.

CLASSIFICATION OF INCLUSION TYPES

Fluid inclusions were classified according to the phases observed in the inclusions at room temperature (approximately 21 °C). Two types of inclusions were observed during this study (Plate 20):

- Type 1: Two-phase, liquid and vapour inclusions (vapour-rich), which homogenizes by expansion of vapour phase upon heating. Type 1 inclusions are generally large ($> 10 \mu$) and mostly ovoid in shape, although irregular shaped inclusions were also observed. These inclusions display clathration and fulfilled all the criteria of primary inclusions.
- Type 2: Three-phase CO₂-liquid bearing inclusions which contain CO₂-liquid, vapour bubble and H₂O liquid. Type 2 inclusion are generally small ($< 5 \mu$), have regular smooth shapes.

RESULTS

HOMOGENIZATION DATA

The Type 1, two-phase primary inclusions in vein quartz from Fosterville gave a homogenization temperature range of T_h (L-V)-L of 248.8 °C to 288.5 °C, with an average of 255 °C. The homogenization temperatures of the Type 2, three-phase, CO₂-liquid bearing secondary inclusions in vein quartz from Fosterville range from T_h (L-V)-L of 138.6 °C to 236.8 °C, with an average of 170 °C (see Figure 6.5).

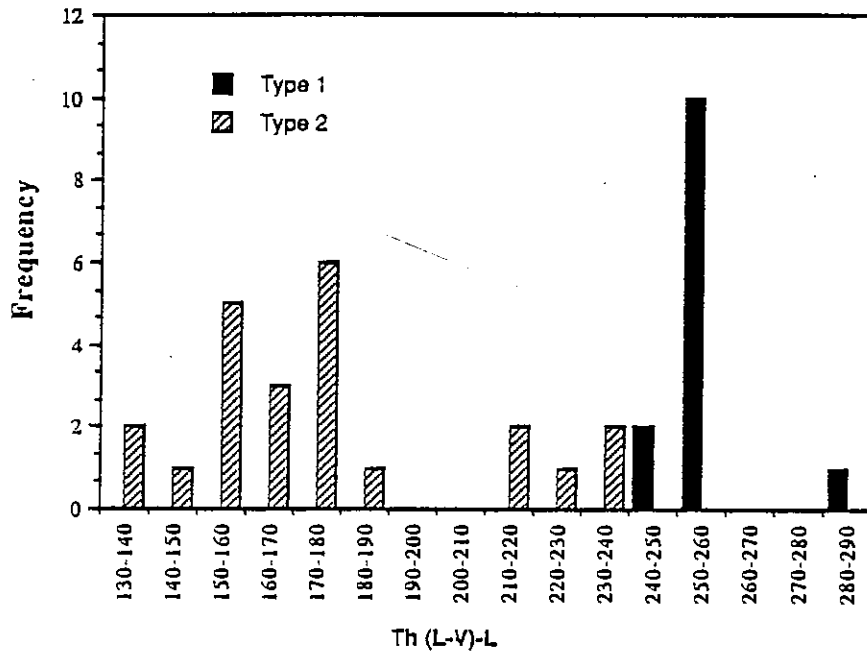


FIGURE 6.5 Distribution of Fluid Inclusion Homogenization Temperatures, (Th (L-V)-L) in °C.

FREEZING DATA

Freezing measurements are useful in obtaining salinity of fluids as the increasing concentrations of salts decreases the freezing point of water.

Type 1 and 2 inclusions display consistent behaviour on freezing. The salinity of the fluid can be calculated by freezing the inclusion and measuring the temperature at which clathrate decomposition occurs (Te-Clathrate) (see Table 6.3) and using the equation of Bozzo et al., 1973 as follows :

$$W_{\text{NaCl}} = 15.52022 - 1.02342 t - 0.05286 * t * t$$

where t - clathrate melting temperature, and

W_{NaCl} - weight percent NaCl in solution.

The salinity of the Type 1, two-phase, primary inclusions in the quartz from Fosterville were measured by clathrate decomposition temperatures, which vary from 5.9-8.6 °C (2.8 to 7.6 NaCl equivalent wt.%). Salinity of the Type 2, three-phase inclusions indicated clathrate decomposition temperature of 2.4-7.6 °C (4.7 to 12.8 wt.% NaCl) (see Figure 6.6).

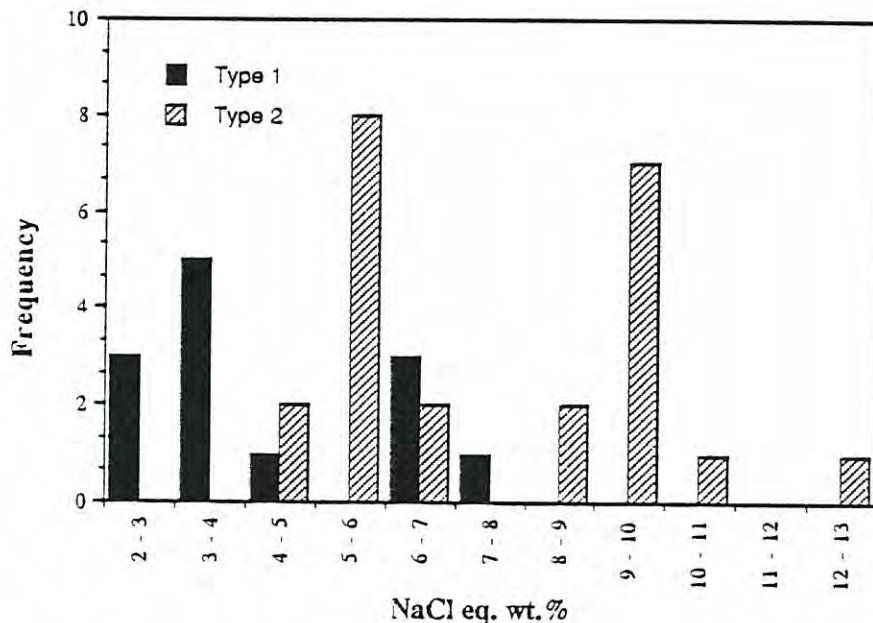


FIGURE 6.6 Distribution of Fluid Inclusion Salinity composition (NaCl eq. wt. %).

ESTIMATES OF CO₂ CONCENTRATION

The small, CO₂ liquid-rich inclusions have T_h CO₂ range from 14.6 °C to 19.1 °C with an average of 17.9 °C. By extrapolating the average T_h CO₂ value on the liquid-vapour curve of CO₂ by Burrass (1981) (see Figure 6.7), a pressure of 54 bars is obtained. The solubility of CO₂ in H₂O at 25 °C and 54 bars is 2.16 mole percent (Figure 6.8). Hence, the total wt.% of CO₂ dissolved in the H₂O phase in the three-phase, CO₂ liquid-rich inclusions is 9.5 wt.%.

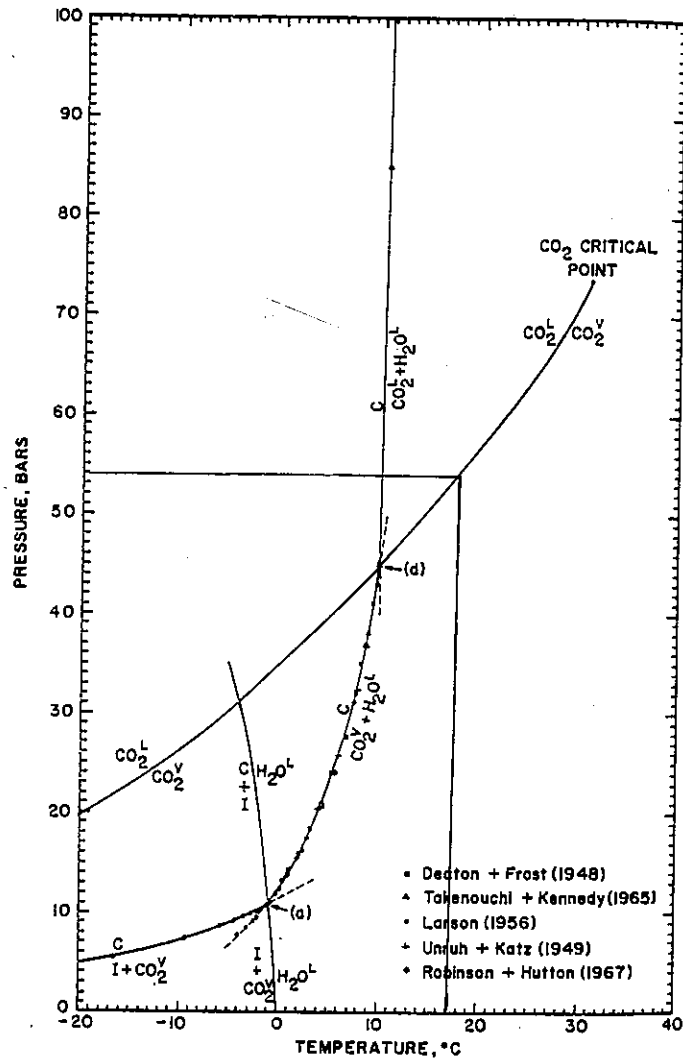


FIGURE 6.7 The quantitative CO₂-H₂O clathrate equilibria (After Buruss, 1981).

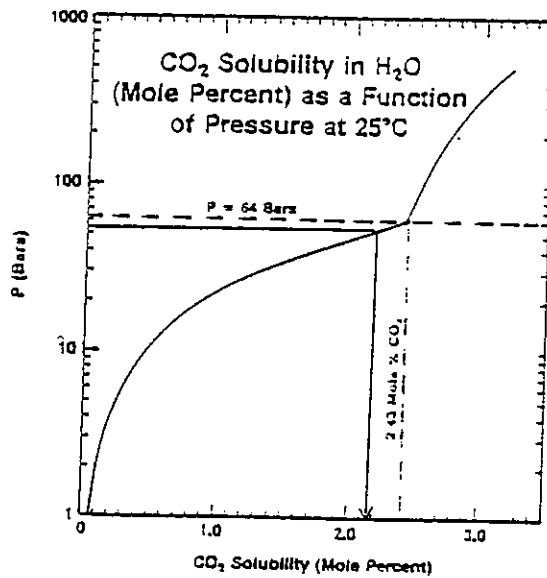


FIGURE 6.8 Solubility of CO₂ in H₂O as a function of pressure at 25 °C (After Bodnar et al., 1986).

ESTIMATES OF CH₄ CONCENTRATION

The melting point of solid CO₂ is -56.6 °C. Type 1, two-phase inclusions have average final melting of solid CO₂ (1st T_m) at -57.5 °C (Figure 6.9).

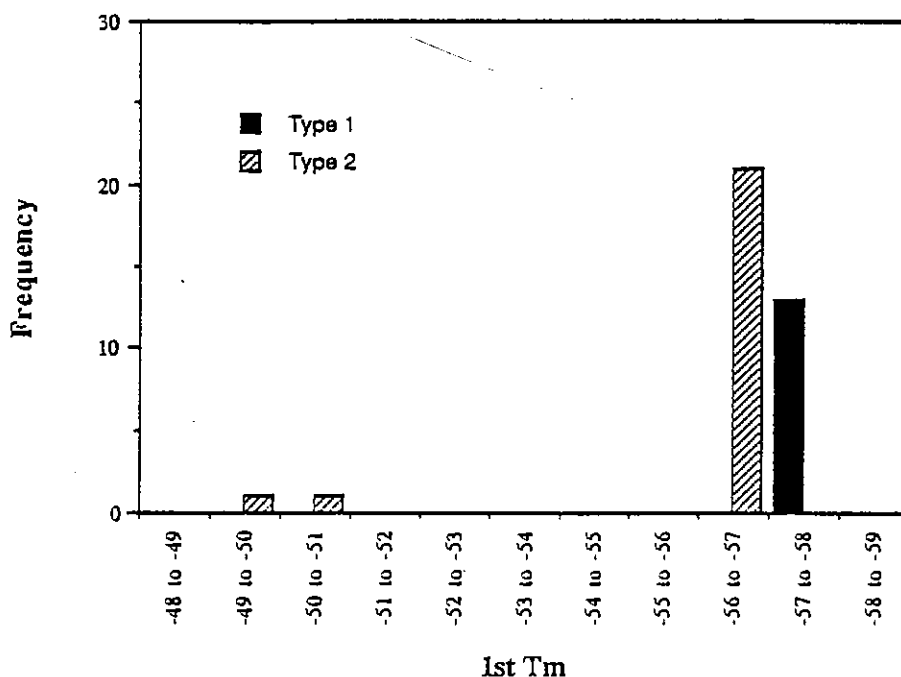


FIGURE 6.9 Distribution of Fluid Inclusion first melting temperature, (1st T_m) in °C.

Since the first T_m of Type 1 inclusions is lower than the melting point of solid CO₂, there is some other vapour phase (as well as CO₂) present in these inclusions. If it is assumed that the other vapour-phase is CH₄, N₂, etc, an estimate of the mole % CH₄ can be obtained from Figure 6.10. Homogenization temperatures of CO₂ (T_h CO₂) for Type 1 inclusions range from 13.6 to 19.1 °C, giving 8 to 10 mole % CH₄.

Type 2, three-phase, CO₂-liquid bearing inclusions have average final melting of solid CO₂ (1st T_m) at -56.7 °C which is similar to the melting point of solid CO₂ suggesting that there was no other vapour phases other than CO₂ present in these inclusions.

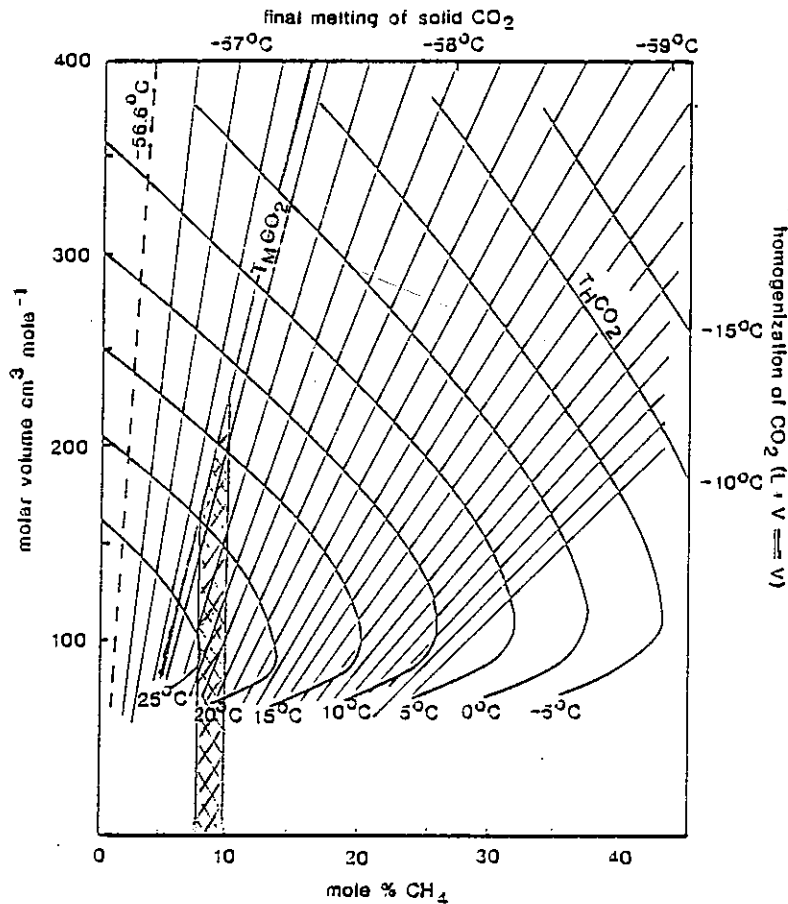


FIGURE 6.10 Graphs for calculating the mole composition of CO₂-CH₄ mixtures using the final melting of CO₂ (1st T_m) and the temperature of homogenization (Th (L-V)-L) (After Sheperd et al., 1985).

Hence, inclusions representing Type 1 phase, which is the original hydrothermal fluid, contains CH₄ as a component whereas Type 2 phase contains CO₂ as a component.

Actual trapping temperature of the inclusions is not equal to the homogenization temperature so a correction is required for a closed lithostatic system.

GEOBAROMETER

The presence of Type 2, CO₂ liquid-rich inclusions provide the basis for an estimation of pressure at Fosterville, since such fluids separate into two immisible components under normal hydrothermal temperature and pressure. The average density

of the CO_2 - rich fluid at Fosterville is approximately 0.6 g cm^{-3} . This was obtained by estimating the volume of each phase in the inclusion. From Figure 6.11, the pressure of trapping, for the average temperature (T_h) of 170°C , for 9.5 wt.% CO_2 is 2 ± 0.5 kbar.

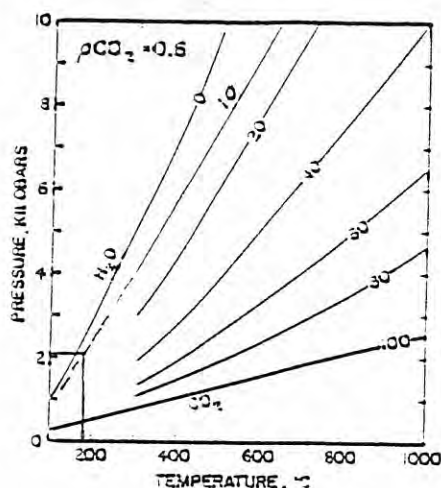


FIGURE 6.11 P-T diagram of bulk fluid isochores for mixed $\text{H}_2\text{O}-\text{CO}_2$ fluid inclusions. The values on the curves are volume % CO_2 for a CO_2 phase density of 0.6 gm/cc (After Brown & Lamb, 1986).

This pressure estimate will give a depth of approximately $8 \pm 2 \text{ km}$ from Figure 6.12. The calculated depth of $8 \pm 2 \text{ km}$ is reasonable since mineralization was pre-peak deformation and hence no overburden was removed at this time.

An alternate way of calculating depth is described below. There are no evidence for boiling of the fluids at Fosterville as fluid inclusions were observed only to homogenize to liquid. Therefore, using the average T_h (L-V)-L of Type 1 inclusions, which is 255°C , and assuming a geothermal gradient of $30-40^\circ\text{C/km}$ (in a granitic intrusive terrain such as Victoria), then a depth of $6.3-8.5 \text{ km}$ is obtained for the mineralizing system.

The homogenization temperature obtained for a fluid inclusion does not correspond to the temperature at which the fluid becomes trapped. This is due to the

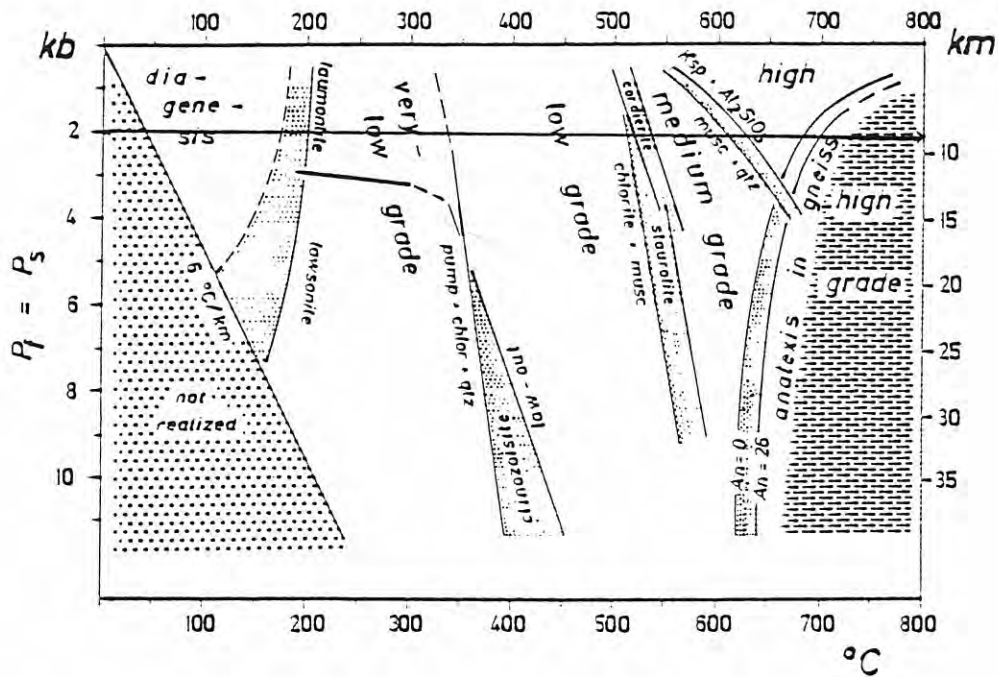


FIGURE 6.12 The four divisions of metamorphic grade representing maximum possible conditions (After Winkler, 1976).

effect of pressure (Roedder, 1984). The trapping temperature can be calculated from the homogenization temperature if the pressure and density of the fluid is known at the time of trapping.

The maximum homogenization temperature of the Type 1 inclusion was 288.5 °C, and hence the density of the fluid in the inclusion with 5 eq. wt. % NaCl is 0.9 g/cm³. This is obtained from extrapolating the data onto Figure 6.13. The pressure of 2 kbar and density of 0.9 g/cm³ gives an extrapolated value of 370 °C, for the trapping temperature of the inclusions (Figure 6.14).

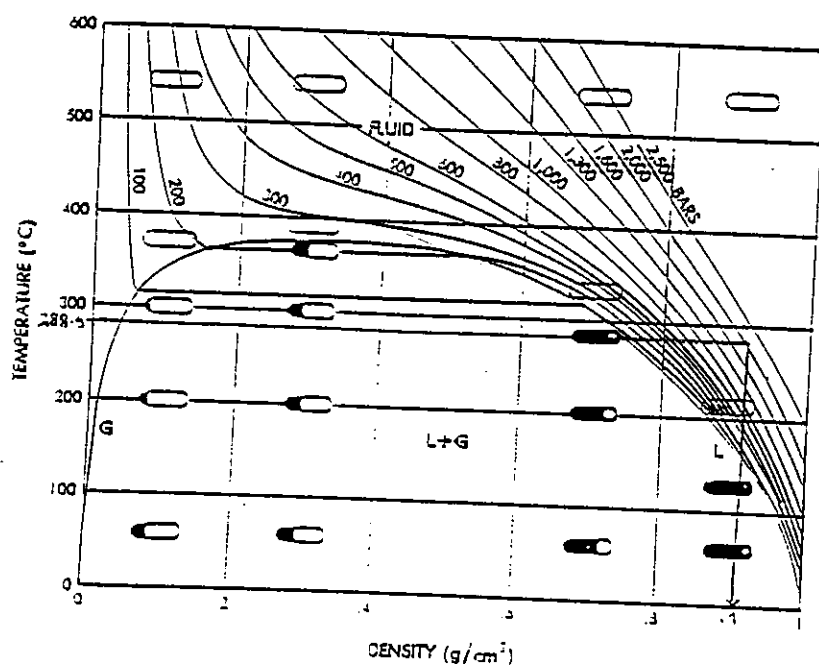


FIGURE 6.13 Temperature-density diagram for the system H₂O. The homogenization behaviour of four inclusions, all trapped at 540 °C (but at different pressures) is indicated. Liquid-black; gas-colourless; fluid-grey (After Roedder, 1984).

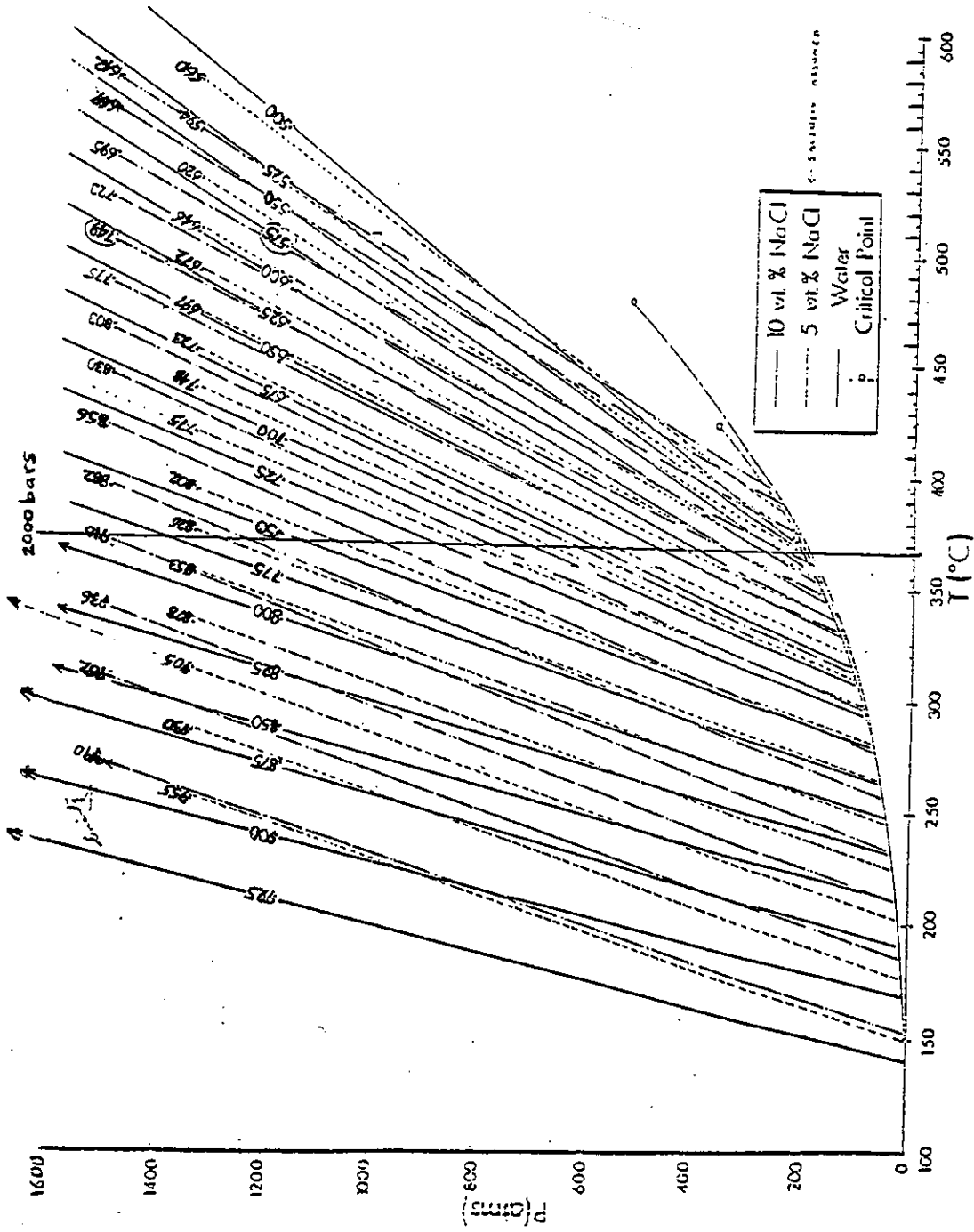


FIGURE 6.14 P-T-density relationships of water, 5 wt. % and 10 wt. %

NaCl solution (After Ohmoto & Rye, 1970).

DISCUSSION

The following conclusions can be made from the fluid inclusion studies on the Fosterville deposit:

- (1) The average homogenization temperature is at least 255 °C for vein quartz associated with mineralization and the trapping temperature obtained from the maximum homogenization temperature of 288.5 °C was 370 °C.
- (2) The Type 1 inclusions have a salinity of 2.8 to 7.6 NaCl equivalent wt.%, and the Type 2 inclusions have a salinity of 4.7 to 12.8 NaCl equivalent wt. %. The salinity of the fluids obtained seem higher than that of seawater, suggesting that another source is present for the higher salinity. This source could be a granite.
- (3) The Type 2 inclusions were enriched in CO₂ with a concentration of approximately 9.5 wt.%.
- (4) The pressure estimated from concentration of CO₂ and homogenization temperature of Type 2 fluid inclusions gave a minimum of 2 ± 0.5 kbar which is equivalent to a depth of 8 ± 2 km, and homogenization temperature from Type 1 fluid inclusions gave a depth of 6.3-8.5 km assuming a geothermal gradient of 30 - 40 °C/km which is not unusual if a granite source is situated beneath the Fosterville goldfield.
- (5) There is no evidence of boiling in the system at Fosterville.

Fluid inclusion studies at Avoca (Green, 1983) and Wattle Gully Mine (Cox et al., 1983) in the Ballarat Trough indicated that both aqueous and CO₂ or CH₄ fluids were present during auriferous reef formation. This is similar to the fluids present during auriferous reef formation at Fosterville.

PART 4 : GOLD-RICH ARSENOPYRITES

INTRODUCTION

Arsenopyrite-pyrite mineralization is restricted to the shear zones at Fosterville, where it is fine grained and disseminated. Arsenopyrite is typically euhedral with rhombic form and between 50 and 350 μm in length. The grains are randomly oriented, although star-shaped (rosettes) clusters are locally developed where the concentrations are high (Plate 21). Pyrite is usually present in association with arsenopyrite, typically as cubic crystals between 60 to 400 μm across. They are generally more common than arsenopyrite in the sediments.

Arsenopyrite is the main gold-bearing mineral in various hydrothermal deposits (Cathelineau et al., 1988), and this is the case for Fosterville. Pyrite also contains gold in the Fosterville deposit, but is in very low concentrations, therefore difficult to analyze.

This study focusses on the analysis, distribution and chemical state of gold in arsenopyrite and the possible correlation of As with Au at Fosterville.

METHOD OF STUDY

Five polished thin sections were examined and the arsenopyrite grains located and marked prior to electron microprobe analysis at the CSL, University of Tasmania. Electron microprobe analyses were carried out on the Cameca SX 50 electron microprobe under the following analytical conditions:

- accelerating voltage = 20 kV
- counting time for gold = 60 (peak)/ 30 (background) seconds
- detection limit for gold = 150 ppm

- counting time for other elements = 10/5 seconds

Systematic electron microprobe analyses were performed on a total of 14 arsenopyrite grains from five different samples from Fosterville. Each grain was analyzed at the core (C) and rim (R), presented in Table 6.4. The grains were analyzed for S, Fe, Cu, As, Au and Ag. The analyses of Fe, Cu and Ag are not included in the table.

Results from Table 6.4 show that arsenopyrite grains do not exhibit much variation for As and S between and within grains. As and S are strongly anticorrelated which is expected, considering the equation $Fe As_{1-x}S_{1+x}$.

Sample No.	Au (%)	As (%)	S (%)	At. conc. As
13/48.0-1C	0.000	48.254	17.153	35.96
-1R	B.D.L	48.459	16.763	36.32
-2C	0.000	48.428	16.687	36.47
-2R	0.000	47.549	16.926	35.88
-3C	0.000	47.787	16.670	36.04
-3R	B.D.L	49.214	16.006	37.53
-4C	0.000	47.998	16.654	36.26
-4R	0.000	48.599	16.174	36.92
-5C	0.000	49.155	15.999	37.28
-5R	0.000	48.377	16.317	36.69
13/71.4-1C	0.016	47.413	16.767	35.74
-1R	0.000	48.661	16.060	36.82
-2C	0.030	48.863	16.140	36.82
-2R	0.000	48.221	16.295	36.61
-3C	0.018	48.560	16.307	36.66
-3R	0.000	47.434	16.822	35.69
12/70.0-1C	B.D.L	46.456	16.641	35.06
-1R	0.000	48.864	15.458	37.25
-2C	0.000	48.005	15.654	36.58
-2R	0.000	48.522	15.310	37.20
13/42.5-1C	0.000	47.475	15.399	36.13
-1R	0.034	48.082	15.117	37.28
-2C	0.031	47.598	15.147	36.92
-2R	0.000	47.505	15.205	36.94
13/48.6-1C	0.000	46.765	17.285	34.95
-1R	B.D.L	47.320	16.884	35.77
-2C	0.028	45.823	17.779	34.31
-2R	B.D.L	47.286	16.798	35.78

TABLE 6.4 Electron microprobe analysis of arsenopyrite. C-core; R-rim:

B.D.L-below detection limit.

GOLD DISTRIBUTION

Gold grade is heterogeneous within arsenopyrite (from cores and rims), giving a range from below the 150 ppm detection limit up to 0.034% (340 ppm). This variable distribution of gold in arsenopyrite makes gold throughout the deposit highly variable. Assuming that the arsenopyrite occupies 3 to 5%, the whole rock would contain approximately 10 ppm Au. Pyrite grains were also analyzed for gold, but found Au to be below the detection limit.

Gold particles in the Fosterville field occurs both as fine granules < 1 to 50 μm in size, and within arsenopyrite and pyrite. Limited testing of sulfide material by Bendigo Gold Limited suggests that 70 to 80% of the gold is associated with arsenopyrite while the remaining 20 to 30% is within pyrite.

There is very good evidence of association between gold and arsenic, which is confirmed by fire assay results of the sediments. Drill holes were sampled over every 1 m interval and approximately 2 kg samples despatched for assay for Au. Drill hole DDH 13 analyzed for Au and As showed a very strong positive correlation (see Figure 6.15).

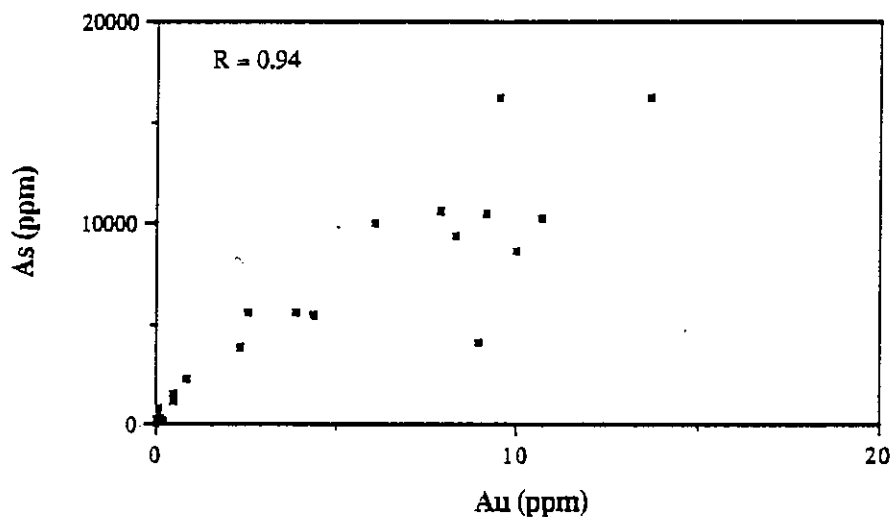


FIGURE 6.15 Scatter plot of As against Au in DDH 13.

Figure 6.16 shows a significant relationship between Au and As with depth for drill hole FO-10. The reason for the high correlation of Au and As at Fosterville is due to the presence of Au in arsenopyrite, and Au and As in pyrite.

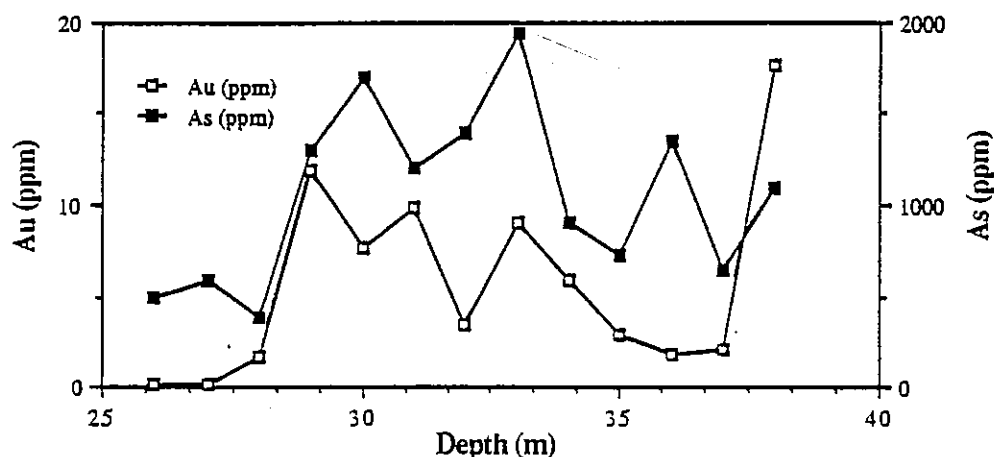


FIGURE 6.16 Line plot of Au and As with depth in FO 10.

Low concentrations of gold in arsenopyrite (such as at Fosterville) makes it difficult to analyze for gold by electron microprobe, and to determine the gold chemical state and distribution within the arsenopyrite grains. To overcome this problem, a multi-disciplinary approach has to be carried out on the arsenopyrite samples, using combined electron microprobe, secondary ion mass spectrometry, atomic absorption and Mossbauer spectroscopy (Cathelineau et al., 1988).

DISCUSSION

There are two possible chemical states of heterogeneously distributed gold in arsenopyrite. These are:

- (1) Gold present in the crystal lattice of arsenopyrite as Au-As bonds.
- (2) Gold present as very fine inclusions within the arsenopyrite and hence, which would be difficult to detected by electron microprobe.

Au-rich arsenopyrites crystallize at relatively low temperatures ranging from 170 to 250 °C (Cathelineau et al., 1988), which is within the observed homogenization temperature range of Fosterville fluid inclusions (part 3). Gold occurs also as fine grains in quartz veins and sediments (which were not observed in this study because the grains were too fine), and within arsenopyrite and pyrite, presumably as inclusions and within their crystal lattice (via electron microprobe analyses). For this reason, there is a good correlation between Au and As at Fosterville.

CHAPTER 7 - GENETIC MODEL AND EXPLORATION STRATEGY

INTRODUCTION

The present geochemical investigation involving sulfur isotope, fluid inclusion and gold geochemistry provides constraints on the origin of the Fosterville deposit and exploration implications. A possible genetic model can be proposed for the Fosterville gold deposit. A set of geological and geochemical criteria can be established for future exploration for similar types of deposits around the Fosterville area.

GENETIC MODEL

The genetic model for Fosterville depends on the sub-vertical fault along which hot solutions (~270 °C) travelled and precipitated gold and sulfides as a result of some physico-chemical changes, such as decrease in temperature and/or sulfur fugacity, occurring in the system. This resulted in a mineral deposit which is restricted to a zone, less than 30 m from the fault.

Ore occurs in brecciated shearzones and stockworks, which are of variable intensity and better developed in sandstones. Oxidation and associated ferruginization occurs to a depth of up to 45m; primary ore occurs below. These breccias and stockworks are usually developed on the east wall of the anticline. Bendigo Gold Limited is currently evaluating near-surface oxidized gold mineralization within the tenements. Deformation and mineralization may be contemporaneous at Fosterville. The shear zones are brittle-ductile and quartz veining is common as well as brecciation. A depth of approximately 6.5-10 km for the system has been obtained from fluid inclusion study.

The role of igneous rocks in the sedimentary rock-hosted gold deposits at Fosterville is genetically important. Firstly, the presence of quartz-feldspar-porphyry dyke at Robbins Hill, on the O'Dywer's line of mineralization, is associated with gold

mineralization and alteration. This dyke may serve as a source for metals and transporting solutions. Secondly, sulfur isotope study on pyrite from Fosterville indicate a magmatic source for the sulfur. Thirdly, the salinity of the fluid inclusions is high compared with seawater, suggesting a magmatic origin for the higher saline fluids. By considering all of the above, it is very likely that the mineralization at Fosterville and Central Ellesmere are related to igneous activity, such as a granite intrusion at some depth beneath the Fosterville goldfield.

The association of iron sulfides with the gold is a key element in the formation of the gold deposit at Fosterville. The gold is either in the crystal lattice or present as minute inclusions in the pyrite and arsenopyrite.

$\text{CO}_2\text{-CH}_4\text{-NaCl-H}_2\text{O}$ are the major components of the solutions from which gold precipitated. There is no evidence of boiling from fluid inclusions hence this is not a mechanism for gold precipitation in this deposit. Gold precipitation was probably due to decrease in sulfur fugacity as a result of precipitation of sulfides. This is reasonable to assume because the gold is incorporated in the sulfides in this deposit.

Romberger (1984) suggested that most hydrothermal solutions in equilibrium with pyrite never reach saturation with respect to gold and gold co-precipitates with sulfides. His suggestion was based on the high solubility of gold in bisulfide solutions (Seward, 1973) and the association between gold and pyrite in most primary ores.

EXPLORATION STRATEGY

Mineralization in the Fosterville field is fault controlled with the fault being the channel along which the gold bearing fluids moved. The shear zones and quartz stockworks acted as reservoirs for the gold.

The Fosterville fault widens into a series of splay faults as it transects the anticlines of the regional folds. Mineralization is intense in areas where sandstones dominate in the core of the anticline and where splay faults have a 300 - 320° orientation (White, 1988). There is also a strong geochemical association between Au

and As in general and trace element analysis of auriferous quartz veins have shown that Ge and paramagnetism of the quartz can be a useful indicator for Au mineralization. The presence of essentially submicroscopic sericite in the quartz and the associated Al, Na, K, Rb, Mg and to a certain extent Li content can also be used as an indicator of the presence of Au in the host rock.

The sets of structural and geochemical controls mentioned above may be useful in exploration for other similar types of deposits around the Fosterville area.

CHAPTER 8 - SUMMARY AND CONCLUSIONS

The rocks within the Fosterville goldfield consists of sandstones, siltstones and shales, of Lower Ordovician age (Lancefieldian), associated with the oxidized brecciated shear zones and associated stockworks of the Fosterville Shear Zone. The fault zone transgresses both fold axes and regional bedding. A quartz-feldspar-porphphyry dyke intrudes the sedimentary rocks at Robbin's Hill and is associated with sericite and carbonate alteration and gold mineralization, similar to alteration and mineralization found at Fosterville and Central Ellesmere.

The style of mineralization present at Fosterville and Central Ellesmere is a sedimentary rock-hosted gold deposit with gold mineralization along the Fosterville Fault Zone occurring in oxidized brecciated shear zones and associated stockworks and silicified sandstones, from surface to 30-45 m depth and primary ore zone below 45 m depth. The mineralized fault breccia and associated stockworks are vertical to sub-vertical and up to 30m wide.

No native gold was observed in drill cores or thin sections. The origin of the Fosterville gold deposit is considered to be genetically related to a granite source from evidence obtained from sulfur isotope study. From fluid inclusion study, the temperature of the mineralizing fluid was approximately 370 °C and the depth of the system was between 6.5-10 km. Gold in the Fosterville goldfield occurs within arsenopyrite and pyrite in crystal lattice and/or as fine native granules and in the quartz veins.

PIXE and AAS analyses have proved to be very useful in analyzing for low trace element concentrations in vein quartz, in particular of germanium and arsenic. The analyses showed positive correlations between the presence of K, Ge, Al and As with the Au in the host rock (analyzed by fire assay) and the intensity of the electron paramagnetic resonance of the quartz.

There is a highly significant positive correlation between the Ge content of the quartz and the intensity of its EPR absorption peak at $g = 2.0027$. The present study indicates that the centre is Ge-Al related. Literature search revealed that Ge is typically enriched in late magmatic and hydrothermal minerals.

The high correlation between Ge, Au and EPR suggests that EPR and Ge may be used as an indicator of gold mineralization in quartz-Au type deposits. In metamorphosed vein quartz systems which lose their paramagnetism through annealing, Ge can probably still be used as an indicator of the presence of gold, as vein quartz is unlikely to lose low level trace element concentrations during metamorphism.

The Al, K, Rb, Mg, Na, and to a lesser extent Li content are probably caused by inclusions of sericite in the vein quartz, and do correlate positively with the Au content of the host rock and the intensity of the EPR signal.

REFERENCES

- ANDERSON, J. H. & WEIL, J. A. 1959. Paramagnetic resonance absorption of colour centres in germanium - doped quartz. *J. Chem. Phys.* 31. p. 427-434.
- BALITSKIY, V. S., SAMOYLOVICH, M. I., TSINOBER, L. I. & ZUBKOVA, E. I. 1969. Some characteristics of the occurrence of Germanium in quartz crystals. *Geokhimiya*, No. 4. p. 421-427.
- BAMBAUER, Von H.U. 1961. Spurenelementgehalte and γ -Farbzentren in Quarzen aus Zerrklüften der Schweizer Alpen. *Schweizerische Mineralogische und Petrographische Mitteilungen*, vol. 4. p. 361-369.
- BARTON, Jr. P. B. & SKINNER, B. J. 1979. Sulfide Mineral Stabilities. In *Geochemistry of Hydrothermal ore deposits*. BARNES, H. L. (Ed.). p. 278-403.
- BLANKENBURG, Von H. J. & SCHROEN, W. 1982. The trace element content of volcanic agates. *Chem. Erde*, 41. p. 121-135.
- BOWEN, K. G. & WHITING, R. G. 1976. Gold in the Tasman Geosyncline, Victoria, in *Economic Geology of Australia and Papua New Guinea*. *Australas. Inst. Min. Metall.* 1. Metals. p. 647-658.
- BOZZO, A. T., CHEN, R. & BARDUHN, A. J. 1973. The properties of hydrates of chlorine and carbon dioxide, in 4th International Symposium on Fresh Water from the Sea; (DELYANNIS, A. & DELYANNIS, E. eds.). vol. 3. p. 437-451.
- BURRASS, R. C. 1981. Analysis of fluid inclusions: phase equilibria at constant volume. *Am. J. Sci.* vol. 281. p. 1104-1126.
- CAS, R. A. F. 1983. Palaeogeographic and tectonic development of the Lachlan Fold Belt of southeastern Australia. *Geol. Soc. Aust. Spec. Publ.* 10.
- CAS, R. A. F. & VANDENBERG, A. H. M. 1988. In *Geology of Victoria* (DOUGLAS, J. G. & FERGUSON, J. A. (ed.)). 663 pp.

- CATHELINÉAU, M., BOIRON, M. C., HOLLINGER, Ph. & MARION, Ph. 1988. Gold-rich arsenopyrites: Crystal-chemistry, gold location and state, physical and chemical conditions of crystallization. *Bicentennial Gold 88*. p. 235-240.
- CHACE, F. M. 1949. Origin of the Bendigo saddle reefs with comments on the formation of ribbon quartz. *Econ. Geol.* **44** (7). p. 561-597.
- CLAPPISON, R. J. S. 1965. The relationship of structure and ore deposition at Stawell goldfield, Victoria. *Proc. Austr. Inst. Mining Metallurgy*, v. **195**. p.1-9.
- CLARK, L. A. 1960a. The Fe-As-S System: Phase Relations and Applications. *Economic Geology*. vol. **55**, No. 7. p. 1345-1381.
- CLARK, L. A. 1960b. Arsenopyrite As:S ratio as a possible geobarometer. *Bull. Geol. Soc. Amer.* **71**, p. 1844 (Abstr.).
- CLAYTON, E. 1986. PIXAN: The Lucas Heights PIXE Analysis Computer Package, Report AAEC/M113. *Aust. At. Comm., Lucas Heights*.
- COX, S. F., WALL, V. J., ETHERIDGE, M. A., SUN, S. S. & POTTER, T. F. 1983. Gold-quartz mineralization in slate belts: the Castlemaine - Chewton example. *Geol. Soc. Austr. Abstracts*, No. 9. p. 260-261.
- CUBITT, J. M. & BUREK, C. V. 1980. A Bibliography of Electron Spin Resonance. Applications in the Earth Sciences. 64 pp.
- FISHER, R. & YATES, F. 1963. Statistical Tables, 6th edition. Oliver and Boyd, Edinburgh. 146 pp.
- FRIEBELE, E. J. & GRISCOM, D. L. 1979. Radiation effects in glass, in TOMOZAWA, M. & DOREMUS, R. H. (eds.). *Treatise on materials science*, vol. 17. New York, Academic Press, p. 257-351.
- FRITZ, J. S. & SCHENK, G. H. 1979. Quantitative Analytical Chemistry. 4th ed. 661 pp.
- FRONDEL, C. 1962. Silica Minerals, Volume III. The System of Mineralogy. Wiley, New York. 334 pp.

- FUKUCHI, T., IMAI, N. & SHIMAKOWA, K. 1986. ESR dating of fault movement using various defect centres in quartz; the case in the Western South Fossa Magna, Japan. *Earth & Planetary Sci. Letter*, **78**. p. 121-128.
- GADSDEN, J. A. 1975. *Infrared Spectra of Minerals and Related Inorganic Compounds*. London: Butterworths. 277 pp.
- GARRISON, E. G., ROWLETT, R. M., COWAN, D. C. & HOLROYD, L. V. 1981. ESR dating of ancient flints. *Nature*, vol. **290**. p. 44-45.
- GRAY, D. L. 1988. In *Geology of Victoria* (DOUGLAS, J.G. & FERGUSON, J.A. (ed.)). 663 pp.
- GREEN, N. 1983. *Geology and Geochemistry at Fiddlers Creek: Unpublished Honours thesis*. University of Melbourne, p. 39.
- GRISCOM, D. L. 1980. Electron spin resonance in glasses. *J. Non-Crystalline Solids*. **40**. p. 211-272.
- GULSON, B. L., ANDREW, A. S., MIZON, K. J., KEAYS, R. R. & STUWE, K. 1988. Source of Gold in Ballarat Slate Belt deposits and Potential Exploration Applications. *Bicentennial Gold 88*. Geological Society of Australia Inc. Abstracts No. 22. p. 331-337.
- HAYDON, R. C. (pers. comm.) Chief Geologist (Fosterville Gold Project). Bendigo Gold Ltd.
- HAMDORF, D. J. 1987. *Geochemical Exploration for Gold in the Mount Read Volcanics: Elliott Bay, South West Tasmania. Unpub. Hons. Thesis*. University of Tasmania.
- HEDENQUIST, J. W. & HENLEY, R. W. 1985. Hydrothermal eruptions in the Waiotapu geothermal system, New Zealand: Their origin, breccia deposits and effect on precious metal mineralization. *Econ. Geol.* vol. **80**, no. 6. p. 1640-1668.
- IKEYA, M. 1985. Dating Methods of Pleistocene Deposits and their problems: IX. Electron Spin Resonance. *Geoscience Canada, Reprint Series*. **2**. p 73-87.

- IKEYA, M., DEVINE, S. D., WHITEHEAD, N. E. & HEDENQUIST, J. W. 1986. Detection of methane in geothermal quartz by ESR. *Chem. Geol.* **56**. p. 185-192.
- IMAI, N., SHIMAKOWA, K. & HIROTA, M. 1985. ESR dating of volcanic ash: *Nature*, v. **314**. p. 81-83.
- KENNEDY, G. C. 1950. A portion of the system silica - water. *Econ. Geol.* **45**. p. 629-653.
- KING, B.C., BLACKBURN, W.H. & DENNEN, W.H. 1987. Inferences drawn from clear and smoky quartz in granitic rocks. *Neues Jahrbuch Miner. Abh.* vol..**156** (3). p. 325-341.
- KRETSCHMAR, U. & SCOTT, S. D. 1976. Phase relations involving arsenopyrite in the system Fe-As-S and their Applications. *Canadian Mineralogist.*, vol. **14**. p. 364-386.
- KRUPP, R. E. & SEWARD, T. M. 1987. The Rotokawa Geothermal System, New Zealand: An active epithermal gold - depositing environment. *Econ. Geol.* **82**, No. 5.
- LEYDERMAN, J. A., WEIL, J. A. & WILLIAMS, J. A. S. 1985. Generation of Paramagnetic centres in crystalline quartz by ultraviolet irradiation. *J. Phys. Chem. Solids*, **46**, No. 4. p. 519-522.
- MANN, A. W., FARDY, J. J. & HEDENQUIST, J. W. 1986. Major and trace element concentrations in some New Zealand geothermal waters. *Proceedings of Symposium 5: Volcanism, Hydrothermal Systems and Related Mineralization. Feb., 1986.*
- MASCHMEYER, D. & LEHMANN, G. 1983. New hole centres in natural quartz. *Phys. Chem. Minerals.* **10**. p. 84-88.
- MATYASH, I. V., BRIK, A. B., MONAKOV, V. I. & DERSKII, L. I. 1982. Formation of native gold in quartz according to EPR data. *Geokhimiya*. p. 1048-51.

- McANDREW, J. & MARSDEN, M. A. H. 1973. Regional Guide to Victorian Geology, 2nd Edition. 224 pp.
- McCONACHY, G. W. 1988. Fosterville. *Bicentennial Gold 88, Excursion No. 2 Guide: Central Victoria*. p. 7-11.
- McMORRIS, D. W. 1970. ESR detection of fossil alpha damage in quartz. *Nature*. vol. 266. p. 146-148.
- MILLER, W. S., DACHILLE, F., SHAFER, E. C. & RUSTUM, R. 1963. The system $\text{GeO}_2 - \text{SiO}_2$. *The American Mineralogist*, vol. 48. p. 1024-32.
- MOREY, G. W. 1957. The solubility of solids in gases. *Econ. Geol.* vol. 52. p. 225-251.
- ODOM, A. L. & RINK, W. J. 1989. Natural accumulation of Schottky-Frenkel defects: Implications for a quartz geochronometer. *Geology*, vol. 17. p. 55-58.
- OHMOTO, H. & RYE, R. O. 1979. Isotopes of Sulfur and Carbon. In *Geochemistry of Hydrothermal ore deposits*. BARNES, H. L. (Ed.). p. 509-567.
- ONISHI, H. & SANDELL, E. B. 1955. Geochemistry of arsenic. *Geochim. Cosmochim. Acta.* 7,1.
- O'SHEA, A. H. 1987. Geochemistry of the alkaline chloride hot springs. *Unpub. Hons. Thesis*, University of Tasmania.
- POOLE, C. P. (1983). *Electron Spin Resonance*, 2nd edition. A Comprehensive Treatise on Experimental Technique. 780 pp.
- POTY, B. 1969. La croissance des cristaux de quartz dans les Filous sur l'exemple du Filou de La Gardette (Bourg d'Oisais) et des Filous du massif du Mont Blanc. *Science de la Terre*, vol. 17. 166 pp.
- RAMSAY, W. R. H. & WILLMAN, C. E. 1988. In *Geology of Victoria*. (DOUGLAS, J. G. & FERGUSON, J. A. (ed)) 663 pp.
- RAMSAY, W. R. H. & VANDENBERG, A. H. M. 1986. Metallogeny and tectonic development of the Tasman Fold Belt system in Victoria. *Ore Geol. Rev.* 1, p. 213-257.

- ROBINS, G. V., SEELEY, N. J., McNEIL, D. A. C. & SYMONS, M. C. R. 1981. Manganese (II) as an indicator of ancient heat treatment in flint. *Archaeometry*, 23. p. 322-332.
- ROEDDER, E. 1984. Fluid inclusions: Reviews in mineralogy, vol. 12. (RIBBE, P. H. series ed.) *Mineralogical Soc. America*. 644 pp.
- ROMBERGER, S. B. 1984. Mechanisms of deposition of gold in low temperature hydrothermal systems: Association of Exploration Geochemists, Program with Abstracts.
- SANDIFORD, M. & KEAYS, R. R. 1986. Structural and tectonic constraints on the origin of gold deposits in the Ballarat Slate Belt, Victoria. In Turbidite hosted gold deposits (KEPPIE, J.D., BOYLE, R. W. & HAYNES, S. J. (eds)). *Geol. Soc. Canada Spec. Pap.* 32. p. 15- 24.
- SCHERBAKOVA, M. Y., SOTNIKOV, V. I., PROSKURYAKOV, A. A., MASHKAVTSEV, R.I. & SOLTNTSEV, V. P. 1976. Use of quartz EPR spectra in the analysis of ore content (as exemplified by gold-ore and copper molybdenum mineralization). *Geologiya Rudnykh Mestorozhdenii*, 18, p. 63-69 (in Russian).
- SCHNADT, R. & RAUBER, A. 1971. Motional effects in the trapped - hole center in smoky quartz. *Solid State Communications*, vol. 9. p. 159-161.
- SCHROEN, W. 1968. Ein Beitrag zur Geochemie des Germaniums: I Petrogenetische Problems. *Chem. Erde*. 27. p. 193-231.
- SCHROEN, W. 1969. Zur Geochemie des Germaniums und des Indiums. *Mineralogie-Lagerstättenlehre*, C 246. 122 pp.
- SEWARD, T. M. 1973. Thiocomplexes of gold and the transport of gold in hydrothermal ore solutions: *Geochimica et Cosmochimica Acta*, v. 37, p. 379-399.
- SHIMAKOWA, K., IMAI, N. & HIROTA, M. 1984. Dating of volcanic rock by electron spin resonance. *Isotope Geoscience*. 2. p. 365-373.

- SHIMAKOWA, K. & IMAI, N. 1985. ESR dating of quartz in tuff and tephra. *ESR Dating and Dosimetry* (IONICS, TOKYO). p. 181-185.
- SPENCER-JONES, D. & VANDENBERG, A. H. M. 1976. The Tasman Geosyncline in Victoria; In *Economic Geology Australia and Papua New Guinea. 1. Metals. Australas. Inst. Min. Metall.* p. 637-646.
- TAYLOR, P. C., BAUGHER, J. F. & KRIZ, H. M. 1975. Magnetic Resonance Spectra in Polycrystalline Solids. *Chem. Rev.* 75. p. 203-239.
- TIKHOMIROVA, V. V. 1966. Geochemistry of Ge in a polymetallic deposit. In: *Mineral raw material*, issue 14, Moscow.
- UZUMASA, Y., NASU, Y. & TOSHIKO, S. 1959. Chemical investigation of hot springs in Japan. XLIX. Germanium content of hot springs. *Nippon Kagaku Zasshi*, 80. p. 1118- 1128.
- VAN MOORT, J. C. 1987. Electron paramagnetic powder spectra of natural vein quartz in Tasmania, especially related to mineralization. *Proc. Pacific Rim Congress, '87.* Australas. Inst. Min. Metall. p. 437-444.
- VAN MOORT, J. C. 1989. The use of EPR powder for the characterization of vein quartz. *Proc. 23rd Symp., Advances in the study of the Sydney Basin, Newcastle.* p. 271-278.
- VAN MOORT, J. C. & RUSSELL, D. W. 1987. Electron Spin Resonance of Auriferous and Barren Quartz at Beaconsfield, Northern Tasmania. *Journal of Geochemical Exploration*, 27. p. 227-237.
- VAN MOORT, J. C. & BARTH, W. H. 1987. EPR powder spectra of some natural quartzes. *Proc. and Abstr. Solid State Symp., Chemistry Division, D.S.I.R., Wellington.* p. 21-24.
- VAN MOORT, J. C. & BARTH, W. H. 1989. The application of paramagnetic to the characterisation of vein quartz. *Proc. International Symposium on Petrogenesis and Mineralization of Granitoids.* (Institute of Geochemistry Academia Sinica, Guangzhon), in press.

- VAN MOORT, J. C. & BRATHWAITE, R. L. 1988. Electron Paramagnetic Resonance spectra of epithermal quartz from the Martha Hill gold-silver deposit, Waihi, New Zealand. *Bicentennial Gold 88*. p. 575-578.
- VAN MOORT, J. C., COHEN, D. D, RUSSELL, D. W. & KATSAROS, A. (in press). Correlations between chemical composition as determined by PIXE and the paramagnetism of auriferous vein quartz. Nuclear Instruments and Physical Research.
- WEDEPOHL, K. H. 1978. *Handbook of Geochemistry*. vol. 11-3. Elements Cr (24) to Br (35). Springer - verlag, Berlin, Heidelberg, New York.
- WEIL, J. A. 1984. A review of Electron spin Spectroscopy and its application to the study of Paramagnetic defects in Crystalline quartz. *Phys. and Chem. of Minerals*, 19. p. 149-165.
- WERTZ, J. E. & BOLTON, J. R. 1986. Electron Spin Resonance. Elementary Theory and Practical Applications. Chapman and Hall, New York, NY. 487 pp.
- WHITE, S. H. 1988. Report to Bendigo Gold Limited on the overall structural controls on gold mineralization in the Fosterville prospect. 8 pp.
- WILMSHURST, T. H. 1967. Electron Spin Resonance Spectrometers. (ed.). p. 1-61.
- WINKLER, H. G. F. 1976. Petrogenesis of metamorphic rocks, 4th edition. Springer-Verlag, New York, Heidelberg, Berlin. 334 pp.
- YIP, K. L. & FOWLER, W. B. 1975. Electronic structure of E' centers in SiO₂. *Phys. Rev. B*. 11. p.2327-2338.
- ZAVOISKII, E. 1945. Paramagnetic relaxation of liquid solutions for perpendicular fields. *Journal of Physics*, Vol.. IX, No. 3. p. 211-216.

APPENDIX 1

TRACE ELEMENT ANALYSIS IN QUARTZ BY A.A.S.

Li, Na, Mg, Al, Zn, Rb, Sr, K, Fe, Ti,

PREPARATION:

Clean laboratory benches and the fume cupboard.

Clean PTFE (teflon) beakers and glassware with HNO_3/HCl .

Heat beakers containing acid and soak volumetric ware overnight at room temperature.

Rinse many times with distilled water.

DIGESTION:

(a) Weigh 1.000g sample (first cleaned in HNO_3 and washed with distilled H_2O) into a clean PTFE beaker.

(b) Add 10 ml hydrofluoric acid and 1 ml nitric acid (A.R. reagents).

(c) Heat on ceramic hotplate until dry.

(d) Add 2ml nitric acid and evaporate dry.

(e) Add 5ml of 10% hydrochloric acid to dissolve all residue. Warm, shake then cool solution. Dilute to 25 ml in a volumetric flask, washing contents of beaker thoroughly with distilled water. (25 x dilution)

Note: Prepare two blanks (reagents only) with each batch of 20-25 samples using the same distilled water.

AAS STANDARDS:

Prepare one litre of 10% HCl acid (100ml conc. HCl /litre).

1000 ppm stock (Li, Na, Mg, Zn, Rb, Sr, K, Fe.)

Weigh the reagents into separate 100ml beakers. Add acid slowly and take care.

If heating is required make sure the solution does not boil over.

Dissolve: 2.662g Li_2CO_3 in ~20% HNO_3

1.2709g NaCl in distilled water

0.5000g clean Mg ribbon in a few ml. 10% HCl

0.5000g Zn metal in 20ml of 1:1HCl

1.4148g RbCl in distilled water

1.2077g $\text{Sr}(\text{NO}_3)_2$ in distilled water

0.9545g KCl in distilled water

0.500g Merck Fe powder in 10ml of 1:1 HCl

Wash each into a 500ml volumetric flask. Make up to mark with water and shake well.

Store in polythene bottle. Date.

0, 0.25, 0.5, 1.0, 2.5, 5.0 ppm Li, Na, Mg, Zn, Rb, Sr, K, Fe (in 2% HCl)

From 1000 ppm stock solution prepare a 25 ppm solution.

Dilute, 5ml 1000 ppm stock ---> 200ml volumetric flask containing 40ml of 10% HCl.

Using 25 ppm solution:-

5 ppm stock

Pipette 20ml of 25 ppm ---> 100ml volumetric flask containing 20ml of 10% HCl

2.5 ppm

Pipette 10ml of 25 ppm ---> 100ml volumetric flask containing 20ml of 10% HCl

1.00 ppm

Pipette 4ml of 25 ppm ---> 100ml volumetric flask containing 20ml of 10% HCl

0.5 ppm

Pipette 2ml of 25 ppm ---> 100ml volumetric flask containing 20ml of 10% HCl

0.25 ppm

Pipette 2ml of 25 ppm ---> 200ml volumetric flask containing 40ml of 10% HCl

0 ppm

Pipette 0ml of 25 ppm ---> 100ml volumetric flask containing 20 ml of 10% HCl

Store standard solutions in polythene bottles.

ALUMINIUM:

1000 ppm Dissolve 0.5000g Al powder in 2M HCl. Dilute to 500 ml.

100 ppm Al Pipette 10ml ---> 100ml volumetric flask containing 20ml of 10% HCl

50 ppm Al Pipette 5ml ---> 100ml volumetric flask containing 20ml of 10% HCl

25 ppm Al Pipette 2.5ml ---> 100ml volumetric flask containing 20ml of 10% HCl

10 ppm Al Pipette 2.0ml ---> 200ml volumetric flask containing 40ml of 10% HCl

TITANIUM:

1000 ppm Dissolve 1.8491g potassium titanium oxalate in distilled water. Dilute to 250ml. The 1000 ppm stock solution is then diluted similar to Aluminium to prepare 100, 50, 20 and 10 ppm standard solutions.

APPENDIX 2

Some EPR spectra typical of the quartz samples from the Fosterville goldfield showing significant paramagnetism. The broad V-shaped peaks at 326.5 ± 5 mT show the most detail. The peaks have shoulders and are not smooth, hence may be composed of at least five smaller, overlapping peaks. One paramagnetic centre can produce more than one peak (Wertz & Bolton, 1972) so the presence of five peaks does not necessarily mean there is presence of five different types of paramagnetic centres. The ± 100 and ± 250 mT peaks are virtually featureless at Fosterville unlike the spectra at Beaconsfield (van Moort & Russell, 1987) and Waihi, New Zealand (van Moort & Braithwaite, 1988).

g values of these signals have been calculated using the ESR marker. When high accuracy is required, the g value is measured by using the magnetic field calibration device. Where high accuracy is not required, measurements can be carried out by using ESR marker as follows: Mn^{2+} in $MgCO_3$ is used as internal ESR marker, containing six ESR signals. Among these, the g value of the fourth signal is $g = 1.981$. With the JES-UCX-2 type cavity resonator, this value remains constant over the cavity resonance frequency range of 9,200 to 9,400 GHz. Let us assume that the measured sample and ESR marker signals have been recorded simultaneously and that data such as shown in Figure 1 is obtained. ΔB represents distance between signal of sample and fourth signal which can be obtained by means of proportional calculation.

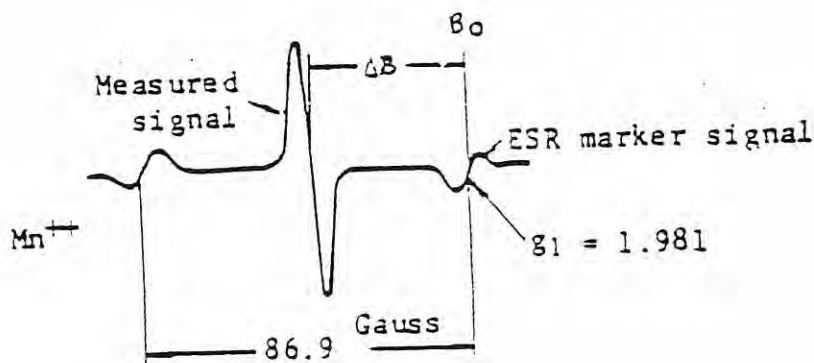


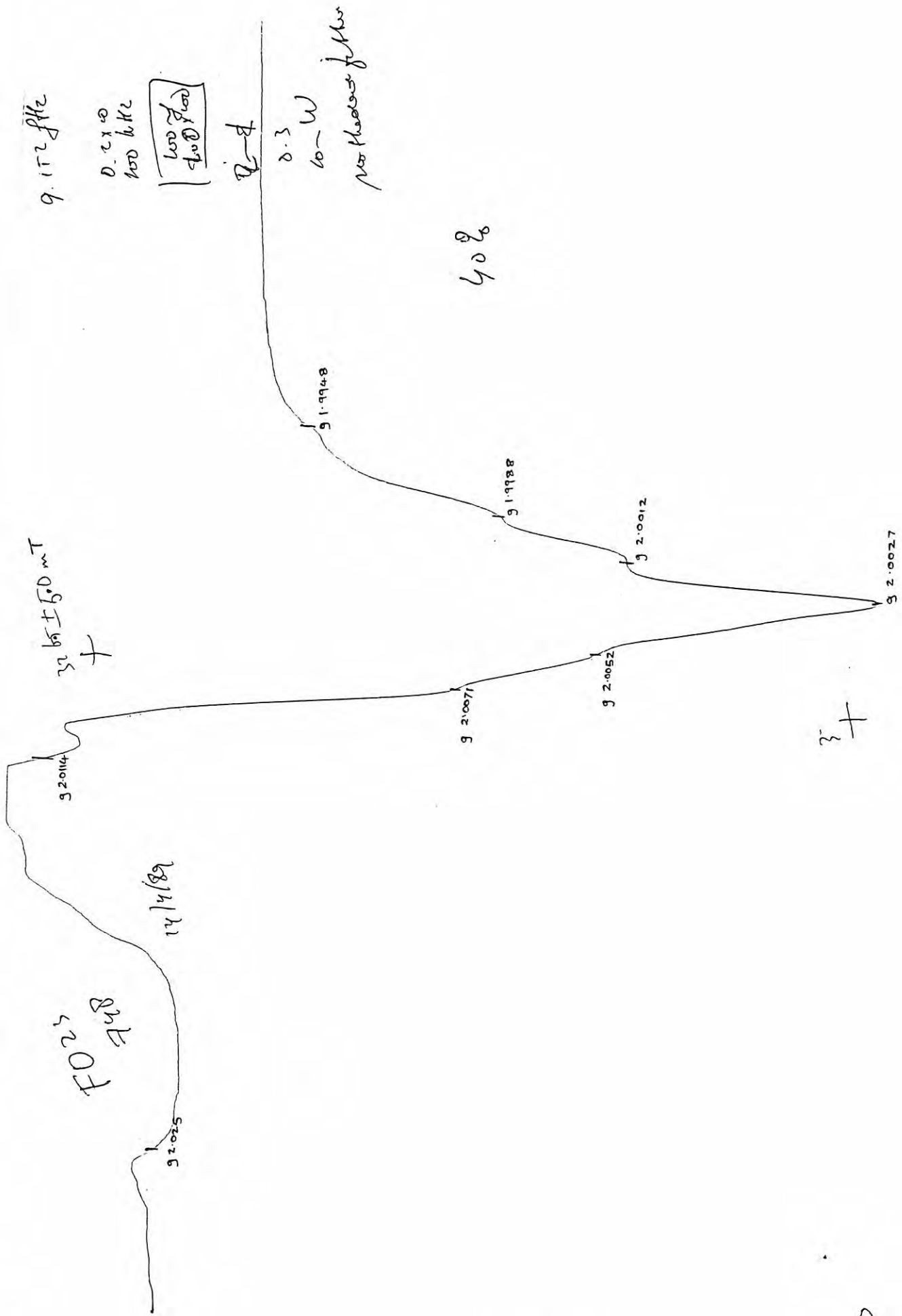
FIGURE 1 Simultaneous recording.

When ΔB is known, the g value of sample can be obtained by;

$$\begin{aligned}
 h\nu &= g_1 \beta B_0 \\
 &= g \beta (B_0 - \Delta B) \\
 g &= \frac{h\nu}{\beta (B_0 - \Delta B)} \\
 &= \frac{h\nu / \beta}{(h\nu / g_1 \beta) - \Delta B} \\
 &= \frac{g_1 \beta B_0}{\beta (B_0 - \Delta B)}
 \end{aligned}$$

The ESR spectrometer in the CSL is subject to sudden drift in the intensity of the magnetic field, which requires calibration of the calculated g values against known spectra necessary. g values in the range 2.3 - 4.0 can be given only to the first decimal because of lack of standards.

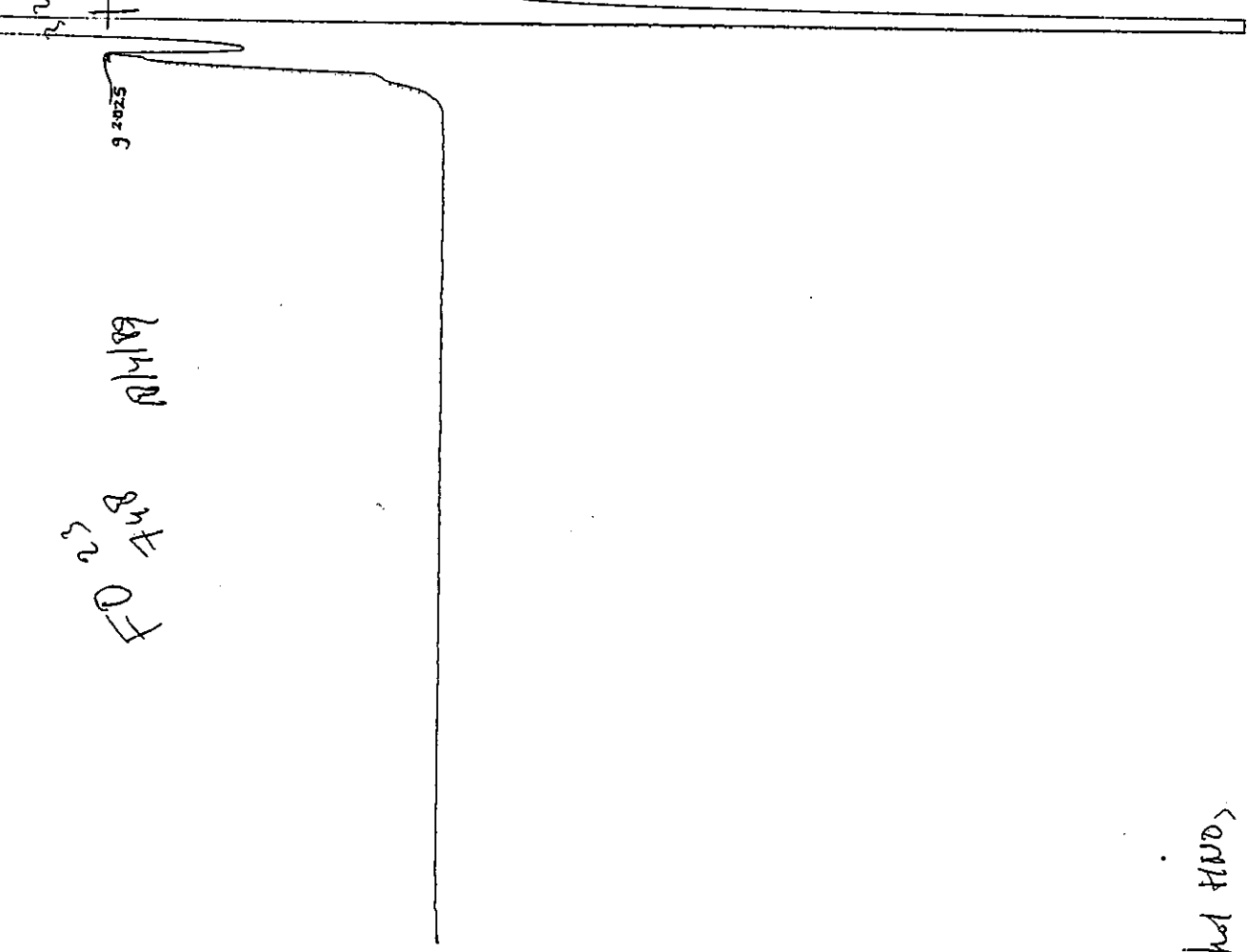
The g values obtained from the observed spectra were 1.995, 1.999, 2.001, 2.003, 2.005, 2.007 and 2.4. The strong signal at g 2.003 (i.e. the peak minimum) is the centre of unknown origin sometimes called "peroxy centre". The shoulder representing g 2.001 is attributed to the oxygen vacancy called E' and g 1.999 could be $[\text{GeO}_4]^0$.



22 bit I 1000 mt

FD 23
4h8
8/1/89

9 2025



9.1 r2 f H2

0.2 x 10
600 H2

$$\frac{600 \cdot 2}{2.1 \times 100} = \frac{1200}{210} = 5.714$$

~~4.2~~ f8.

2.5 W

90 W
... 1000000

had HIND>

9.152 of Hz

2.2 x 10

100 kHz

600 ft
2-T (wood)

0.3

4m-166

10m W

no pressure failure

32.188 + 2.500 m-T

3.2-0027

18/4/89

F023
748

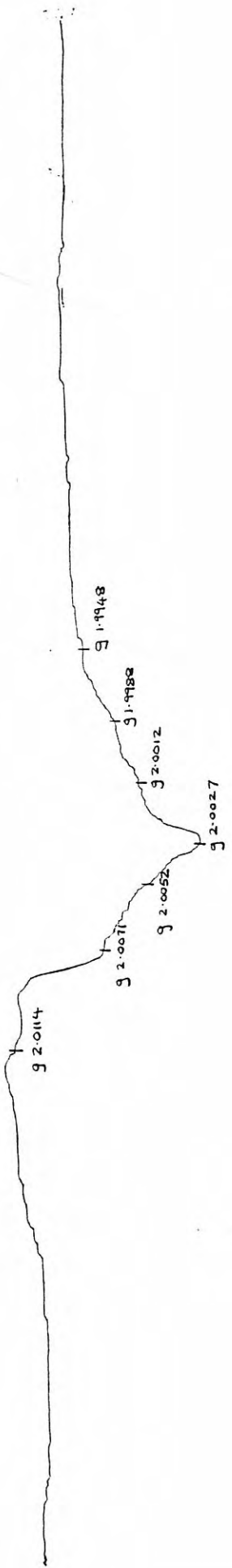
6/11/07

FO 41
2857

70-7-87

$3265 \pm 50 \text{ mT}$
+

9.125 GHz
0.2x10
100 kHz
100 mg
2.5 X 100
0.3
2 min / 4 min
10 mW
no standard



+

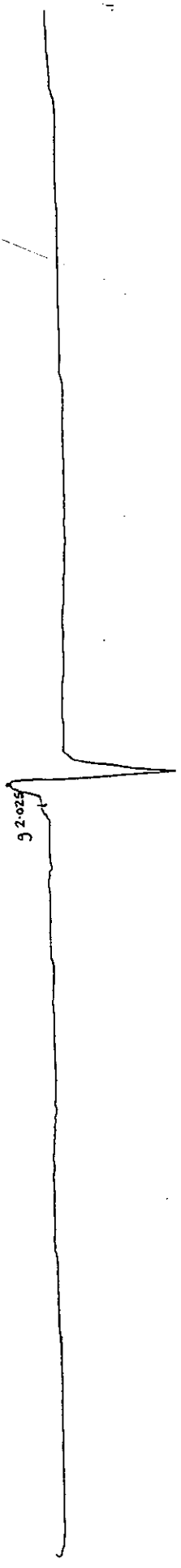
Hot
HNO₃

FO 41
K857

20-8-89

3265 ± 1000 mT
+

9.125 GHz
0.2 x 10
100 kHz
100 mg
25 x 100
0-3
4 min / 8 min
10 mV
no standards



Hot
HNO3

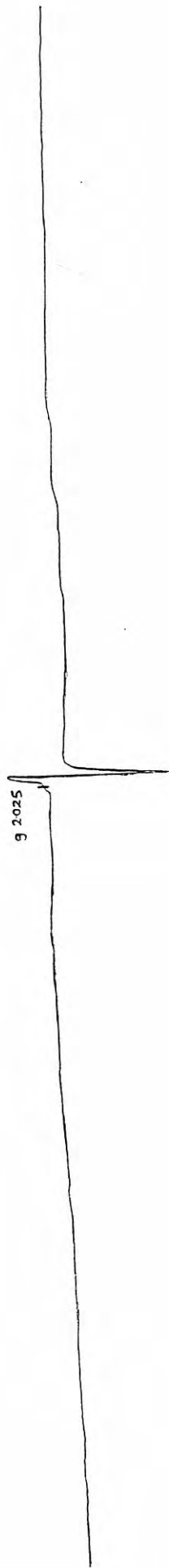
9.125 GHz
0.2 x 10
100 kHz
100 mg
2.5 x 100
0.3
4 min / 16 min
10 mW
no standard

3765 + 2500 mT
+

18-2-06

2657
A of H

g 2.025



+

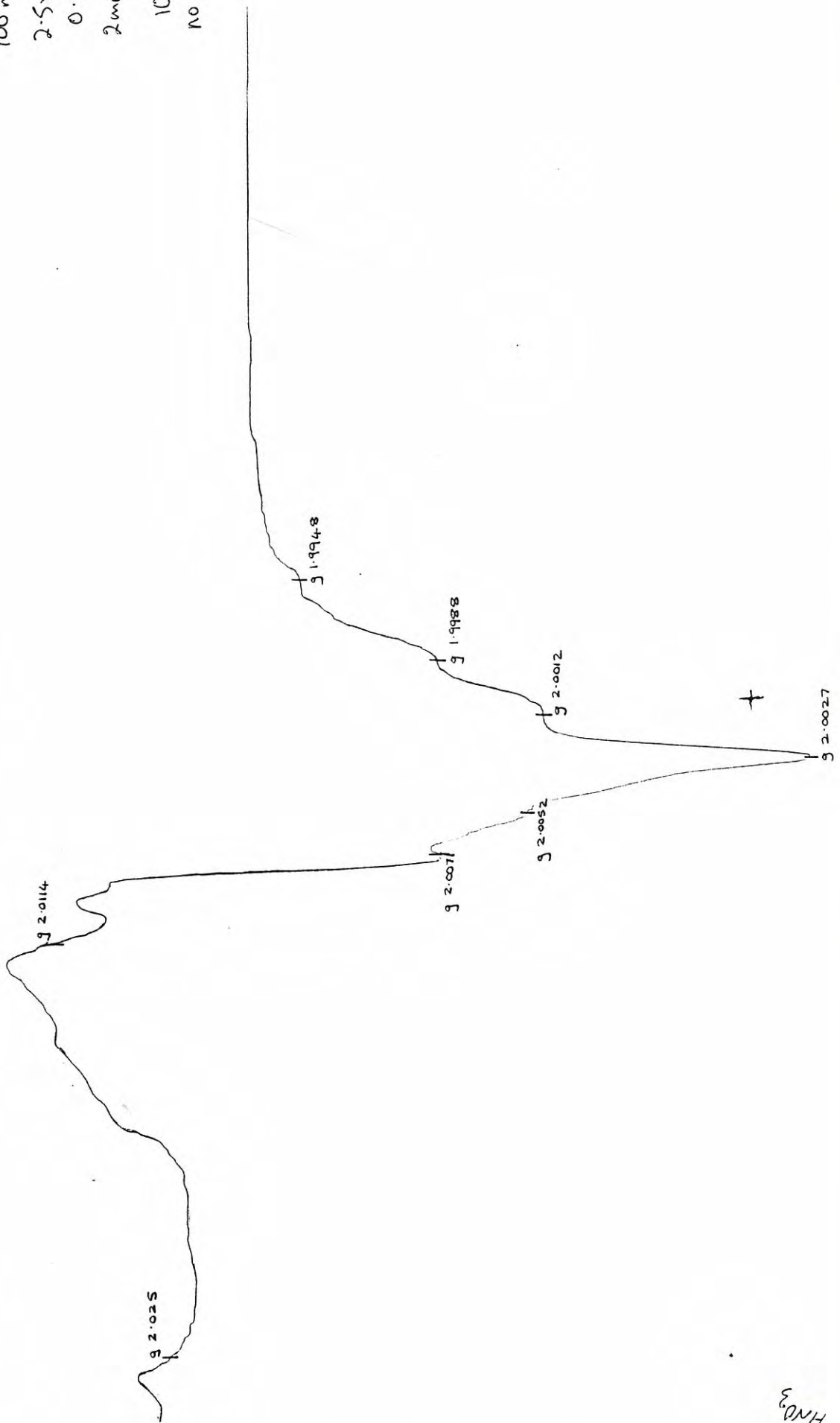
Hot
HND₂

FO
6736
109

70-7-89

3265150 mT
+

9.125 GHz
0.2x10
100 KHz
100 mg
2.5x100
0.3
2 min / 4 min
10 mW
no standard



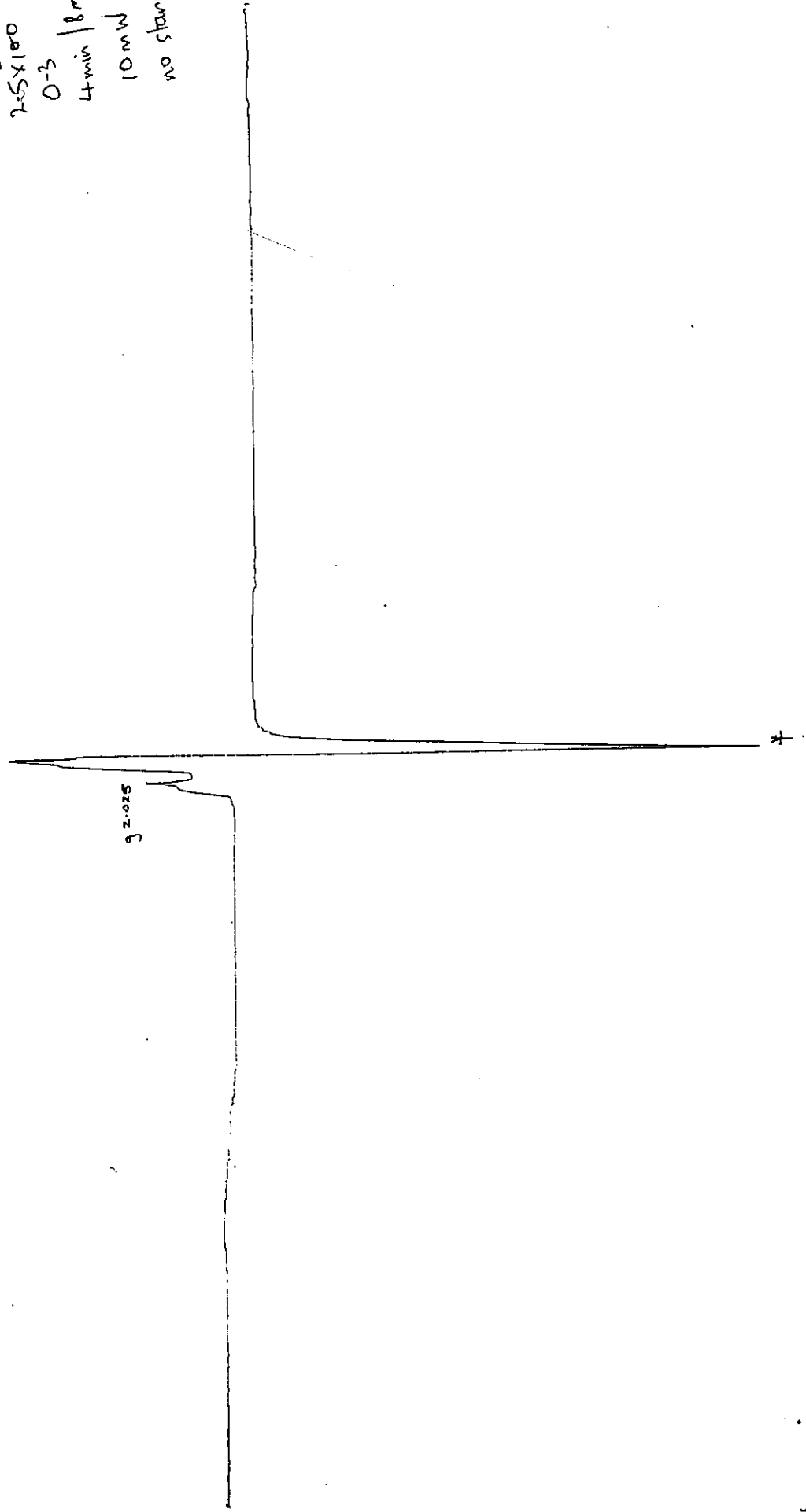
Hof
HND₃

9.125 GHz
0.2x10
100 kHz
100 mg
2.5x100
0-3
4 min / 8 min
10 mW
no standard

3265 ± 1000 mT

20-7-89

6736
Fo 109



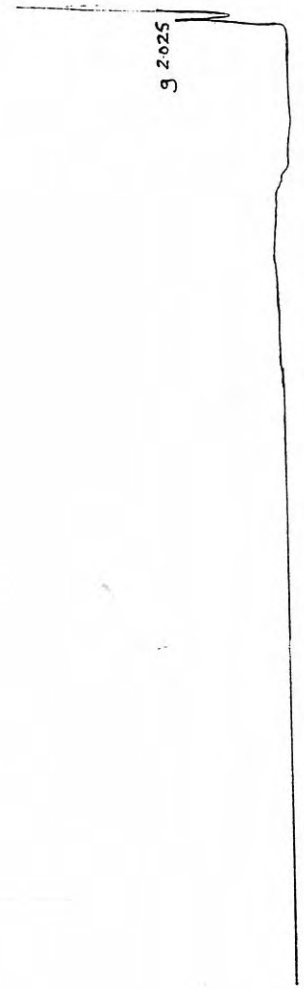
Hof
H103

6736
Fo 109

20-7-89

3265 + 2500 mT
+

9.125 GHz
0.2 x 10
100 KHz
100 mg
2.5 x 100
0.3
4 min / 16 min
10 mW
no standard



Hot
HM03

+

10/1/72

FD 148
1579

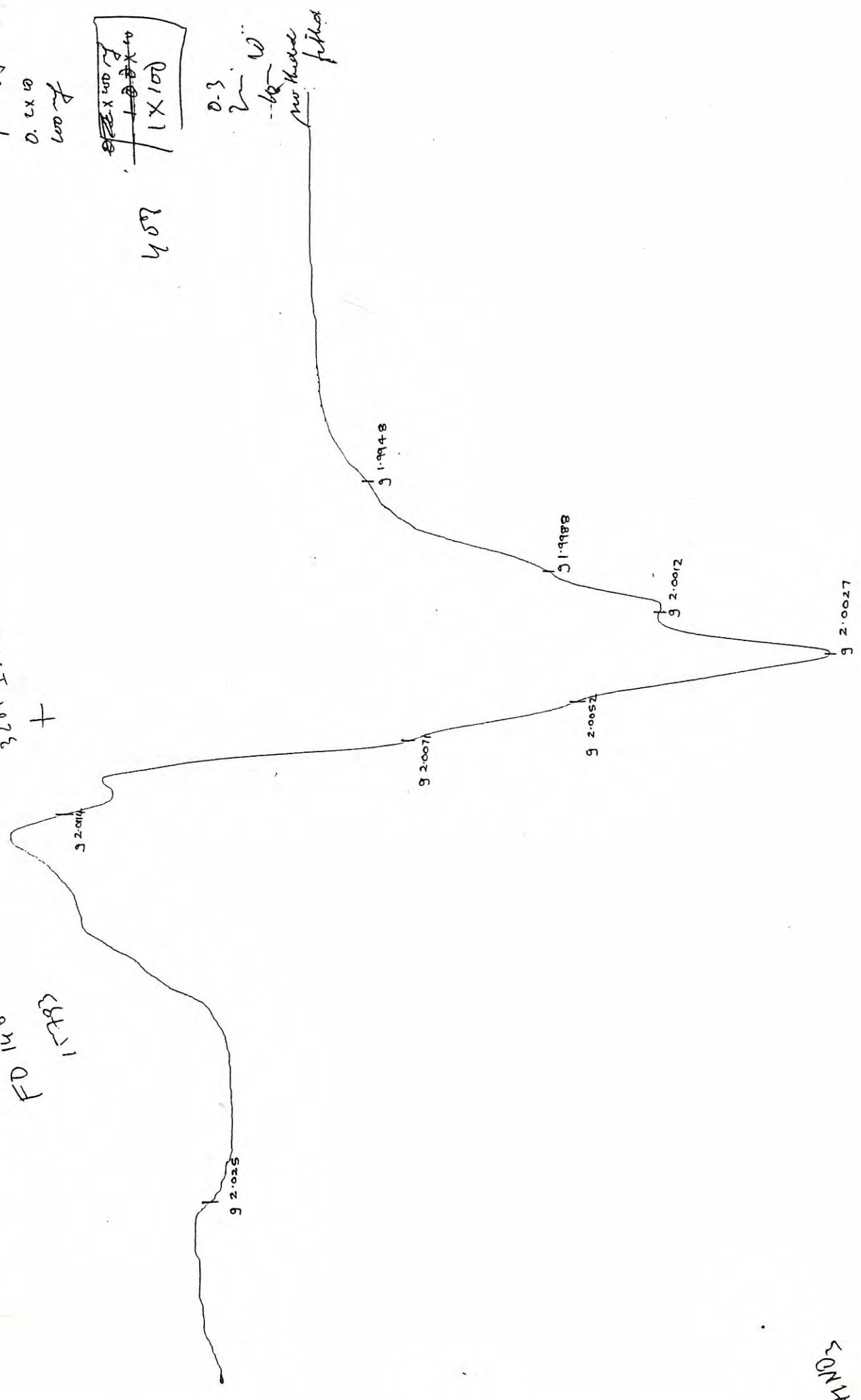
3265 FSD MT
+

9.152 fktz
0.2 x 0
0.007

201X1
1X100
201X100

457

0.3
2
-60
no. 1000
filled



10/1/72

FO 148

17793

2/14/89

3265 ± load mt

+

92025

+

9-174 Hz

0.2x10

600 Hz

100
1 x 100

40%

0.7

2-18

6-40

no-thin fiber

64 x 100

FO 148
15793

27/1489

32 65 ± 2000 mT

9.1574 MHz

0.250
100 MHz

600 f
7 V/m

304 MHz

0.3
16 W
100 W
in through

9 2025

201

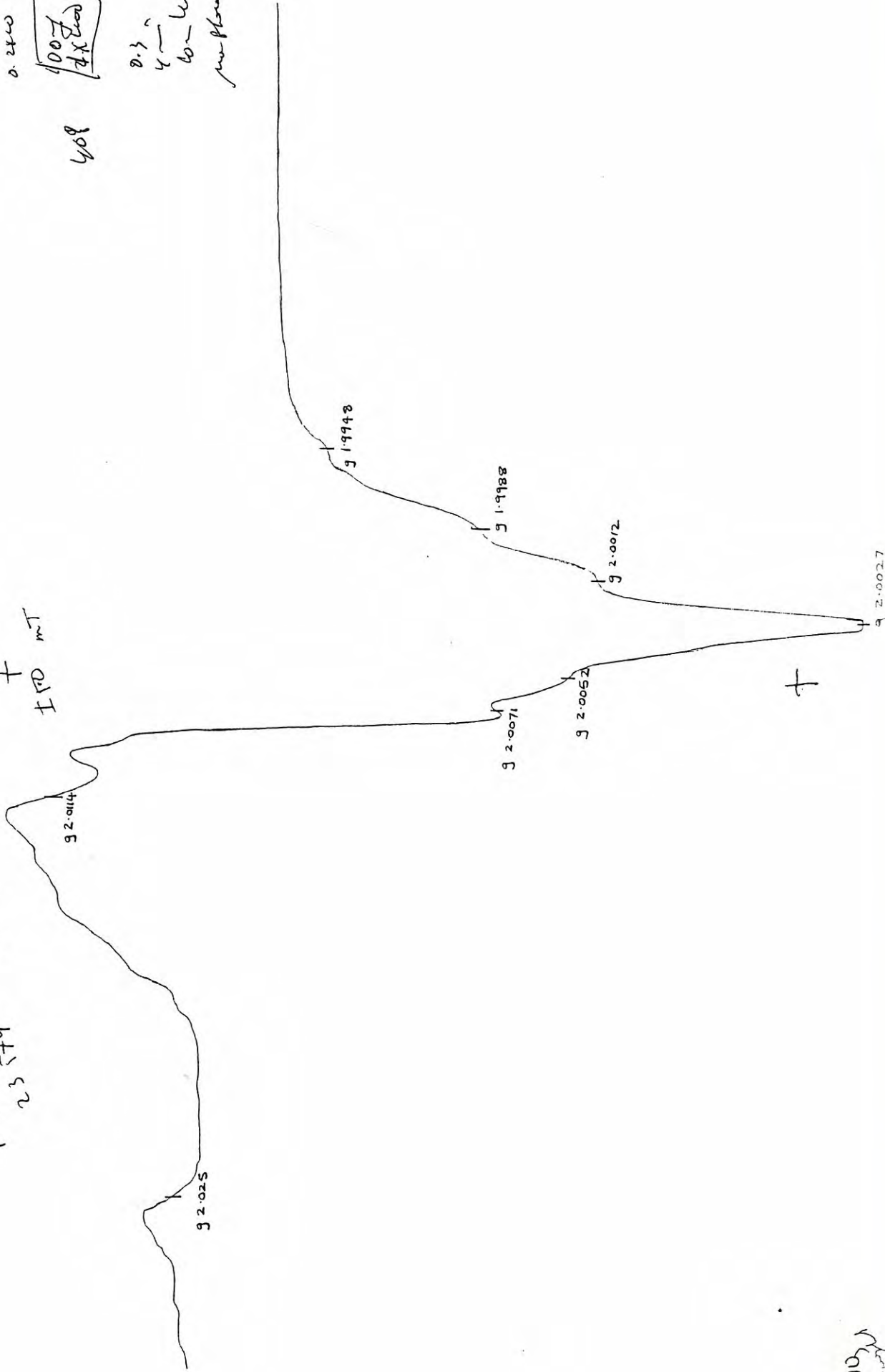
FO 276
23 574

K12189

3265
+
IFD MT

91125
100 1112
0.2400
1000
4 X 1000
408

0.3
4
60-11
per phone bedid



W1111111111

FO 276
23574

11/18/89

3265

I ROAD MT

9 2025

8.15% f the

600 k the
0.220

40% $\frac{600}{11 \times 100}$

4-18

D.S
600 W

per theory fiction

+

just HAD to
write

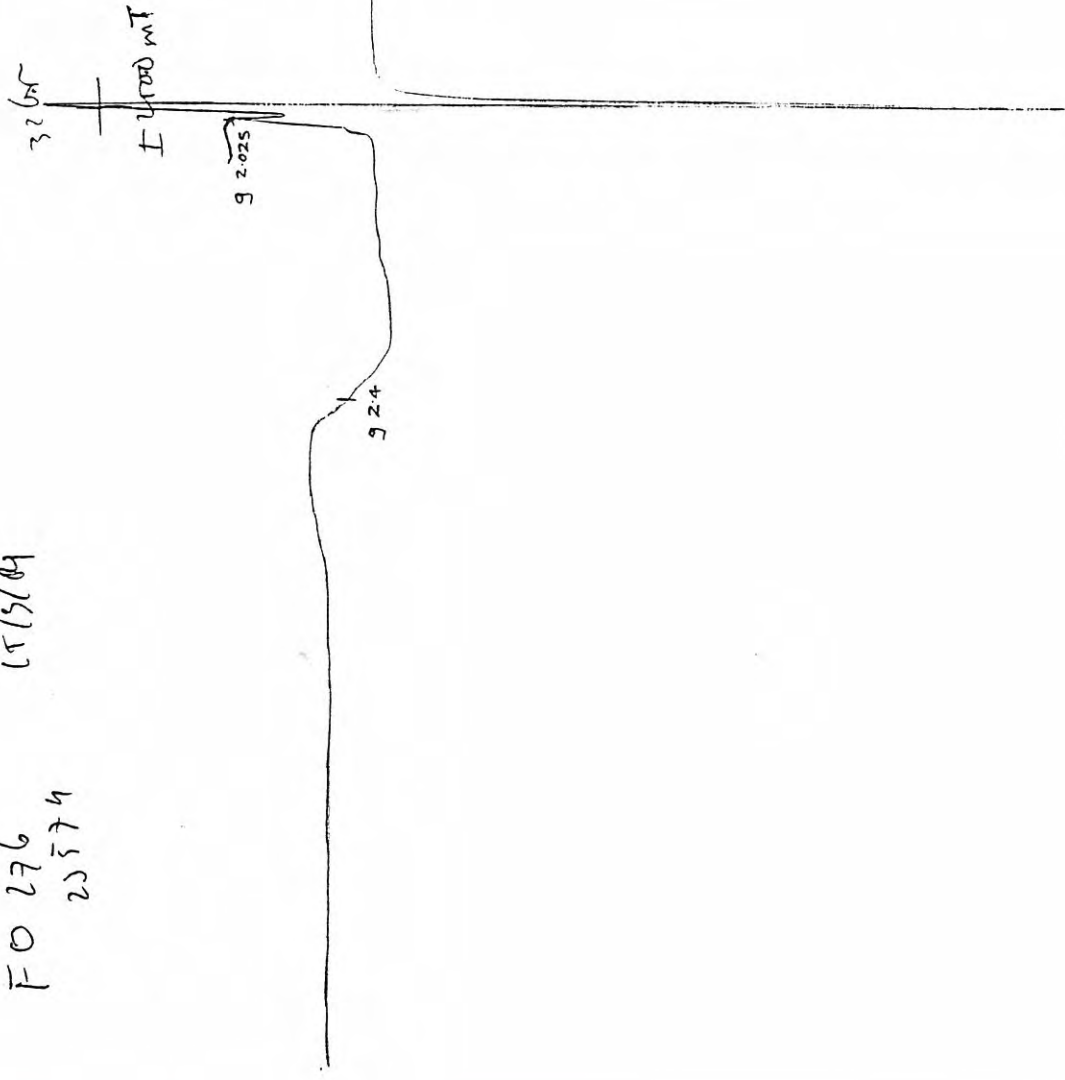
FO 276
20574

15/5/04

2-4-1 flk
0-2-2
600 bbl

400
[1000
1000
1000]

8.1
4
600 W
per-Mon-fill



Kenyon

APPENDIX 3

EPR spectra of samples FO23-748 (Ge=5.4 ppm) and FO 41-2857 (Ge=0.0 ppm) after irradiation with Au x-ray tube.

NB: Ge hole at g 1.9988 becomes visible after irradiation.

P. 154 of K

also
to KHC

Box
X 1

304

0.3

4m
W

Mr. K...

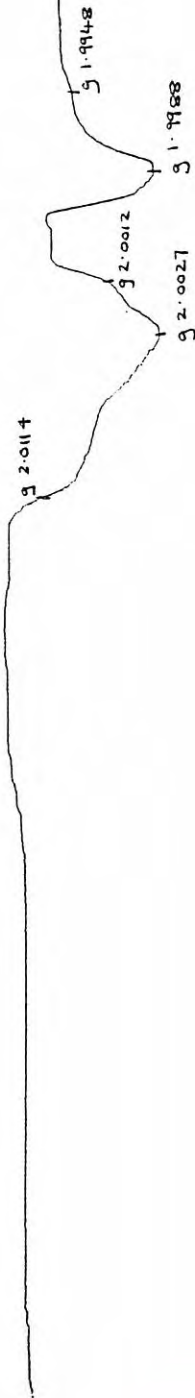
Box
X 1

SECRET MT
+

~~FOUO~~
~~748~~

FO 41
2857

(0.05m)



+

working
W - Y - ...
An table

APPENDIX 4

EPR spectra of samples FO23-748 and FO 41-2857 15 hours after irradiation with Au x-ray tube.

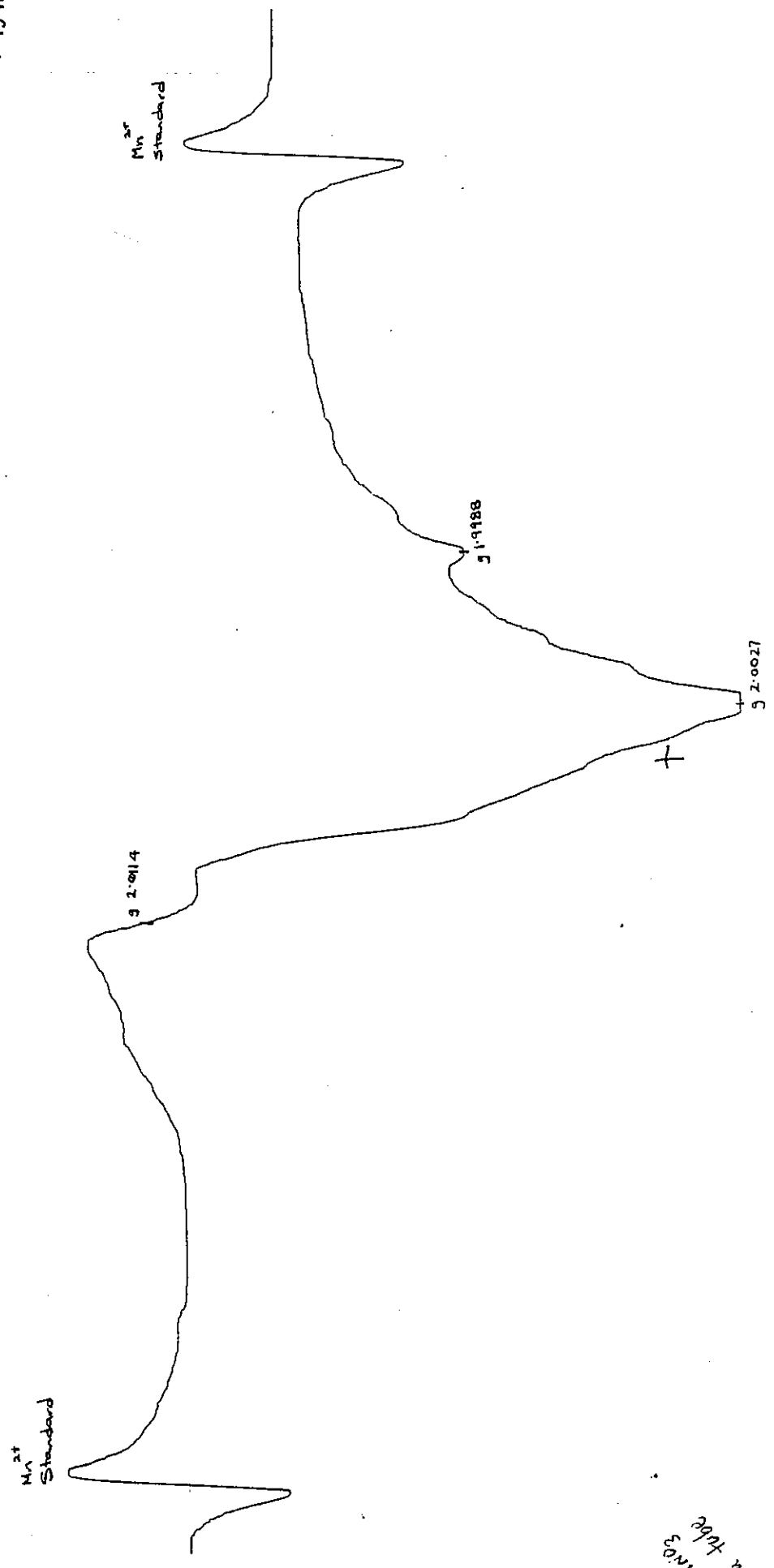
NB: Ge hole at g 1.9988 has decayed after 15 hours for sample FO41-2857 (Ge=0.0 ppm). Ge hole

at g 1.9988 is still visible after 15 hours for sample FO23-748 (Ge= 5.4 ppm).

9.151 GHz
0.2x10
100 KHz
1x100
100mg
0.3
8 min
Minst Standard
X-ray → 10 min
* 15 hrs

3265 ± 50 mT
+

F0 23
748



Hof 1103
the tube

9.151 GHz

0.2 x 10

100 kHz

1 x 100

100 mg

0.3

8 min.

Mn²⁺ Standard

X-ray → 10 min

Mn²⁺ Standard * 15 hrs

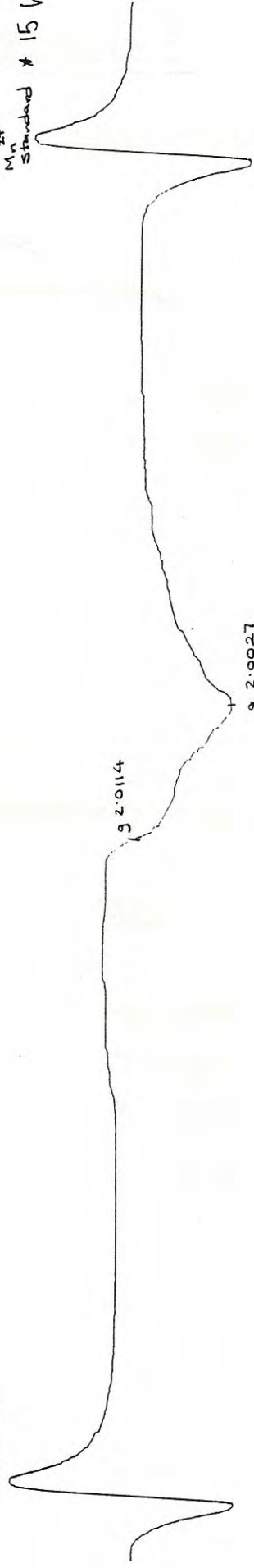
3265 ± 50 mT

+

F041

2857

Mn²⁺ Standard



32014

320027

Hot HNO₃ Au-fibre

+

APPENDIX 5ELECTRON MICRO-PROBE ANALYSIS OF TWO TYPES OF CARBONATES IN
SEDIMENTS AT FOSTERVILLE.(1) Average composition of nine samples of siderite :

<u>CARBONATE</u>		<u>Wt %</u>	<u>CATIONS</u>
Mg(CO ₃)	1.2560	Mg 0.3618	0.0341
Ca(CO ₃)	0.1561	Ca 0.0624	0.0036
Mn(CO ₃)	2.4425	Mn 1.1665	0.0486
Fe(CO ₃)	96.9621	Fe 46.7067	1.9138
Sr(CO ₃)	0.0000	Sr 0.0000	0.0000
Total	100.8167		2.0000

(2) Average composition of twelve samples of Fe-Mg carbonate :

<u>CARBONATE</u>		<u>Wt %</u>	<u>CATIONS</u>
Mg(CO ₃)	38.2107	Mg 11.0066	0.9133
Ca(CO ₃)	0.4041	Ca 0.1617	0.0081
Mn(CO ₃)	0.5136	Mn 0.2453	0.0090
Fe(CO ₃)	61.4634	Fe 29.6070	1.0694
Sr(CO ₃)	0.0119	Sr 0.0070	0.0002
Total	100.6036		2.0000

APPENDIX 6 - ROCK CATALOGUE

UTGD No.	Sample No.	Preparation	Description	Location & Depth	Azimuth	Declination
72331	FO3-23	PP, PC,	Brown sand, interbedded with silt.	10397N, 1651E; 23m	70	60
72332	FO3-30	PP, PC,	Shale. Qtz veins present.	10397N, 1651E; 30m		
72333	FO3-36	PP, PC,	Oxidized sand. Qtz veins present.	10397N, 1651E; 36m		
72334	FO10-30	PP, PC,	Grey sand. Fe stained qtz veins.	10481N, 1663E; 30m	70	55
72335	FO10-31	PP, PC,	Grey sand. Fe stained qtz veins.	10481N, 1663E; 31m		
72336	FO10-32	PP, PC,	Grey sand. Fe stained qtz veins.	10481N, 1663E; 32m		
72337	FO23-747	PP, PC,	Brown sand, interbedded with shale. Qtz veins.	10158N, 1711E; 33m	70	60
72338	FO23-748	PP, PC,	Brown sand, interbedded with shale. Qtz veins.	10158N, 1711E; 34m		
72339	FO41-2853	PP, PC,	Fe stained qtz veins.	10449N, 1652E; 51m	70	55
72340	FO41-2854	PP, PC,	Brown sand, with Fe stained qtz veins.	10449N, 1652E; 52m		
72341	FO41-2857	PP, PC,	Brown sand, with Fe stained qtz veins.	10449N, 1652E; 55m		
72342	FO41-2867	PP, PC, PT, PH	Brown sand, with Fe stained qtz veins.	10449N, 1652E; 65m		
72343	FO52-3637	PC,	Brown sand, with Fe stained qtz veins.	10481N, 1668E; 31m	70	55.5
72344	FO59-4159	PP, PC,	Grey sand, with py & asp. Qtz veins.	7808N, 1873E; 39m	250	55
72345	FO59-4160	PP, PC,	Grey sand, with py & asp. Qtz veins.	7808N, 1873E; 40m		
72346	FO59-4164	PP, PC,	Grey silt, interbedded with sand. Py & asp present.	7808N, 1873E; 44m		
72347	FO106-6468	PP, PC,	Brown sand, with interbedded silt. Qtz veins.	7783N, 1886E; 21m	249	56
72348	FO106-6516	PP, PC,	Interbedded sand, silt. & shale. Py & asp present.	7783N, 1886E; 69m		
72349	FO106-6523	PP, PC,	Interbedded sand, silt. & shale. Py & asp present.	7783N, 1886E; 76m		
72350	FO108-6640	PC,	Brown silt. Minor shale. Qtz veins present.	7583N, 1831E; 26m	69	55
72351	FO108-6641	PP, PC,	Interbedded brown sand, & silt. Qtz veins.	7583N, 1831E; 27m		
72352	FO108-6645	PP, PC,	Brown sand, Fe stained qtz veins.	7583N, 1831E; 31m		
72353	FO109-6735	PP, PC,	Brown silt. Qtz veins abundant.	10158N, 1696E; 48m	69	57
72354	FO109-6736	PC,	Interbedded brown sand, & silt. Qtz veins.	10158N, 1696E; 49m		
72355	FO116-7278	PP, PC,	Brown sand, Qtz veins abundant.	10482N, 1653E; 49m	70	55
72356	FO116-7279	PP, PC,	Brown sand, Fe stained qtz veins.	10482N, 1653E; 50m		
72357	FO147-15736	PC,	Interbedded brown sand, & silt. Qtz veins present.	10392N, 1712E; 22m	70	55
72358	FO148-15789	PP, PC,	Interbedded brown sand, & silt. Qtz veins present.	10392N, 1692E; 33m		
72359	FO148-15793	PP, PC,	Interbedded brown sand, & silt. Qtz veins present.	10392N, 1692E; 37m		
72360	FO172-17031	PP, PC,	Interbedded cream sand, & silt. Qtz veins.	7803N, 1873E; 32m	249	50
72361	FO172-17032	PC,	Interbedded sand, & silt. Qtz veins present.	7803N, 1873E; 33m		
72362	FO172-17035	PP, PC,	Brown sand, Qtz veins present.	7803N, 1873E; 36m		
72363	FO172-17039	PP, PC,	Interbedded grey sand, & shale. Py & asp present.	7803N, 1873E; 40m		
72364	FO224-20626	PP, PC,	Brown sand, Fe stained qtz veins.	10698N, 1660E; 13m	69	50
72365	FO224-20640	PC,	Brown sand, Fe stained qtz veins.	10698N, 1660E; 27m		
72366	FO236-21309	PP, PC,	Interbedded silt. Sand, & shale with py & asp. Qtz.	7429N, 1871E; 69m	249	50
72367	FO236-21317	PP, PC,	Interbedded grey sand, & shale with py & asp.	7429N, 1871E; 77m		
72368	FO237-21381	PP, PC,	Interbedded brown sand, & silt. Qtz veins	8190N, 1826E; 52m	69	50
72369	FO276-23574	PP, PC,	Interbedded grey sand, & shale. Py & asp present.	7803N, 1818E; 69m	69	70
72370	FO276-23601	PP, PC,	Grey sand, with shale. Py & asp present. Qtz veins	7803N, 1818E; 96m		
72371	FO327-28797	PP, PC,	Brown sand, & shale. Qtz veins.	7934N, 1646E; 35m	69	50
72372	FO327-28804	PP, PC,	Brown sand, Qtz veins.	7934N, 1646E; 42m		45
72373	DDH10-45.0	PT, PH	Sand, with qtz veins.	10483N, 1647E; 45m		55
72374	DDH11-52.9	PT, PH, F	Interbedded sand, & silt. Qtz veins.	10197N, 1756E; 52.9m		45
72375	DDH12-41.5	PT, PH, R	Grey, ferruginized sand.	7853N, 1908E; 41.5m		
72376	DDH12-43.0	PP, R, F	Ferruginized sand.	7853N, 1908E; 43m		
72377	DDH12-53.0	R, PT, PH	Grey/green shale.	7853N, 1908E; 53m		
72378	DDH12-54.5	PP, R, PT, PH	Interbedded silt. & shales. Qtz veins.	7853N, 1908E; 54.5m		
72379	DDH12-58.6	PP, R, PT, PH	Interbedded silt. & shales. Qtz veins.	7853N, 1908E; 58.6m		
72380	DDH12-70.0	PT, PH	Grey sand, with interbedded silt. Qtz veins.	7853N, 1908E; 70m		47
72381	DDH13-6.6	PP, R,	Weathered sand.	7787N, 1817E; 6.6m		
72382	DDH13-33.4	R, PH	Massive sand.	7787N, 1817E; 33.4m		
72383	DDH13-41.0	PT, PH, P, D	Lamprophyre dyke	7787N, 1817E; 41m		
72384	DDH13-42.5	PP, R, PT, PH	Qtz cataclasis (ex sand). Qtz veins.	7787N, 1817E; 42.5m		
72385	DDH13-46.5	PP, R,	Py/asp with interbedded silt. & sand. Qtz veins.	7787N, 1817E; 46.5m		
72386	DDH13-48.0	R, PT, PH	Py/asp with interbedded silt. & sand. Qtz veins.	7787N, 1817E; 48m		
72387	DDH13-48.6	PP, R, PT, PH	Py/asp with interbedded silt. & sand. Qtz veins.	7787N, 1817E; 48.6m		
72388	DDH13-52.0	PT, PH	Py/asp with interbedded silt. & sand. Qtz veins.	7787N, 1817E; 52m		
72389	DDH13-71.4	PP, R, PT, PH	Massive sandstone. Qtz veins.	7787N, 1817E; 71.4m		
72390	DDH13-74.5	PT, PH, R	Silt, with py & asp.	7787N, 1817E; 74.5m		

UTGD No. - UNIVERSITY OF TASMANIA GEOLOGY DEPARTMENT
NUMBER

PP	-	PIXE PILL	Sand.	-	Sandstone
PC	-	PERCUSSION DRILL CHIP SAMPLES	Silt.	-	Siltstone
PT	-	POLISHED THIN SECTIONS	Py	-	Pyrite
PH	-	PHOTO	Asp	-	Arsenopyrite
F	-	FLUID INCLUSION CHIPS	Qtz	-	Quartz
P	-	X-RAY PILL			
D	-	X-RAY DISC			